iberiancomsolconference.com

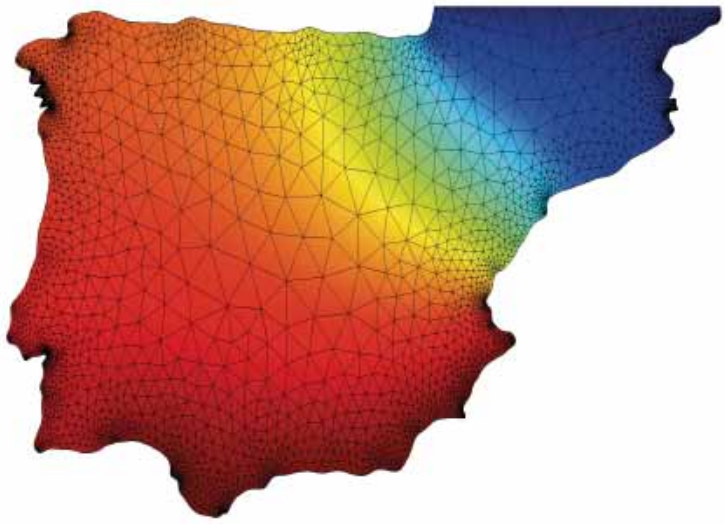

Iberian
COMSOL Multiphysics CONFERENCE
Málaga. May 29, 2014

Organised by:

COMSOL

Uma

NAFEMS

Addlink Software Científico

In collaboration with:

Andalucía Tech

FGUMA

EPS

scbi

Sponsored by:

SIE

Addlink Software Científico

Iberian
COMSOL Multiphysics
Conference 2014
Málaga, May 29, 2014

Conference book, abstracts and papers

ISBN 978-84-617-1737-8

Contents

Welcome to Iberian COMSOL Multiphysics Conference 2014 in Málaga!

It is with great pleasure that we welcome you in Málaga to participate in the Iberian COMSOL Multiphysics Conference 2014.

In the conference we have tried to bring together a community that is scientifically diverse in an event that allows for inspiring contacts about the use of COMSOL Multiphysics, with the creation of a premier Iberian event for Multiphysics Modelling & Simulation. It is an event to connect with the Spanish and Portuguese COMSOL Multiphysics users and participate in training opportunities and events explicitly designed for the academic and engineering community. Oral and poster presentations highlight achievements in multiphysics modelling and simulations using COMSOL.

In addition to being inspired by new methods, ideas and knowledge, we hope you will also discover and enjoy the city of Málaga. Very ancient Phoenician and Punic archaeological sites have been found in Málaga. It was a Roman municipality and during the Moorish era became the capital of a small independent kingdom. Since the 1960s, it has been an international tourist destination and the centre of one of the most thriving regions in southern Spain. Málaga is a city for all tastes with activities for everyone, and a perfect city for shopping while exploring the downtown core. With more than twenty museums, fifteen of them concentrated in the same area, Malaga has truly become a City of Museums. In the historic downtown core alone, including the new projects that will come on stream shortly, there are up to 24 museums making Malaga's historic downtown core one of the most densely developed in terms of museums.

Finally, we would like to thank Addlink Software Científico, COMSOL AB, the Technical Secretariat of the FGUMA, the University of Málaga, the Scientific Committee and the invited lectures for their assistance, and all the helping hands whose efforts will undoubtedly make Iberian COMSOL Multiphysics Conference 2014 a conference to remember!

The organizing committee of Iberian COMSOL Multiphysics Conference 2014.

Program

Thursday May 29

Morning	
9:00	**Registration opens**
9:30 – 9:45	**Welcome and introduction**
9:45 – 10:15	**Keynote presentation.- News in COMSOL 4.4.** Anders Ekerot. COMSOL AB, Sweden.
10:15 – 10:45	**User's presentations.** Session 1.
10:45 – 11:15	Coffee break
11:15 – 12:15	**Solver's Minicourse.-** Anders Ekerot. COMSOL AB, Sweden.
12:15 – 12:45	**User's presentations.** Session 2.
12:45 – 13:15	**Keynote presentation.- Simulation of discharges in gaseous particle detectors for CERN's RD51 collaboration.** Paulo Jorge Ribeiro da Fonte, LIP – Laboratory of Instrumentation and High Energy Particle Physics, Portugal
13:15 – 14:45	Lunch

Afternoon	
14:45 – 15:15	**Keynote presentation. – CFD Model*l*ing for Hydrogen Energy Technologies.** Ernesto Amores Vera. Research Department, National Hydrogen Centre, Spain.
15:15 – 15:45	**User's presentations.** Session 3.
15:45 – 16:30	**Poster session**
16:30 – 17:00	Coffee break
17:00 – 17:30	**Keynote presentation. – Using COMSOL Multiphysics to Describe Solid/Liquid Flows.** Maria Graça Rasteiro. Universidade de Coimbra, Portugal.
17:30 – 18:00	**Keynote presentation. – Multiphysics Simulations for Geosciences and Environmental Engineering.** Elena Abarca. Amphos 21, Spain.
18:00	Closing words. Conference ends
20:30	Conference Cocktail

10:15 – 10:45 **User's presentations.** Session 1.

10:15 - 10:30 Modelling Vaporization in Radiofrequency Ablation of Biological Tissue, Y. Fatieieva, E. Berjano and M. Trujillo.

10:30 - 10:45 Implementation of Advanced Soil Mechanics Models in COMSOL Multiphysics, V. Navarro, L. Asensio, J. Alonso, Á. Yustres and X. Pintado.

12:15 – 12:45 **User's presentations.** Session 2.

12:15 - 12:30 Mixed Elasticity with Discontinuous Pressure Interpolation, J. J. Anza.

12:30 - 12:45 Hydro-Mechanical-Chemical Coupled Modelling of Copper Heap Leaching with iCP, O. Silva, A. Nardi, J. Molinero, G. Román-Ross and P. Quesada.

15:15 – 15:45 **User's presentations.** Session 3.

15:15 - 15:30 NO_x Remediation in Monolith Channel with NH_3-SCR, U. de la Torre, F. Dhainaut, B. Pereda-Ayo and J.R. González-Velasco.

15:30 - 15:45 Assessment of the Validity Range of the Standard Linear Perturbation Models of Electrophoresis with High Electric Field Calculations, E. Ruiz-Reina and F. Carrique.

15:45 – 16:30 **Poster session.**

P1: Ethanol Steam Reforming for Hydrogen Generation, S. Rosell, R. Torres, J. Grau, and J. López.

P2: Generalized Plane Strain Problem: Application To Heterostructure Nanowires, H. T. Mengistu and A. García-Cristóbal.

P3: Equivalent Resistance Factor for Vapour Diffusion in Building Materials and Components, J.A. Millán, J.M. Hidalgo, J.M. Sala and I. Gómez.

P4: A Computer Modelling Study of the Influence of Blood Blow inside a Large Vessel as a Thermal Protection Mechanism from Thermal Damage to its Wall during RF-assisted Resection, A. González-Suárez, M. Trujillo, F. Burdío, A. Andaluz and E. Berjano.

Keynote presentations and minicourse

Anders Ekerot, COMSOL AB, Sweden.
M.Sc. in engineering physics specialized in scientific computing. Anders has been with COMSOL since 1999, starting out at the development department. He currently works with global technical support and product development at the Swedish office.

Keynote presentation.- News in COMSOL 4.4. Topics: New Windows User Interface, Mixer Module and New functionality in established products.

Solver's Minicourse.- COMSOL Multiphysics gives precise control over the way in which your multiphysics models are solved. This minicourse covers the fundamental numerical techniques and underlying algorithms used, and explains the reasons behind the default solver settings. Building upon this knowledge, attendees will learn various techniques for achieving or accelerating convergence of nonlinear multiphysics models.

Ernesto Amores Vera.
Research Department,CNH_2 – National Hydrogen Centre, Spain
Graduated in Mechanical Engineering at Castilla-La Mancha University. Later he joined a company dedicated to PV solar energy. Since 2010, he works in the Research Department at Centro Nacional del Hidrógeno (CNH2) on several aspects of hydrogen energy and simulation CFD applied to investigate electrolyzers, fuel cell and safety issues of H2 technologies. He has assisted to several COMSOL Conferences and in 2011 the CNH2 received the "Best Paper Award" for the article "Study of an alkaline electrolyzer powered by renewable energy"

Keynote presentation.- CFD Modeling for Hydrogen Energy Technologies
Hydrogen is an ideal energy storage system for the future. It can be produced from Renewable Energy (RE) surplus and later it can be used to produce electricity through a fuel cell. In this way, H_2 production allows us to reduce emit greenhouse gases. However, transition to a RE-H_2 requires a large R&D effort to improve technologies for production, storage and use of H_2. In this sense, the development of models using simulation CFD software is key to achieving the H_2 economy. For example the modeling of an alkaline electrolysis cell powered by a PV-module using "Electric Currents" and "Two phase-flow" modules of COMSOL; or the study of H_2/H_2O separation considering laminar or turbulent flow are strategic models to predict the behavior of these technologies.

Elena Abarca.
Amphos 21, Spain.

Elena received her B.Sc. in Geology, M.Sc. in Hydrogeology, and Ph.D. in Civil Engineering. She is Project Manager and Senior Consultant at AMPHOS 21. She was previously a Postdoctoral Associate at MIT with 11 years of experience in numerical modeling of groundwater flow and contaminant transport in porous media. She has a wide experience in numerical modeling of groundwater flow and transport of (conservative and reactive) contaminants in porous media using COMSOL Multiphysics.

Keynote presentation.- Multiphysics Simulations for Geosciences and Environmental Engineering.

Porous media flow simulations for geoscience applications are characterized by coupled processes occurring over very different spatial and temporal scales. We present some multiphysics simulations accounting for groundwater flow and reactive transport processes occurring in complex geological media for applications in the nuclear waste disposal, mining and oil and gas industries. For coupling subsurface flows and geochemical processes, we have developed the interface iCP, which couples COMSOL Multiphysics and the geochemistry code PHREEQC.

Maria Graça Rasteiro.
Universidade de Coimbra, Portugal

Professor of Chemical Engineering. She did her PhD in Chemical Engineering in 1988, and it was focused in the topic of Hydraulic Transport. In 2012 she was awarded the aggregation degree in the field of Chemical Engineering. She is, presently, coordinator of the Research Center on Chemical Processes and Forest Products Engineering (CIEPQPF) at the University of Coimbra. Her field of expertise is Particle Technology, with a special focus on studies of particle/particle interactions (both modeling and experimental) and multiphase flows. Under her direction, three PhD students have been developing, in the last years, their thesis in this last domain, studying the flow of solid/liquid suspensions (spherical particles and suspensions of cellulose fibers) with the aid of COMSOL Multiphysics for the numerical simulations.

Keynote presentation.- Using COMSOL Multiphysics to Describe Solid/Liquid Flow

A great number of industrial applications heavily depend on the conveying of particles in pipelines. Amongst the ever increasing number of fields where particle conveying is

of great importance we can outline the production of chemicals, energy, pharmaceuticals or foodstuffs, papermaking, composites and also the transportation of minerals and wastes. The team of CIEPQPF working in this field has been dealing with both the flow of concentrated fiber suspensions and of concentrated suspensions of spherical particles. The work which will be presented in this lecture details numerical studies using the Mixture Model present in COMSOL Multiphysics to simulate the behavior of concentrated solid-liquid suspensions conveyed in pipelines. This model was employed for neutrally buoyant and heavy particles, with varying sizes and particle concentrations. In order to be able to describe adequately these flows, several modifications had to be introduced in the Mixture Model. With these modifications good agreement with experimental data was obtained. These modifications depend on the type of particles being conveyed, buoyant particles or heavy particles and, in general, on the flow regime.

Paulo Jorge Ribeiro da Fonte
LIP – Laboratory of Instrumentation and High Energy Particle Physics, Portugal.

Paulo Fonte is professor at ISEC-Instituto Superior de Engenharia de Coimbra and researcher at LIP-Laboratory of Instrumentation and High Energy Particle Physics, Portugal. He and his group at LIP have been on the front line of the development of timing Resistive Plate Chambers, which opened the way to much more economic time-of-flight particle detectors, featuring excellent time and position resolutions, compact mechanics, magnetic field compatibility and large-area capability. COMSOL Multiphysics is often used for modeling different aspects of such detectors.

Keynote presentation.- Simulation of discharges in gaseous particle detectors for CERN's RD51 collaboration.

The RD51 Research &Development collaboration, based at CERN, aims at facilitating the development of advanced gas-avalanche detector technologies (gaseous detectors) and associated electronic-readout systems, for applications in basic and applied research. The movement of electrical charges in several micropattern gaseous detectors, leading to avalanches and eventually to "streamer" discharges is here modeled in COMSOL Multiphysics within a hydrodynamic model, yielding insights into fundamental features of these detectors.

Abstracts oral presentations

Modeling Vaporization in Radiofrequency Ablation of Biological Tissue

Yu. Fatieieva[*1], E. Berjano[2], and M. Trujillo[3]

[1]Zaporizhzhye National University, Zaporizhzhye, Ukraine, [2]Biomedical Synergy, Electronic Engineering Department, Universitat Politècnica de València, Spain, [3]Instituto Universitario de Matemática Pura y Aplicada, Universitat Politècnica de València, Spain.
*Presenting and corresponding author: Department of Applied Mathematics, Zaporizhzhye National University, Zhukovsky str., 66, 69600. Zaporizhzhya, Ukraine.
E-mail: fateevajulia@gmail.com

Abstract

Radiofrequency ablation (RFA) is a minimally invasive technique used to destroy different kind of tumors [1]. RFA consists of the passing of electrical currents (≈ 500 kHz) through the biological tissue which produces the heating of the target tissue. When tissue temperature achieves 50^{o}C, cells die due to protein denaturation. When tissue temperature achieves 100^{o}C water vaporization occurs. This phenomenon has an important effect during RFA since electrical and thermal conductivities depends on the water content of the tissue, and this phenomenon removes energy employed for heating.

The objective of the RFA is to obtain a lesion size in tissue which destroys completely the tumor. However, during the heating, the electrical impedance increases and produces charring and dehydration in the tissue around the electrode, which reduces energy diffusion and limits the lesion size. Changes in the power delivering protocol or in the electrode design are the primary ways to overcome this limitation. For instance, cooled internally electrodes prevent the adjacent tissue from charring and consequently can produce larger lesions than the conventional electrodes. Although cooled electrodes are commonly used, the lesion size obtained do not allow destroy completely the tumor. To increase the lesion size, wet electrodes have been proposed, which infuse saline solution into the tissue. The saline improves thermal and electrical tissue conductivities, and hence prevents fast water evaporation in the tissue.

In theoretical modeling, there are two approaches to introduce water evaporation in the tissue: moving mesh methods and fixed mesh methods [2]. We are focus on fixed mesh methods since they are easier to include in the problem formulation and they provide satisfactory results for RFA problems. Specifically, we focus on the enthalpy method and water content modeling method. The enthalpy method is based on a modification of bioheat equation. However, this method does not taken into account the water content of tissue which would be useful for the RFA models which use wet electrodes. The aim of this work is to compare enthalpy and water content method to determine the correct use of them in the RFA modeling with different kind of electrodes.

To compare enthalpy and water content methods, we consider a theoretical RF hepatic ablation model. When vaporization is formulated using enthalpy method a

coupled thermo-electric problem is solved numerically using COMSOL Multiphysics software (COMSOL, Burlington MA, USA). To implement the water content method we add a PDE general form problem in COMSOL.

The results suggest that the enthalpy method presents an easier formulation and more appropriate for the RFA models employing dry and cooled electrodes. However, for the formulation of RFA models which use wet electrodes could be better to employ the water content method.

References

1. E. J. Berjano, Theoretical modeling for radiofrequency ablation: State-of-the-art and challenges for the future Biomed. Eng. Online, 18, 5-24, 2006.
2. T. Patz, T. Preusser, Composite Finite Elements for a Phase Change Model, SIAM Sci Comput, 31(5), 1372-91,2012.

Implementation of Advanced Soil Mechanics Models in COMSOL Multiphysics

V. Navarro[1], L. Asensio[*1], J. Alonso[1], Á. Yustres[1] and X. Pintado[2]

[1]Universidad de Castilla-La Mancha (Spain), [2]B+Tech Oy (Finland)
*Presenting and corresponding author: E.T.S.I. Caminos, Canales y Puertos, Avda. Camilo José Cela s/n, 13071 Ciudad Real, Spain. Laura.Asensio@uclm.es

Abstract

Introduction.- COMSOL Multiphysics includes several stress-strain constitutive models. In particular, the Geomechanics module introduces geomaterials models such as the Drucker-Prager and Mohr-Coulomb yield criteria and the modified Cam-Clay model, which are especially useful in soil mechanics. However, when a user wishes to implement a non-linear model of their choice that contains implicit relationships involving state functions, difficulties can arise. Then, in the case that the Solid Mechanics interface, or any other interface for which COMSOL computes symbolic derivatives of the terms by automatic differentiation (like a General Form PDE, Gobbert et al., 2009), is used, a circular dependence is obtained and the problem cannot be computed in COMSOL Multiphysics.

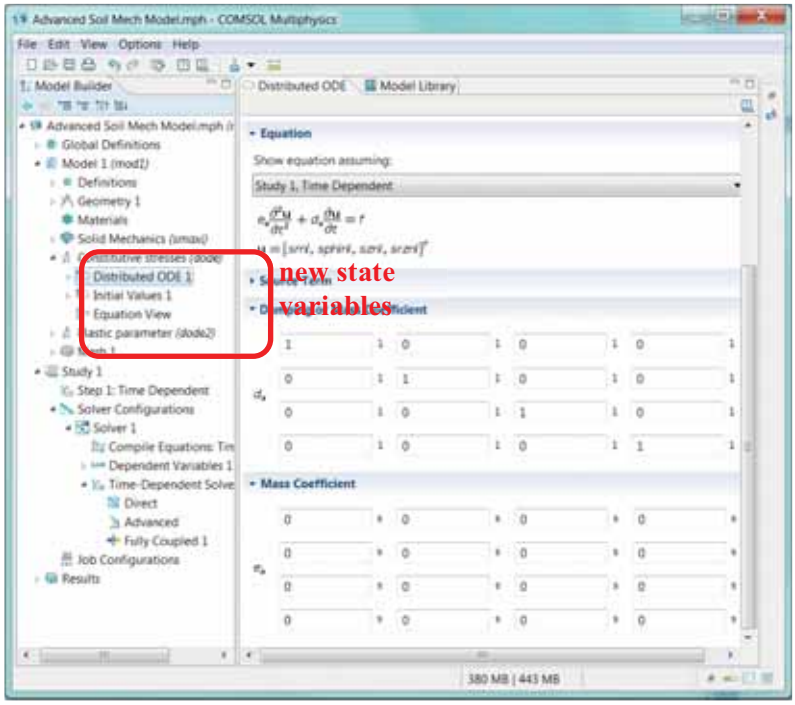

Figure 1

Use of COMSOL Multiphysics.- This work presents a strategy to overcome this problem. The use of a mixed method is proposed, as presented in Navarro et al. (2014). The stresses and plastic parameters are introduced as new state variables in the problem, making use of the equation-based modelling with a Domain ODE interface, in addition to the equilibrium solved with the Solid Mechanics interface (Figure 1). This way, consistence between the new state variables solved and the equilibrium block is enforced.

Results.- Advanced geomechanical models have been successfully implemented into COMSOL Multiphysics 4.3a using the proposed methodology. A Time-Dependent, Fully Coupled Solver has been used to compute transient problems. This way, quality solutions are obtained.

Conclusions.- The strategy presented enables the direct implementation by the user of advanced soil mechanics models, beyond the built-in models, into COMSOL Multiphysics, through the use of a mixed method. Thus, we believe it can be of great use for the modellers in the COMSOL community.

References

1. Gobbert M.K., Churchill A., Wang G. and Seidman T.I., Multiphysics for efficient solution of a transient reaction-diffusion system with fast reaction. In: Rao Y. (ed.) *Proceedings of the COMSOL Conference 2009*, Boston (2009).
2. Navarro V., Asensio L., Alonso J., Yustres Á. and Pintado X., Multiphysics implementation of advanced soil mechanics models, *Computers and Geotechnics*, **60**, 20-28 (2014).

Mixed Elasticity with Discontinuous Pressure Interpolation

Juan Jose Anza

Department of applied mathematics, University of the Basque Country, Bilbao, Spain
*Alameda de Urkijo s/n, Bilbao 48013, Spain , juanjose.anza@ehu.es

Abstract

Introduction.- In this paper we are interesting in using COMSOL as a platform for new developments. The work presented deals with elasticity in the incompressible limit where standard formulation has to be substituted by the mixed one, and finite element interpolations might be ill conditioned conducting to pathological behavior.

For such cases COMSOL offers in the Structural Mechanics toolbox, a mixed Formulation that represents de pressure as a dependent variable in addition to the displacement components. This formulation is implemented with continuous quadratic interpolation of displacements and continuous linear interpolation of pressure, a good combination to avoid mesh locking and pressure modes (ref 1) .

This work implements using COMSOL tools, a mixed formulation with continuous linear displacements and constant discontinuous pressure, which gives better precision, less unknowns and the possibility to work with linear elements near the incompressible limit.

Use of COMSOL Multiphysics.

1) Using the "pde (mathematics)\general formulation form" interface, define linear deformation and stresses from displacements and solve a cantilever beam (ref 1) for 0.3 and 0.499 Poisson modulus.
2) Using the "pde (mathematics)\weak form pde" interface, add the equation for the pressure and solve the previous problem.
3) Using the Solid Mechanics interface, compute the elastic deformation of the cantilever beam and compare with previous results and exact formulas.
4) Using the physics interface builder , build a new physics interface named "Linear Elastic Mixed Model (*mxe*), implementing the functionality developed in previous steps 1 and 2 with Dirichlet and Neumann boundary conditions, which can be used with any general geometry defined by COMSOL.
5) Using the physics interface builder , build a new physics interface named "Hyperelastic Mixed Model (*mxh*), with non linear stress (Piola) and non linear deformation (Green). Apply to any general geometry, for example, a torus under compression with large deformations (ref 2).
6) Using the Solid Mechanic interface, compute the hyperelastic deformation of the torus under compression, and compare with previous step.

Figure 1 shows the vertically compressed torus and the corresponding mesh for one eighth of the torus by symmetry.

Figure 2 shows Von Misses stress and deformation for the standard elastic formulation with Poisson modulus 0.4999 and linear interpolation of displacements.

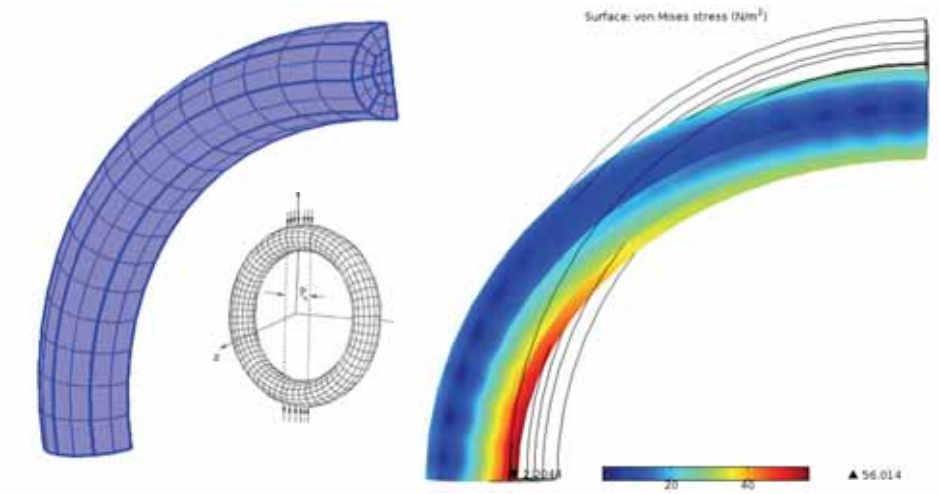

Figures 1 and 2

Figure 3 shows the deformation for the mixed hyperelastic formulation, with quadratic displacement and linear pressure interpolation.

Figure 4 shows the deformation obtained with the new Hyperelastic Mixed Model (mxh) interface, with linear displacement and constant pressure interpolation.

Mesh locking can be observed in figure 2, as well as the identical deformation obtained with both implementations of the mixed formulation, being the second (figure 4) much faster.

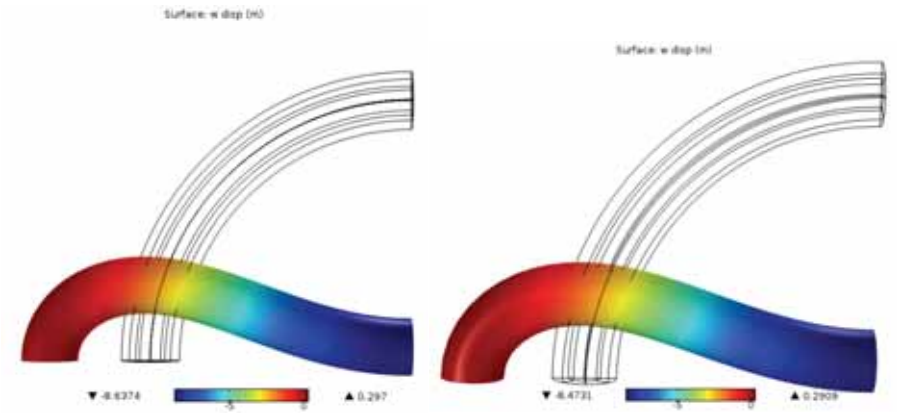

Figures 3 and 4

References

1. T.J. Hugues, "The Finite Element Method. (Linear Static and Dynamic Analysis)", *Prentice Hall*, 1987.
2. K.S. Chavan, B.P. Lamichhane, BI. Wohlmuth, "Locking-free finite element methods for linear and non linear elasticity in 2D and 3D"Non linear continuum mechanics for finite element analysis", *Computer Methods in Applied Mechanics and Engineering,* 196 issue 41-44 p. 4075-4086, 2007.

Hydro-Mechanical-Chemical Coupled Modeling of Copper Heap Leaching with iCP

Orlando Silva[*1], Albert Nardi[1], Jorge Molinero[1], Gabriela Román-Ross[1] and Pablo Quesada[2]

[1]Amphos 21 Consulting S.L., Spain, [2]Amphos 21 Consulting Perú S.A.C., Perú
*Presenting and corresponding author: Passeig Garcia i Faria, 49-51, 08019, Barcelona, Spain, orlando.silva@amphos21.com

Abstract

Heap leach pads constitute a common practice in the copper mining industry. It is defined as a mineral processing technology whereby large piles of crushed Run-of-Mine (ROM) rock are leached with various chemical solutions to extract the valuable minerals (Figure 1). In their design and management it is not common to take into account criteria based on coupled Hydro-Mechanical-Chemical (HMC) processes and these are of paramount importance for two reasons: (i) they could play an important role on the physical stability of the pad and; (ii) they are keys for the metallurgical efficiency, especially in the mid-long term. Several coupled HMC processes are involved during the construction and operation of a heap leach pad. Due to the complexity of the problem, common existing heap leaching models solve the different phenomena in an uncoupled or partially coupled way. Also, it is common to assume the system composed by a single copper-containing mineral and a single mineral representing the gangue. However, they could result in poor predictions of the composition of the pregnant solution and consequently, an over- or under- estimation of the copper recovery and acid consumption. Further, mechanics stability and mineral recovery efficiency cannot be estimated accurately without considering multiple coupling of the complex chemistry, soil mechanics and hydrodynamics.

Here we present a coupled HMC model that accounts for the kinetics of several mineral species and the evolution of a muti-lift heap. The governing equations are solved with the numerical interface COMSOL-PHREEQC (iCP) (Nardi *et al*., 2014). iCP is a Java interface that couples COMSOL Multiphysics and the geochemical simulator PHREEQC (Parkhurst and Appelo, 2013). In brief, the tool is based on implementing an operator splitting technique for solving the hydro-mechanical problem (a coupled or uncoupled system of partial/ordinary equations and algebraic differential equations) on COMSOL and the chemical system of algebraic and differential equations on PHREEQC.

We simulated the construction and operation of a synthetic copper heap leach pad consisting of five ore layers that are simulated sequentially, mimicking the sequence of construction and operation of a real heap leach pad. The stacked ore consists of an artificial mineral mixture made from Chrysocolla, Chalcopyrite, Pyrite, Albite and K-Feldspar, whose chemical evolution is assumed to be governed by kinetics reactions. Equilibrium precipitation-dissolution reactions of Jarosite-K, Jurbanite, Basaluminite,

$FeOH_3$(a) and Schwertmannite were also taken into account. The results show that changes in porosity and permeability due to mineral dissolution/precipitation (Figure 2) and irrigation time affect significantly the hydromechanical behavior of a heap leach pad (Figure 3), and vice versa. A strong advantage of the present model is that it can treat multiple chemical species simultaneously, providing solutions that are best for interpreting all the chemical interactions within a leaching system. The stability of the pad, the ore recovery efficiency and the acid consumption (Figure 4) can be predicted with more accuracy because the model considers the interaction between variable saturated flow, mechanical deformation and chemical reactions during the construction and operation of the heap.

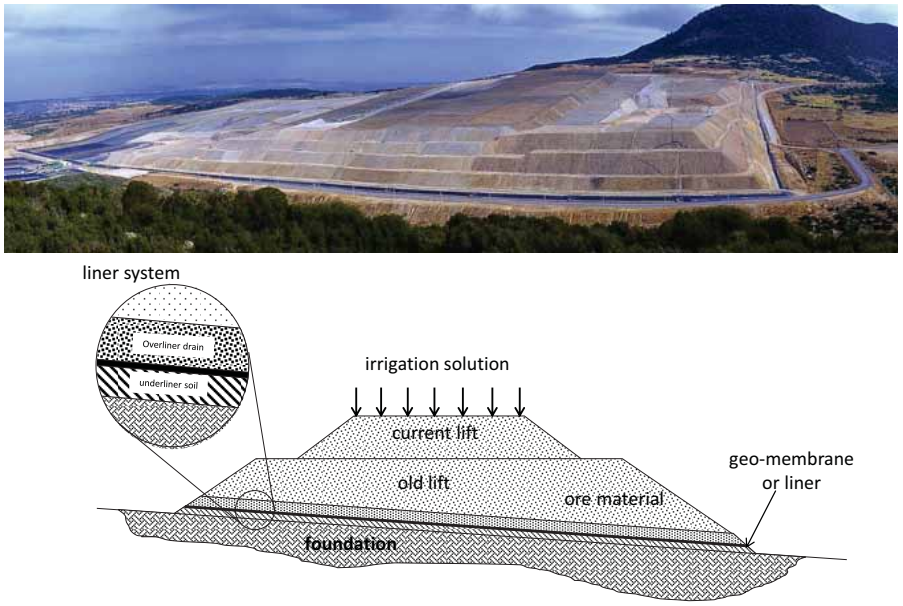

Figure 1 *View of a multi-lift heap pad (upper) and sketch of a heap leach pad system (bottom).*

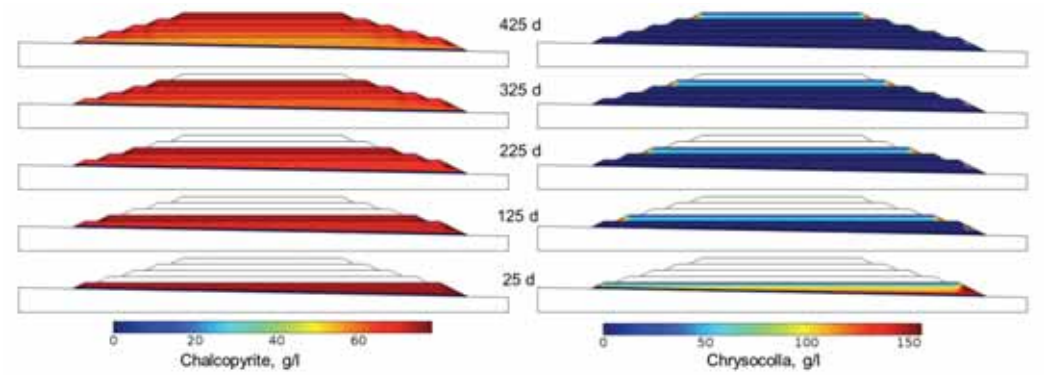

Figure 2 *Evolution of the Chalcopyrite (left) and Chrysocolla (right) concentrations in the leach pad.*

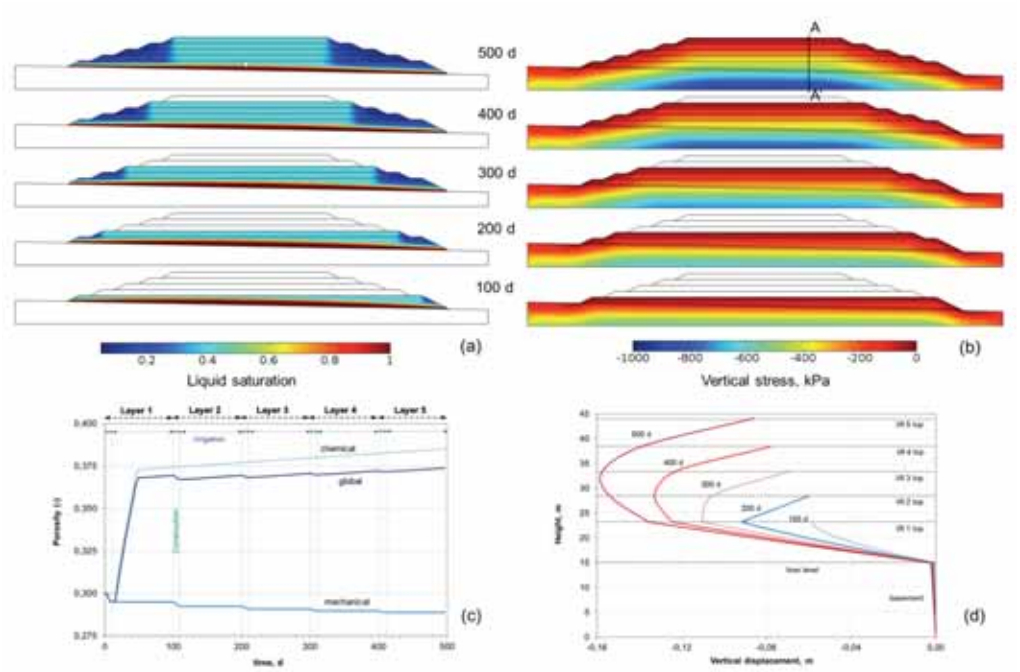

Figure 3 *Evolution of liquid saturation (a), vertical stress (b), porosity at the center of first lift (c) and vertical displacement at the cross section A-A' (d).*

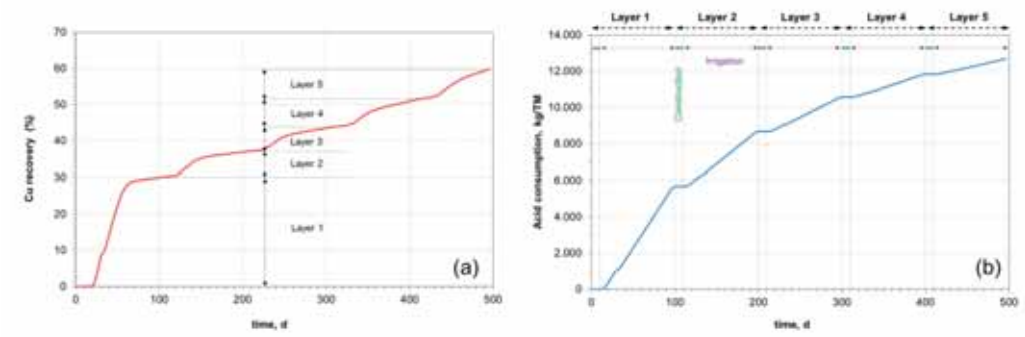

Figure 4 *Predicted copper recovery (a) and acid consumption (b).*

References

1. Nardi, A., Idiart, A., Trinchero, P., de Vries, L. M. and Molinero, J., Interface Comsol-PHREEQC (iCP), an efficient numerical framework for the solution of coupled multiphysics and geochemistry, *Computer & Geosciences*, submitted (2014).

2. Parkhurst, D. L., and Appelo, C. A. J., *Description of input and examples for PHREEQC version 3—A computer program for speciation, batch-reaction, one-dimensional transport, and inverse geochemical calculations*, U.S. Geological Survey Techniques and Methods, book 6, chap. A43, 497 p., available only at http://pubs.usgs.gov/tm/06/a43/ (2013).

NO_x Remediation in Monolith Channel with NH_3-SCR

U. De La Torre[1*], F. Dhainaut[2], B. Pereda-Ayo[1] and J.R. González-Velasco[1*]

[1]Chemical Engineering Department, Faculty of Science and Technology, University of the Basque Country, UPV/EHU, Leioa, 48940, Spain, [2] UCCS, Université Lille 1, Villeneuve d'Ascq, France.
*Presenter: unai.delatorre@ehu.es; Corresponding author: juanra.gonzalezvelasco@ehu.es

Abstract

Diesel engines have the highest thermal efficiency, and consequently release less CO_2 into the atmosphere as main gas contributing to global warming. The engine operates in excess of oxygen, with an air-to-fuel ratio higher than stoichiometric, making the conventional three-way catalyst (TWC) ineffective under such net oxidizing environment [1]. Among different alternatives, engine manufacturers and catalyst suppliers are considering the use of SCR with NH_3 as reductant for NO_x removal in end-of-pipe technologies. Additionally, the automobile application requires the development of a structured catalyst (Figure 1) in order to limit the pressure drop under real operation. Thus, the walls of a cordierite monolith (2 cm in length and diameter, 175 channels) were washcoated with a layer of previously exchanged Cu-zeolite catalyst where NH_3-SCR reaction occurs.

In this work, kinetic values determined from experimental run data analysis were used for creating a model in COMSOL 4.4. Actually, NH_3 adsorption-desorption, NH_3 oxidation and standard SCR ($4NH_3 + 4NO + O_2 \rightarrow 4N_2 + 6H_2O$) reactions were considered. Here, we have validated the model with experimental results obtained at 300 ºC and we have also evaluated the catalyst surface coverage ammonia and the NO_x removal along the channel for different geometries of the structure –typical squared or cylindrical channels in 3D.

The COMSOL Multiphysics Fluid Dynamics module was used to model the fluid flow along the monolith channel while solving the diffusion−convection equations with reactions occurring simultaneously on the catalyst surface. The use of the Transport of Diluted Species and Surface Reaction COMSOL modules allowed us to determine simultaneously the evolution of the concentration of NH_3 and NO at the outlet as well as the surface coverage of adsorbed NH_3 species in the washcoat.

The NO conversion *vs* time representation (Figure 2) confirms that the steady state has been reached after 500 seconds of reaction, with NO conversion around 48%. These results are in good agreement with experimental for square cell monolith elsewhere reported [2]. From Figure 2 it can also be deduced that NO conversion is not sensitive to the monolith geometry (cylindrical and parallelepiped channels). On the other hand, Figure 3 shows the NO conversion along the channel surface as well as at the reactor exit (end of channel) after 500 s of NH_3-SCR reaction. It can also been observed how the NO concentration is decreasing abruptly along the monolith length from the entry to the exit where NO conversion close to 100% is achieved over the wall. However, at the

exit cross section the NO concentration in not uniform distributed but in the middle of the channel –far from the walls− higher concentration is detected, as expected according to the fact that the catalytic reaction is occurring over the washcoated channel walls. Finally, Figure 4 shows the evolution of the ammonia surface coverage after 50 and 450 seconds of NH_3-SCR reaction. It can be observed that adsorption sites are not saturated of NH_3 even when the steady state has been reached, since adsorbed species are being oxidized as well as used for the NO reduction.

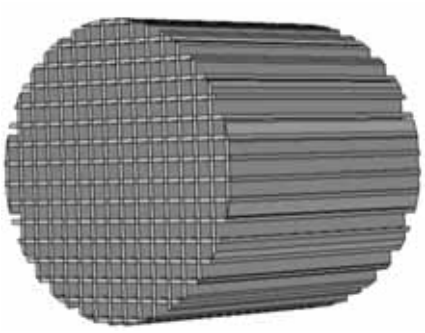

Figure 1. *Cordierite monolith (2 cm in length and diameter).*

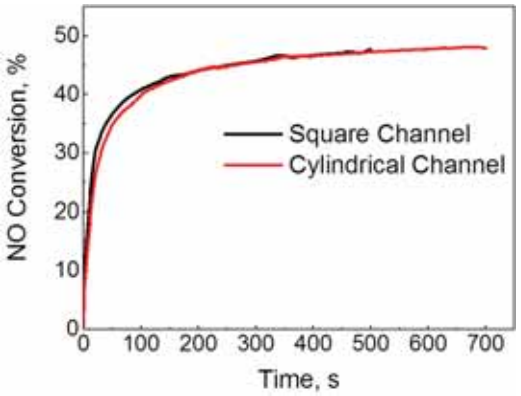

Figure 2. *NO conversion evolution with time at the exit, for cylindrical and square geometry channels.*

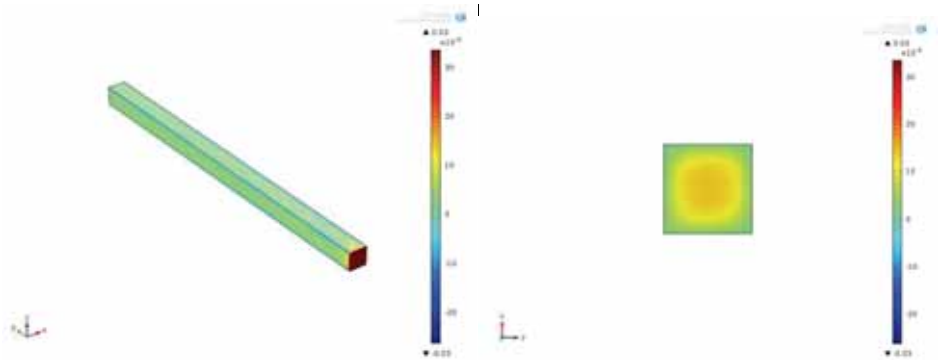

Figure 3. *NO concentration profile along the channel (left) and at the cross section at the end of the channel (right), after 500 s of NH_3-SCR reaction.*

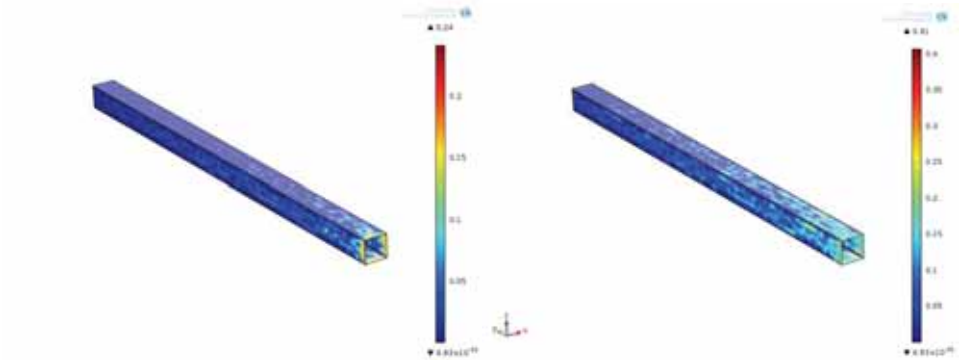

Figure 4. *Catalyst surface coverage with ammonia along the channel walls, after 50 s (left) and 450 s (right) of NH_3-SCR reaction.*

References

1. J.R. González-Velasco, M.A. Gutiérrez-Ortiz, J.L. Marc, M.P. González-Marcos, G. Blanchard, Selectivity of high surface area $Ce_{0.68}Zr_{0.32}O_2$ for the new generation of TWC under environments with different redox character, *Appl. Catal. B: Environmental*, **33**, 333–314 (2001).

2. B. Pereda-Ayo, U. De La Torre, M. Romero-Sáez, A. Aranzabal, J.A. González-Marcos, J.R. González-Velasco, Influence of the washcoat characteristics on NH_3-SCR behavior of Cu-zeolite monoliths, *Catal. Today*, **216**, 82-89 (2013).

Assessment of the Validity Range of the Standard Linear Perturbation Models of Electrophoresis with High Electric Field Calculations

E. Ruiz-Reina*[1] and F. Carrique[2]

[1]Department of Applied Physics II, University of Málaga, Málaga, Spain,
[2]Department of Applied Physics I, University of Málaga, Málaga, Spain
*Presenting and corresponding author: eruizr@uma.es

Abstract

Very recently, the synthesis and experimental study of a new class of highly charged polymer particles has been described, which spontaneously charge in non-aqueous low-polarity solvents [1,2]. These suspensions are an example of what is known as salt-free systems. The study of suspensions of charged colloidal particles in a salt-free medium is nowadays increasing [3]. The term salt-free does not mean that there are not ions present in the suspension because those ions coming from the charging process of the colloidal particles, which are known as "added counterions", will always dissolve into the supporting medium. This fact implies that the electric double layers that surround the colloidal particles in non-aqueous suspensions are constituted by one single ionic species.

For those systems, there is a non-linear singular relationship between the surface potential and the surface charge density. While for low surface charge density this relation is roughly linear, above a critical value of the surface charge density, the surface potential in-creases very slowly. This phenomenon is related to the counterion condensation effect, i.e., the generation of a compact layer of counterions that develops very close to the particles surface, and can considerably affect the macroscopical physical behavior, such as the electrokinetics, the rheology, etc., of these suspensions. Striking non-linear effects in the presence of high electric fields, as the unbinding of counterions from the condensation regions, have been observed in electrophoresis experiments [1,2].

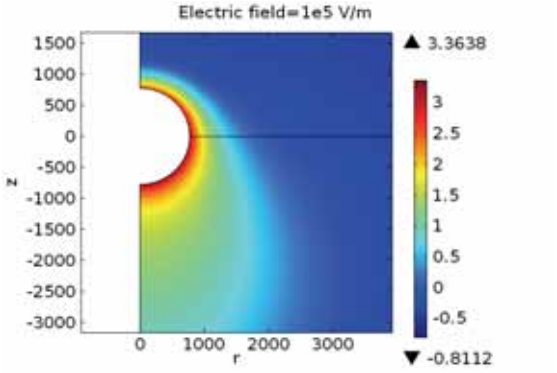

Figure 1 *Stationary ionic distribution for a electric field of 10^5 V/m.*

In this work we have performed some initial calculations with the finite element method using COMSOL Multiphysics for solving the full time-dependent non-linear governing equations inside a unit Wigner-Seitz cell. In the theoretical study of the electrophoretic mobility against the applied electric field, we have successfully reproduced the numerical results of the standard linear perturbation model in the limit of low applied electric fields and test its range of validity. From this starting point we have explored the electrophoretic behavior as the electric field is increased.

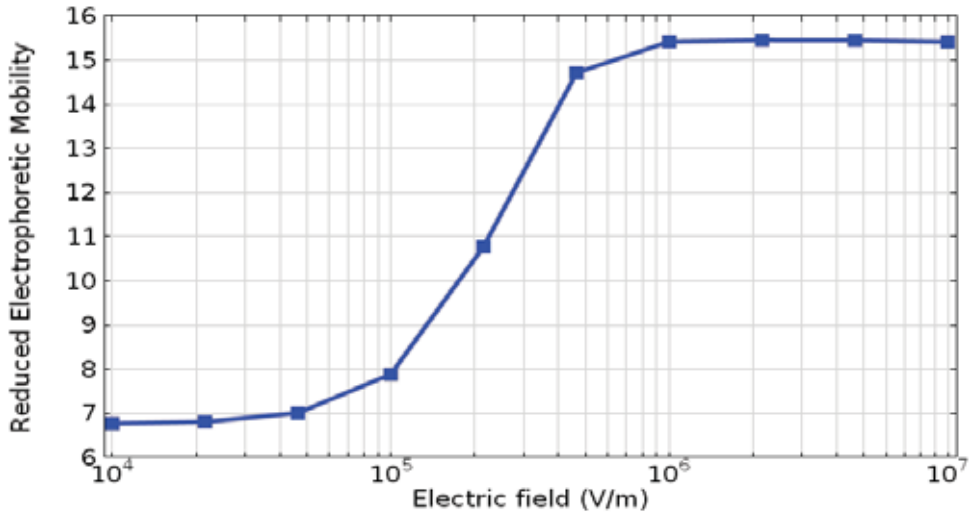

Figure 2 *Stationary reduced electrophoretic mobility as a function of applied electric fields. The electric field is applied at time t = 0 s over the equilibrium electric double layer.*

References

1. D. A. J. Gillespie, J. E. Hallett, O. Elujoba, A. F. C. Hamzah, R. M. Richardson, P. Bartlett, Counterion condensation on spheres in the salt-free limit, *Soft Matter*, **10**, 566 (2014).
2. G. Hussain, A. Robinson, P. Bartlett, Charge Generation in Low-Polarity Solvents: Poly(ionic liquid)-Functionalized Particles, *Langmuir*, **29**, 4204 (2013).
3. F. Carrique, E. Ruiz-Reina, F. J. Arroyo, M. L. Jiménez, A. V. Delgado, Dynamic electrophoretic mobility of spherical colloidal particles in salt-free concentrated suspensions, *Langmuir*, **24**, 2395 (2008).

Abstracts poster presentations

Ethanol Steam Reforming for Hydrogen Generation

S. Rosell[*1], R. Torres[1], J. Grau[1], J. López[2]

[1]Fluid Mechanics Dpt (EUETIB - Universitat Politècnica de Catalunya)
[2]Physics and Nuclear Engineering Dpt (EUETIB – Universitat Politècnica de Catalunya)
*Sergi Rosell: Universitat Politècnica de Catalunya, Compte Urgell 187, 08036 Barcelona, Spain.Tel.: +34 93 413 74 00; Fax: +34 93 413 74 01, srosellbochaca@gmail.com.

Abstract

It has been carried out a three dimensional computational fluid dynamics simulation study of ethanol steam reforming (ESR) in microreactors. Has been established and implemented in the codes a kinetic model describing the ESR on a Rh-Pd/CeO_2 catalyst. The model includes the ethanol decomposition into hydrogen, methane and carbon monoxide, the water gas shift (WGS) reaction, the reforming, in presence of water, of the methane (MSR) produced to carbon monoxide or carbon dioxide. To these ends, a 20mm tube filled with square channels of 0.9mm of characteristic size has been used (Figure 1).

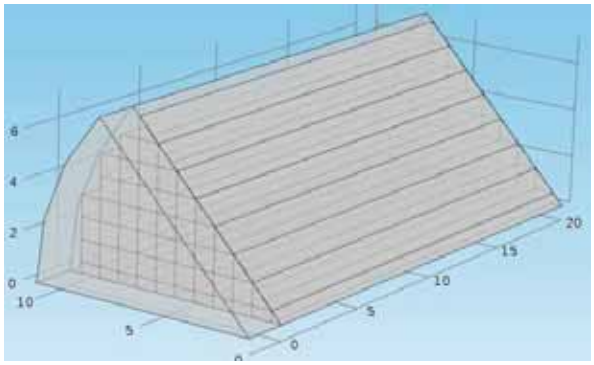

Figure 1. *Geometry of the microreactor.*

For solving the problem three different COMSOL modules has been used. First of all, the Creeping Flow (CF) is used to solve the fluid flow, NS equations, through the device. Second of all, the Heat Transfer in Fluids module has been chosen to calculate heat and temperature variations on the fluid, since there are exothermic, endothermic reactions and an exterior heat source. Third of all, to simulate the transport of species the Transport of Concentrated Species has been elected, choosing a Fick's Law to simulate the diffusion phenomena.

Finally, the rate expressions have been introduced as variables, as well as the enthalpy of reaction as a function of the temperature, in addition to the diffusion coefficients using the Chapman-Enskog approximation.

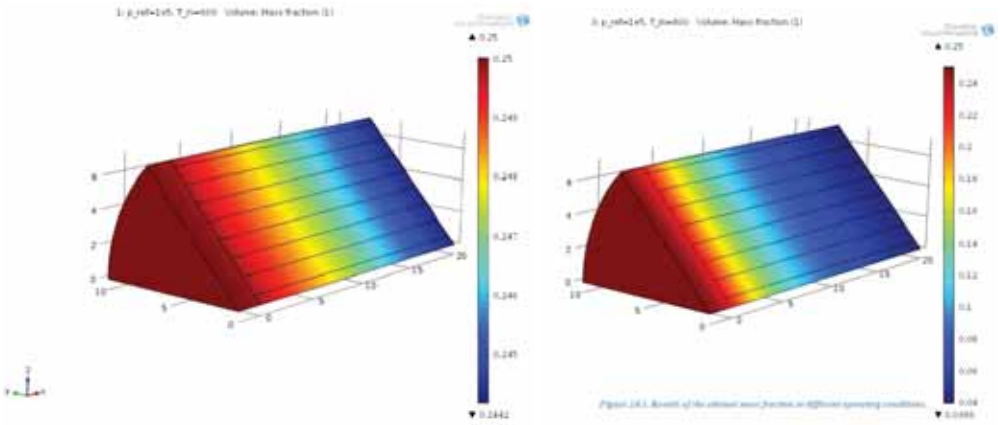

Figures 2 and 3. *Results of the ethanol mass fraction at different operating conditions.*

As of yet, a parametric study has been ran, varying the temperature from 600 to 800°C, the pressure from 1 to 6 bars, and some discrete values of the average inlet velocity that guarantee a Re below 5. All results have not been analyzed yet, but the small part analyzed accomplish with the expectative. A clear dependence on the temperature can be seen (figures 2 and 3) in the decomposition of ethanol at same pressure and velocity.

It also has been found that the variation between the inlet and outlet temperatures do not almost vary when the pressure increases. As said, the data obtained need further manipulation in order to see properly what has been obtained. It is expected that some of the multiple simulations results will achieve operating conditions that guarantees more than 95% of ethanol decomposition, as well as a high hydrogen yield, quotient between H_2 outlet molar flow rate and the ethanol inlet molar flow rate.

References

1. E. López, J. Llorca, N. J. Divins, A. Anzola, S. Schbib, D. Borio, Ethanol steam reforming forhydrogen generation over structured analaysis, *International Journal of Hydrogen Energy*, **38**, 4418-4428 (2013).
2. Elshishini S, Elnashaie S, *Modeling, simulation and optimization of industrial fixed bedcatalytic reactors*, 50-77. Gordon and Breach Science, London (1993).
3. I. Uriz, G. Arzamendi, E. López, J. Llorca, L.M. Gandía, Computational fluid dynamicssimulation of ethanol steam reforming in catalytic wall microchannels, *Chemical Engineering Journal*, **167**, 603-609 (2011).
4. A. Casanovas, M. Domínguez, C. Ledesma, E. López, J. Llorca, Catalytic walls and micro-devices for generating hydrogen by low temperature steam reforming of ethanol, *Catalysis Today*, **143**, 32-37 (2009).

Generalized Plane Strain Problem: Application to Heterostructure Nanowires

H. T. Mengistu[1*] and A. García-Cristóbal[1]

[1]Institut de Ciencia dels Materials, Universitat de Valencia,46980 Paterna (Valencia), Spain
[*]E-mail: heruy.mengistu@uv.es

Abstract

The possibility to dispose of two-dimensional (2D) approaches to problems originally posed in a three-dimensional (3D) geometry is always desirable since it reduces significantly the computing resources needed for the numerical studies. In this work we report on a new 2D approach suitable for the study of elasticity problems under general conditions and apply it to the calculation of the strain fields in heterostructure (core-shell) nanowires. Under this sole hypothesis, the original 3D problem can be very well approximated by a so-called 2D Generalized Plane strain (GPS) problem [1]. The GPS approach is able to accommodate any cross section geometry, symmetry and a wide range of compatible boundary conditions. Therefore, the GPS approach is well suited to treat elasticity problems in core-shell nanowires of any material type under different kinds of externally applied constraints or stresses (such as hydrostatic pressure, bending moments...).

The numerical calculations are performed on a discretized form of the GPS problem in the framework of continuum mechanics by using COMSOL Multiphysics. We consider a nanowire with periodic boundary conditions along the axial direction of the nanowires to have the effect of infinite length. As a result all the cross-sections of the core-shell nanowire along the axial direction will be at identical conditions, and hence all the strain components depend only on in-plane coordinates x_1 and x_2 [2].

References

1. Tungyang Chen and Donsen Lai , *Proc. Soc. Lond A*. 453, 2689-2713 (1997)
2. Chyanbin Hwu, ,Anisotropic Elastic Plates, *Springer*, pp. 29-52 (2010)

Equivalent Resistance Factor for Vapor Diffusion in Building Materials and Components

J.A. Millán[*1], J.M. Hidalgo[2], J.M. Sala[1], I. Gomez[1].

[1]UPV/EHU University of the Basque Country.
[2]Laboratory for the Quality Control in Buildings. Basque Government.
* Pza. de Europa, 20018 San Sebastian, Spain, j.millan@ehu.es

Abstract

The action of moisture on construction materials affects the thermal insulation of the building, the healthiness of its spaces and the durability of its enclosures; in short, it affects the comfort within the walls that make up the internal volume of the building.

While it is customary to know the thermal properties of most construction materials, less research has been conducted on the characterization of their hygroscope properties and their performance against moisture.

The objective of the simulation is to obtain the vapor transmission properties of the whole block geometry, to obtain a value for the equivalent permeability and the resistance factor to vapor diffusion of the geometry of the blocks.

Introduction.- In experiments, a material's vapor permeability is determined using a diffusion test; however, the resulting properties can only be considered representative if the construction product is homogenous and does not contain other elements in its finish.

However, in more complex cases is very difficult to obtain accurate and reliable measures of the vapor flow in experiments, as the vapor permeability of big blocks it, therefore the first step would be to calculate this through simulation.

Figure 1. *Termoarcilla Block*

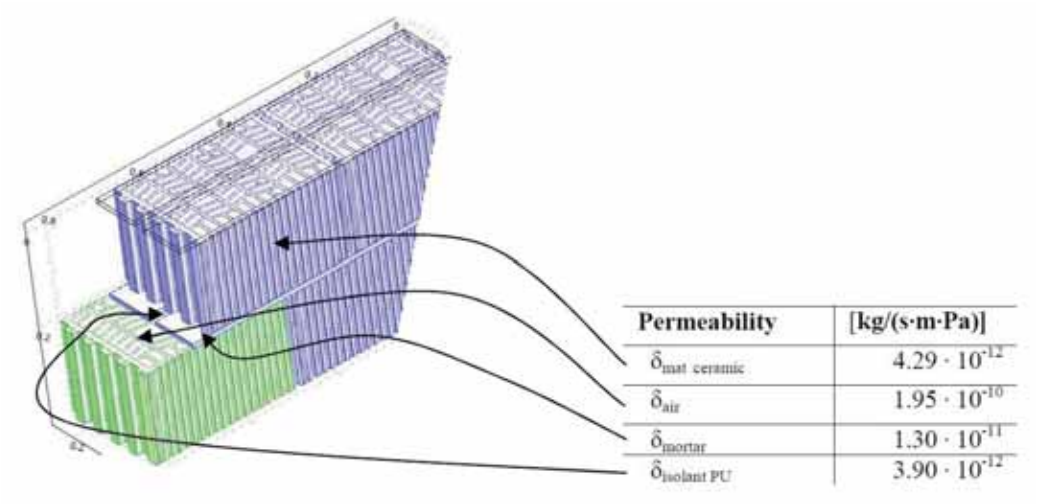

Figure 2. *Spatial representation of discontinuous joint model*

For practical purposes, it is necessary to know the average properties of the construction system in which these blocks are used and define equivalent ones for simulation. (Figures 1 and 2).

Use of COMSOL Multiphysics.- The finite element method was used to evaluate coupled 2D and 3D thermal and vapor transport by means of COMSOL v.4.3b. Modules have been combined heat transfer and diffusion of dilute species.

Heat transfer, according to Fourier's Law is:

$$q = -\lambda \nabla T$$

A general form of the moisture transfer (g) using partial vapor pressure as the potential:

$$g = g_v + g_\ell$$

$$g_v = -\delta_p \cdot \nabla p$$

$$g_\ell = -D_w \cdot (\xi / p_{sat}) \cdot \nabla p$$

Results.- The results of simulation using COMSOL numerical integration of a surface for different types of joints are shown in Table 1.

Block 24. Model TM-EF.		TYPE A	TYPE B	TYPE C	TYPE D
	RH (%)				
Equivalent resistance factor of wall $\mu_{eq} = \frac{h_1+h_2+h_3}{\frac{h_1}{\mu_1}+\frac{h_2}{\mu_2}+\frac{h_3}{\mu_3}}$	27	18.80	18.55	18.30	18.74
	64	15.47	15.26	15.04	15.39
	80	19.50	19.21	19.06	19.46

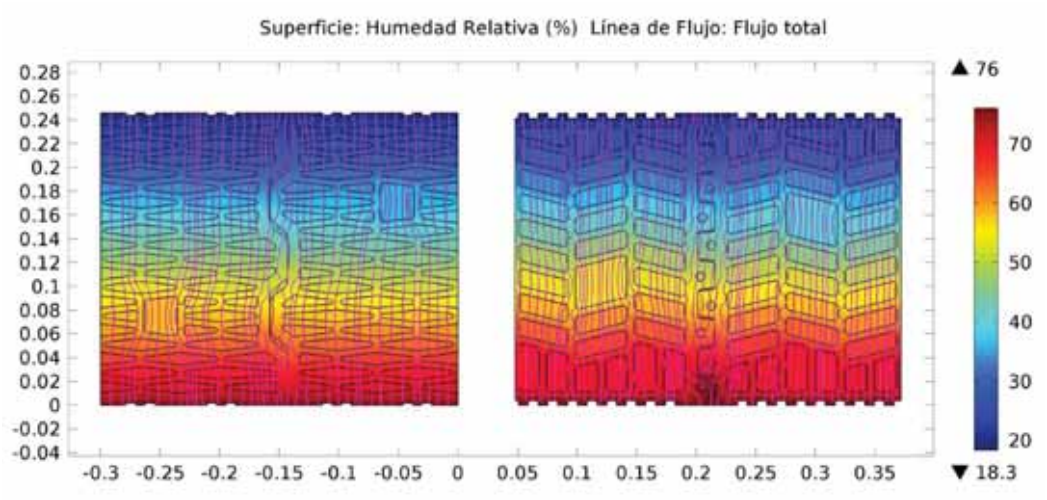

Figure 3. *Comparison between two different blocks.*

Conclusion.- The findings showed that the resistance factor of the block to vapor diffusion is not a constant value, since it depends on the average relative humidity to which the block is exposed.

The maximum value obtained for meq corresponds to the maximum relative humidity of the test. The Termoarcilla blocks, have a higher resistance to water vapor diffusion than the value assigned to them in the databases.

References

1. W. M. van Schijndel, Multiphysics Modeling of Building Physical Constructions. *Building Simulation: International Journal*, 4(1), 49-60 (2011).
2. I. Gomez, Characterization of Moisture Transport Properties for Lightened Clay Brick, *Journal of Building Physics* 31, 179-194 (2007).

A Computer Modeling Study of the Influence of Blood Blow inside a Large Vessel as a Thermal Protection Mechanism from Thermal Damage to its Wall during RF-assisted Resection

A. González-Suárez*[1], M.Trujillo[1], F. Burdío[2], A. Andaluz[3] and E. Berjano[1]

[1]Universitat Politècnica de València, [2]Hospital del Mar, [3]Universitat Autònoma de Barcelona
*Presenting and corresponding author: Camino de Vera s/n 46022, angonsua@eln.upv.es

Abstract

Introduction.- Medical devices based on radiofrequency (RF) energy are usually employed during surgical resection to thermally coagulate medium and small vessels and consequently minimize intraoperative blood loss [1]. Unfortunately, there is a potential risk of vessel wall damage when the RF device is used in the proximity of large vessels. In this case, some surgeons prefer to substitute RF-based dissectors for ultrasonic dissectors when removing tissue around these large vessels, since these dissectors have a low penetration depth and minimal lateral energy spread [2]. The aim of this study was to assess whether the heat sink effect inside a large vessel (portal vein) could protect the vessel wall from thermal damage close to an internally cooled electrode during RF-assisted resection. We considered the 8 mm diameter Coolinside device (Apeiron Medical, Valencia, Spain), which is designed to coagulate and dissect hepatic parenchyma by a laparotomy approach [3].

Use of COMSOL Multiphysics.- Three-dimensional model based on a coupled electric-thermal problem, was solved numerically using the Finite Element Method (FEM) with COMSOL Multiphysics software (COMSOL, Burlington, MA, USA). The model is composed by a partially isolated metallic electrode in total contact with a fragment of hepatic tissue and at a distance (D) below a large vessel (Figure 1).

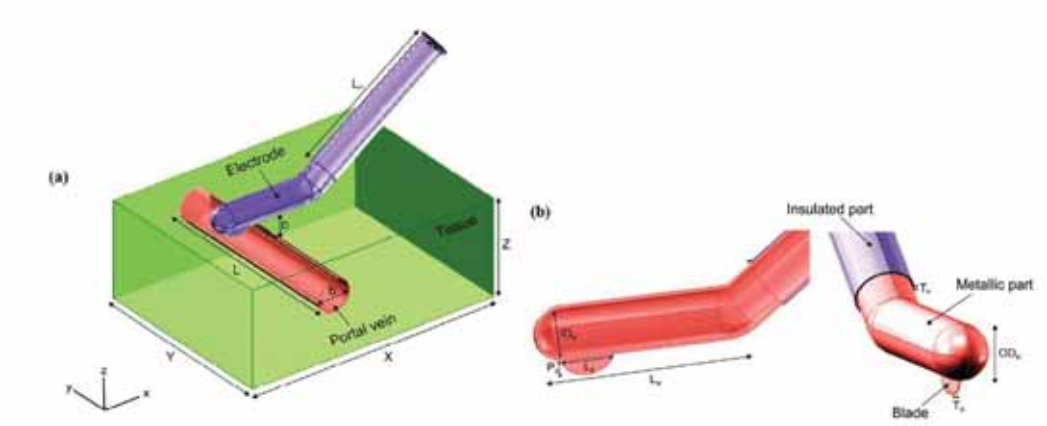

Figure 1 *(a) Geometry and dimensions of the three-dimensional model built for the study. Tissue dimensions X, Y and Z (Z = Y/2) were obtained from a convergence test. The portal vein, with a diameter b and a length L, is located perpendicular to and at distance D below the electrode. LP:*

length of the insulated section of the electrode. (b) Internal and external view and dimensions of the RF-assisted device. LM: length of the metallic part in contact with the tissue; ODM and IDM: outer and inner diameter; PB: insertion depth of the blade; LB: blade length; TB: blade thickness; TP: thickness of the insulated section.

We studied the effect of different factors such as device-tissue contact, vessel position and vessel-device distance on temperature distributions and thermal lesion shapes near a large vessel, specifically the portal vein. The geometry of the thermal lesion around the portal vein after RF heating was obtained for each case by solving the Arrhenius equation and considering the thermal damage contour $\Omega = 1$ (63% probability of cell death).

Results.- The thermal lesion shape created around the portal vein was significantly modified by the heat sink effect in all the cases considered (Figure 2).

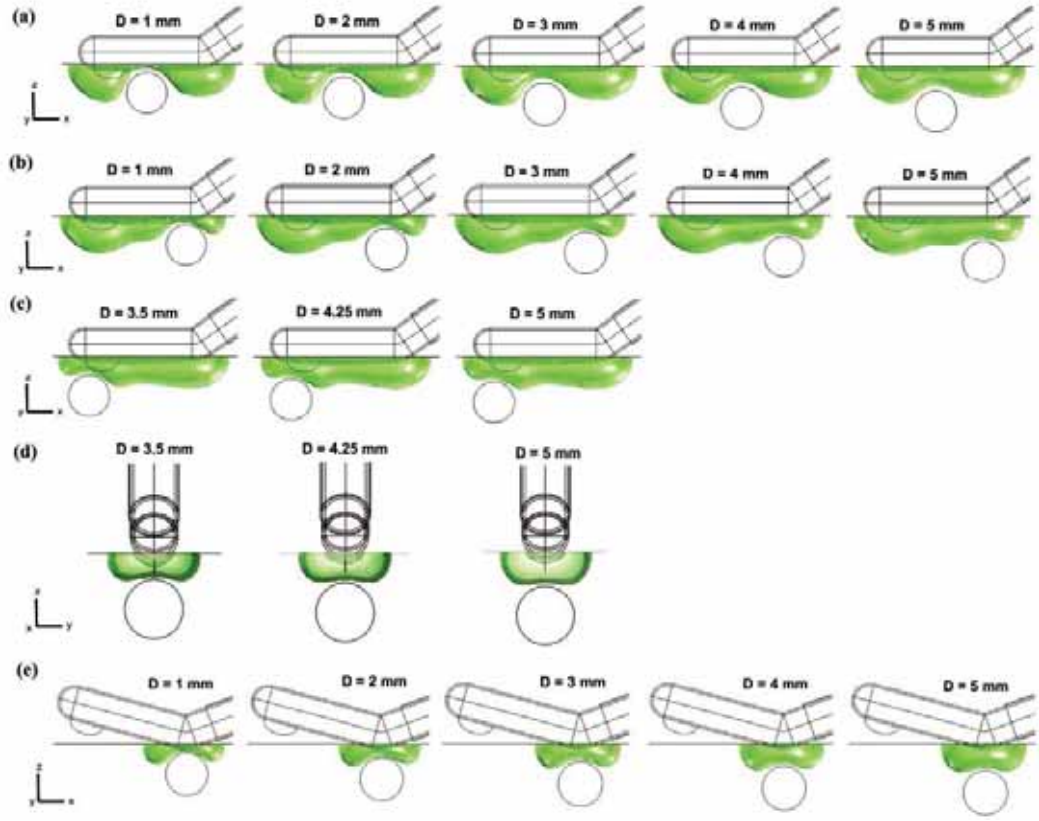

Figure 2 *Thermal lesions created around the portal vein after 45 s of RF heating for different vessel device distances (D), device-tissue contact conditions, and relative position of the vessel. Cases: total vessel-device contact and vessel perpendicular below the center of the device (a), below its proximal end (b) and below its distal end (c), vessel parallel to the device (d), and only proximal vessel-device contact and vessel perpendicular to the device (e). The thermal damage surface corresponds to* $\Omega = 1$.

Thermal damage to the portal vein wall was inversely related to the vessel-device distance. It was also more pronounced when the device-tissue contact surface was reduced or when the vessel was parallel to the device or perpendicular to its distal end (blade zone), the vessel wall being damaged at distances less than 4.25 mm (Figure 3).

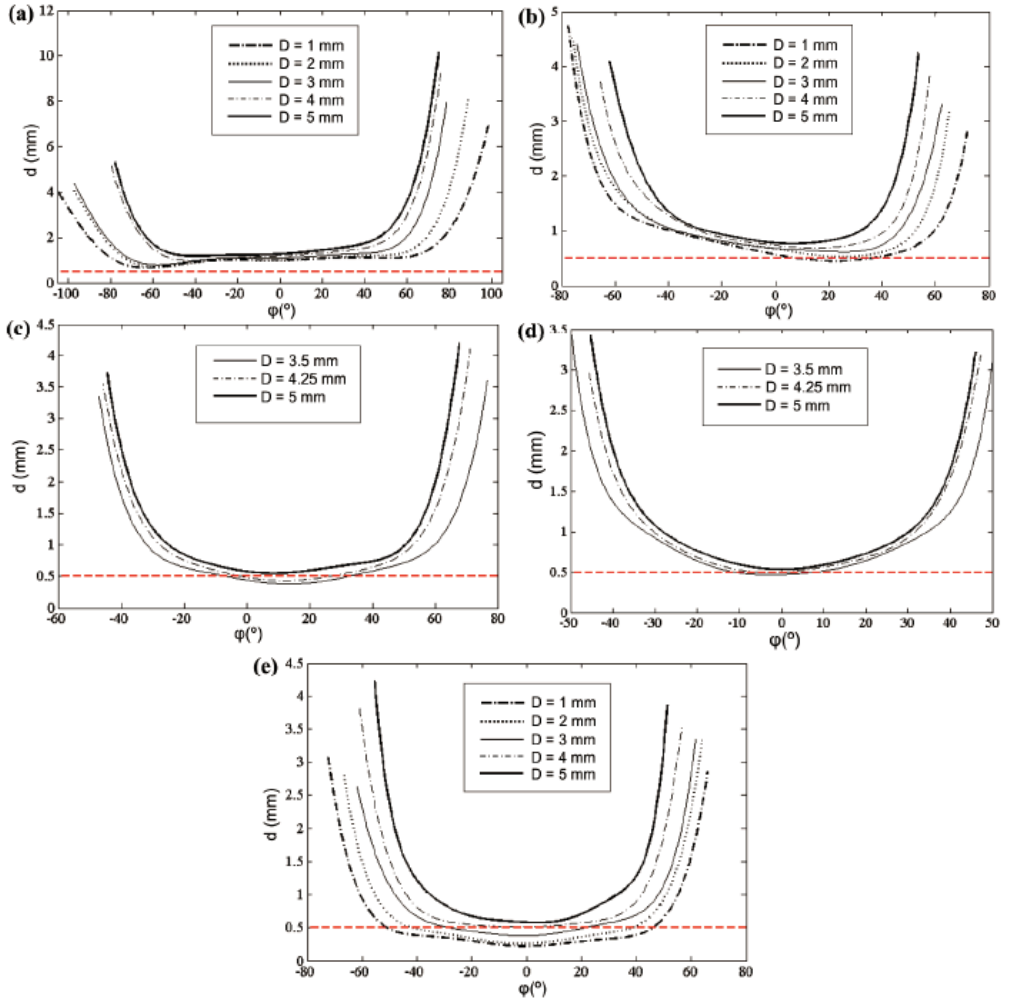

Figure 3 *Distances obtained between the portal vein and the thermal lesion in order to assess thermal damage in the vessel wall for different vessel-device distances (D), device-tissue contact conditions, and relative position of the vessel. Cases (see Fig. 2 for more details): total vessel device contact and vessel perpendicular below the center of the device* ***(a)****, below its proximal end* ***(b)*** *and below its distal end* ***(c)****, vessel parallel to the device* ***(d)****, and only proximal vessel device contact and vessel perpendicular to the device* ***(e)****. The horizontal dashed line represents the vessel wall thickness (0.5 mm).*

Conclusion.- Our computational findings suggest that the heat sink effect could protect the portal vein wall for distances equal to or greater than 5 mm, regardless of its position and distance with respect to the RF-based device. We think that our findings might be useful for surgeons involving in RF-assisted surgical resection, since knowing the conditions under which the heat sink effect inside the vessel thermally protects its wall could be help them in making a preliminary assessment of vascular damage in their treatment plans.

References

1. Poon RT, Fan ST, Wong J, Liver resection using a saline-linked radiofrequency dissecting sealer for transection of the liver, *J Am Coll Surg*, **200**(2), 308-313 (2005).
2. Sutton PA, Awad S, Perkins AC et al, Comparison of lateral thermal spread using monopolar and bipolar diathermy, the Harmonic Scalpel and the Ligasure, *Br J Surg*, **97**(3), 428-433 (2010).
3. Burdío F, Grande L, Berjano E et al, A new single-instrument technique for parenchyma division and hemostasis in liver resection: a clinical feasibility study, *Am J Sur*, **200**(6):e75-80 (2010).

Papers

Modeling of avalanches and streamers in gaseous detectors with COMSOL

P. Fonte[1,*]

LIP - Laboratory of Instrumentation and Experimental Particle Physics, Coimbra, Portugal
*Corresponding author: LIP, Dep. de Física da Univ. de Coimbra, 3004-516 Coimbra, Portugal, fonte@coimbra.lip.pt

Abstract: Gaseous detectors are widely used in Nuclear Physics experiments for identifying elementary particles. These detectors achieve the amplification of the primary ionization by means of Townsend avalanches, which sometimes evolve to undesirable streamers. In this note we will describe the modeling of these gaseous discharges by COMSOL Multiphysics.

Keywords: Gaseous detector, avalanche, streamer.

1. Introduction

The science and technology of gaseous particle detectors has been extensively reviewed (e.g. [1-4] and references therein) and in this note we will not elaborate on the subject.

A fundamental limitation on the working conditions of these detectors is that there is a maximum value of electric charge in each avalanche, which, if exceeded, will cause the occurrence of a streamer discharge and subsequent spark [4]. Therefore it is important to model the avalanche streamer transition, trying to better understand its features.

2. Physical model

An important approach to the modeling of avalanches and streamers treats the distribution of charges, electrons and ions, as fluids governed by hydrodynamic like equations [5]. The forces on such fluids are determined by electrostatic considerations, to be solved simultaneously.

An important effect to be included is the emission of light by the avalanche, which may cause secondary avalanches in the gas itself (gas self-photoionization) and in the surrounding solid surfaces. This effect may be modeled approximately as a diffusion-like process [6] acting on a photon flow distribution.

Altogether, the equations to be simultaneously solved are listed in Table 1. Eqs. a) to d) are the differential equations to be solved while eqs. e) to i) are functional relations. Eq. a) is Poisson's equation applied to the charge densities in presence. Eq. b) describes the drift, diffusion and multiplication of electrons, described by the source term *S*, which has several components, g) to i), corresponding to different physical sources of ionization (producing electron-ion pairs). Eq. c) just states that for each electron created a corresponding ion is also created. Eq. d)

approximates the description of the flow of photons by a Helmholtz equation [6].

$$
\begin{cases}
-\vec{\nabla}^2 V = \dfrac{q_p}{\varepsilon_0}(n_{i+} - n_e) & a) \\
\dfrac{\partial n_e}{\partial t} + \vec{\nabla}\cdot(\vec{W}_e n_e) = S + D_e \nabla^2 n_e & b) \\
\dfrac{\partial n_{i+}}{\partial t} = S & c) \\
-\dfrac{1}{3\mu}\vec{\nabla}^2 \Psi_0 + \mu \Psi_0 = \delta S_e & d) \\
\vec{E} = -\vec{\nabla} V + \vec{E}_0 & e) \\
S = S_e + S_{gas} + S_{surface} & f) \\
S_e = \alpha \left|\vec{W}_e\right| n_e & g) \\
S_{gas} = QE_{gas} \mu \Psi_0(\vec{r},t) & h) \\
S_{surface} = QE_{surface}\, \Psi_0(\vec{r},t) & i)
\end{cases}
$$

$n_{e,i+}(\vec{r},t)$ = numerical density of electrons and ions in space and time
$\Psi_0(\vec{r},t)$ = photon flux
V = electric potential arising from space-charge
$\vec{E}(\vec{r},t)$ = electric field
$\vec{E}_0(\vec{r})$ = applied electric field
$\vec{W}_e(\vec{E})$ = electron velocity
$\alpha(|\vec{E}|)$ = first Townsend coefficient
$D_e(|\vec{E}|)$ = electron's diffusion coefficient
δ = photon yield per ionization
QE_{gas} = quantum efficiency of the gas to its own radiation
$QE_{surface}$ = quantum efficiency of the surfaces to the gas radiation
μ = photon's absorption coefficient
S = total source term for electron-ion pairs
S_e = pair production by impact ionization
S_{gas} = gas self-photoionization
$S_{surface}$ = electron extraction from surfaces
q_p = elementary electrical charge

Table 1: *Mathematical model of the drift, multiplication and diffusion of electrons, ions and photons under an applied electrostatic electric field.*

The photonic parameters are supposed to be effective values averaged over all wavelengths, a matter that is far from being trivial. The remaining physical parameters are reasonably known from reference data.

3. Numerical solution

In terms of COMSOL Multiphysics 4.1, Eq. a) is modeled as "Electrostatics", Eqs b) and c) as "Transport of diluted species" (therefore the units of $n_{e,i+}$ will be mol/m^3) and eq. d) as "Coefficient form PDE".

The example presented in this note corresponds to a detector called Gaseous Electron Multiplier (GEM - see [4]), which consists on a fine array of holes through a thin double sided printed circuit board. Only one such hole will be modeled, on an axisymmetric geometry.

4. Results

Figures 1 to 7 represent the electron and ion densities during the process of amplification of an initial charge cluster on the GEM hole. The amount of charge generated is sufficient to distort the applied electric field, creating the conditions for the formation of a streamer discharge. The streamer eventually reaches the cathode setting the conditions for a spark.

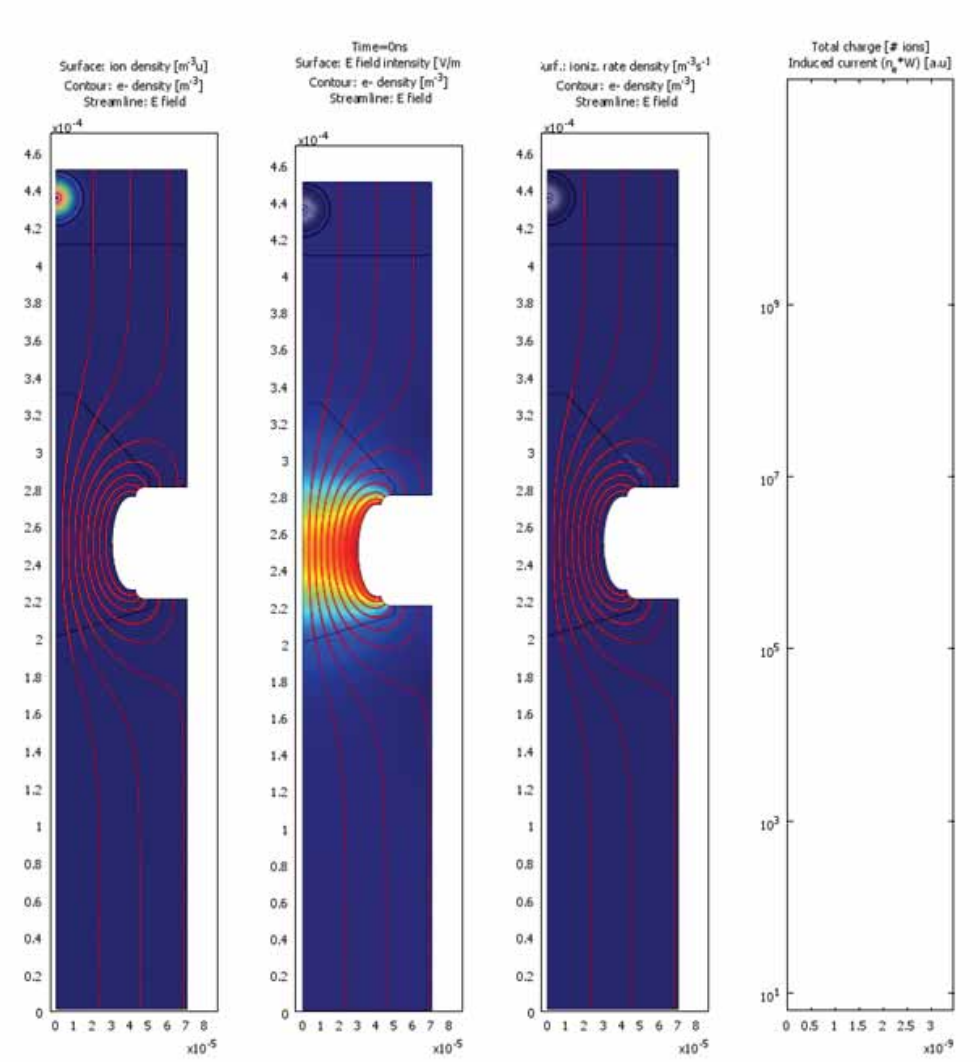

Figure 1 *Representation of the GEM hole and the initial cluster of electron-ion pairs. In the far-left pane the colorwash represents the ion density, in the center-left pane it represents the electric field strength and in the center-right pane represents the ionization rate density (*S*). In all cases the gray contours represent the electron density and the red lines the electric field streamlines. The far-right pane shows the total amount of ionic charge in the volume (red line) and the current observable externally (blue line) as a function of time.*

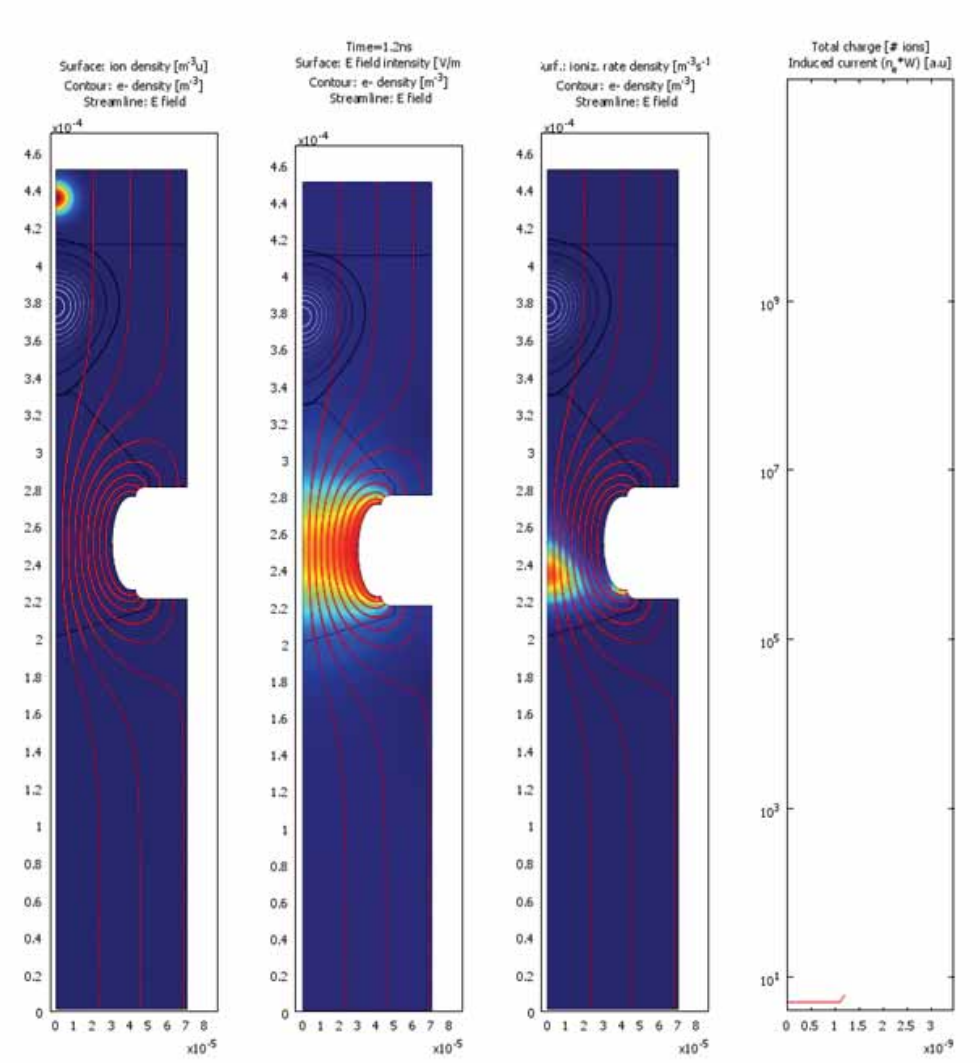

Figure 2 *After 1.2 ns the electrons drifted towards the GEM while the initial electrons remain stationary. There is no charge multiplication so far.*

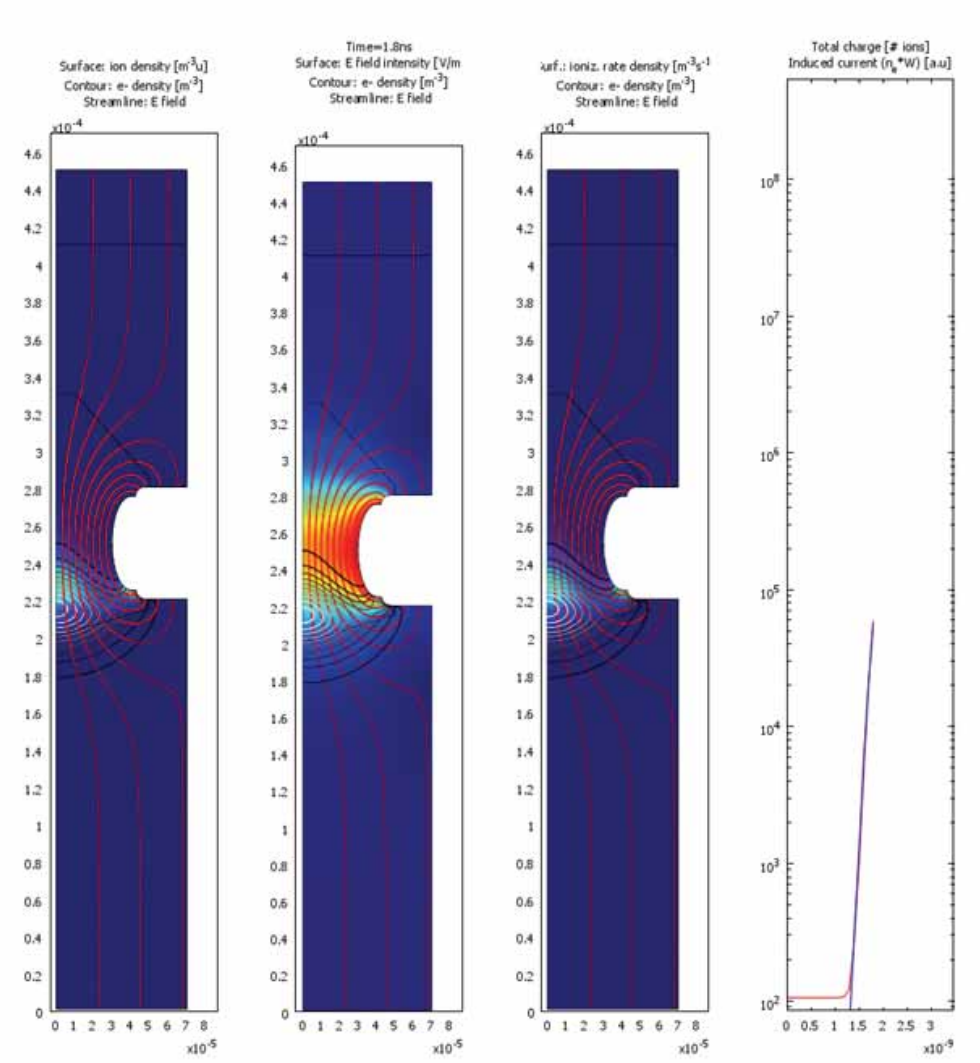

Figure 3 *After 1.8 ns the electrons reached the GEM hole and multiply there, growing exponentially in time the amount of charge and the current. The electric field remains undisturbed.*

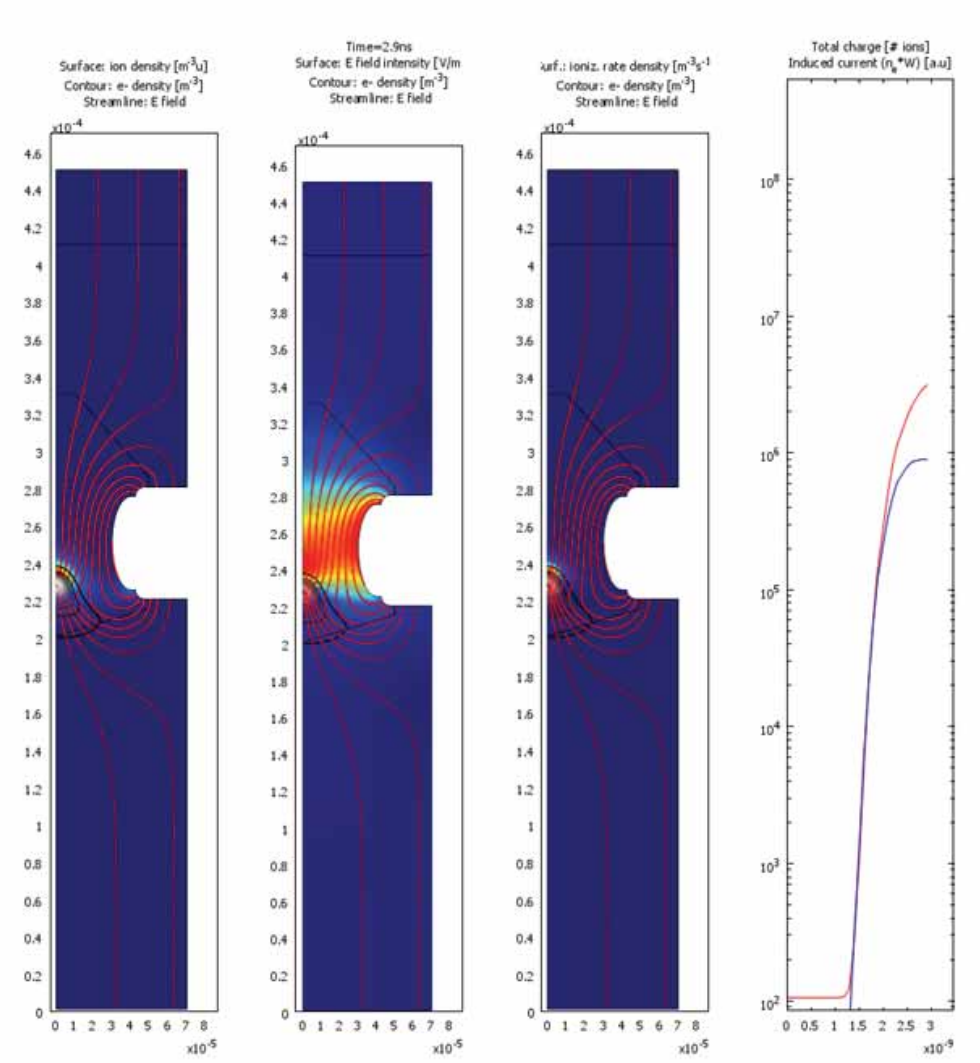

Figure 4 *After 2.9 ns the initial electron cloud has passed through the hole and the current stalls its exponential growth. However the electric field is now disturbed by the large concentration of ions close to the bottom of the hole.*

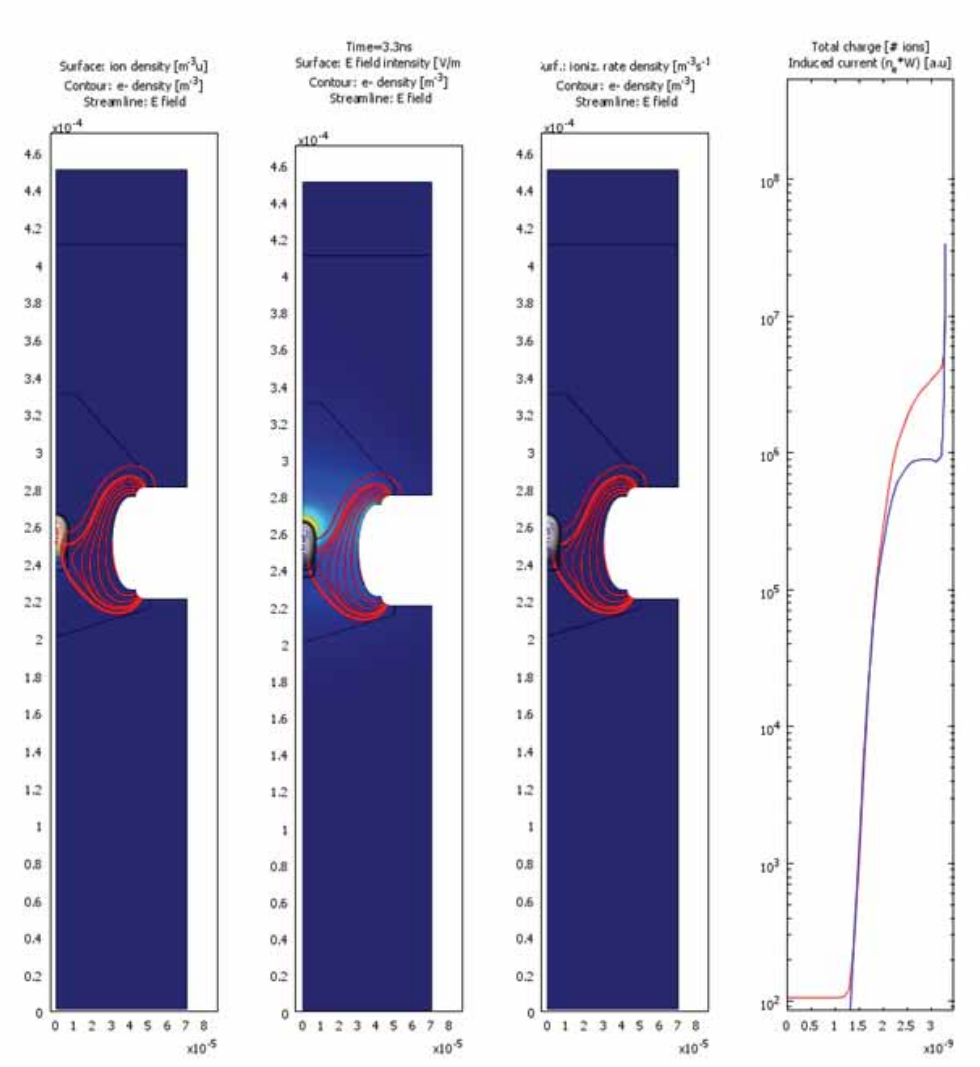

Figure 5 *After 3.3 ns the streamer has formed and now it dominates the electric field in the hole, overcoming the applied field. The streamer races up, generating a strong current surge.*

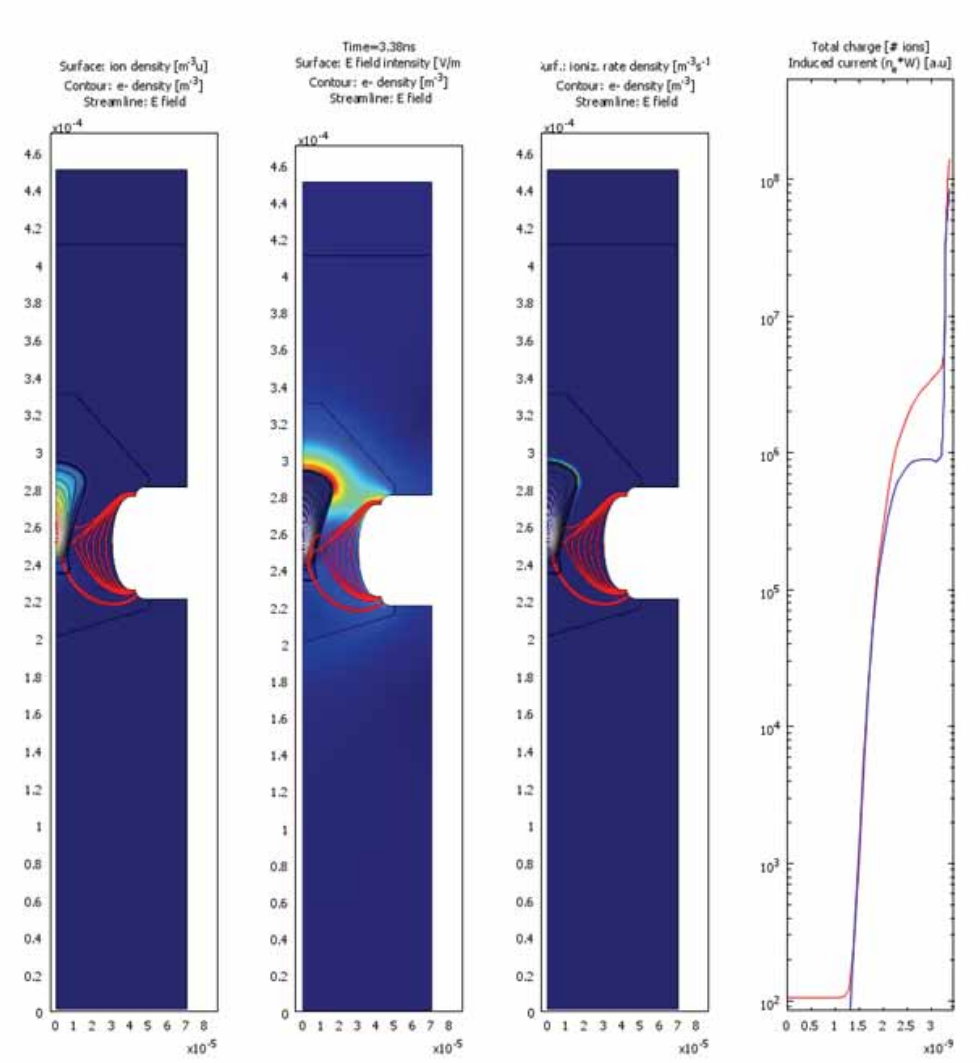

Figure 6 *After 3.38 ns the streamer reaches the top of the hole and starts to branch towards the upper positive electrode (cathode).*

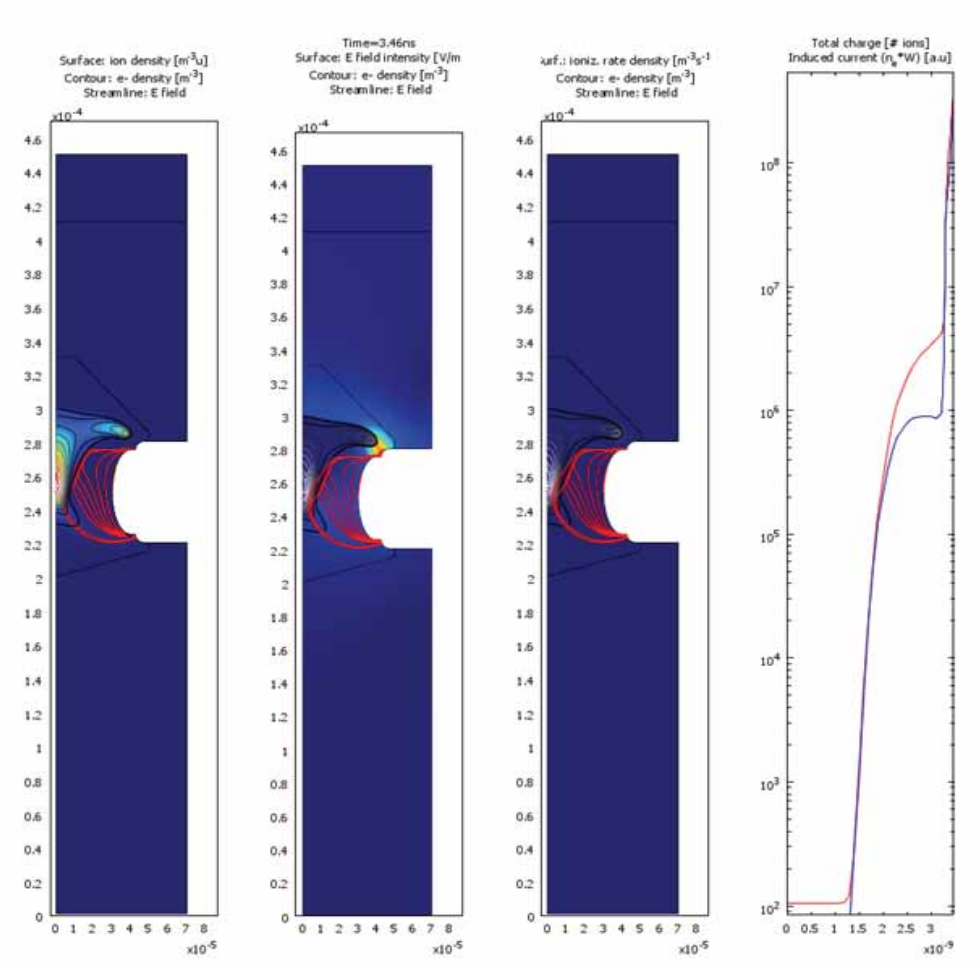

Figure 7 *After 3.46 ns the streamer reaches the cathode, leaving behind a plasma column through which the subsequent spark will flow.*

5. Conclusions

The drift, multiplication and diffusion of electrons, ions and photons under an applied electrostatic electric field in a gaseous detector (GEM) were modeled in a hydrodynamic approach. The emergent phenomenon of streamer formation was apparent and its physical nature investigated.

6. References

1. C. Grupen, *Particle Detectors*, Cambridge Monographs on Particle Physics, Cambridge University Press (1996).
2. K. Kleinknecht, *Detectors for Particle Radiation*, Cambridge University Press (1998).
3. D. Green, *The Physics of Particle Detectors*, Cambridge Monographs on

Particle Physics, Cambridge University Press (2000).
4. P. Fonte and V. Peskov, On the physics and technology of gaseous particle detectors, *Plasma Sources Sci. Technol.* **19** 034021 (2010).
5. A.J. Davies and C.J. Evans, The Theory of Ionization Growth in Gases Under Pulsed and Static Fields, *CERN 73-10* (1973).
6. J. Capeillère *et al*, The finite volume method solution of the radiative transfer equation for photon transport in non-thermal gas discharges: application to the calculation of photoionization in streamer discharges, *J. Phys. D : Appl. Phys.* **41** 234018 (2008).

7. Acknowledgement

This work was performed in the framework of the RD51 collaboration and financed by the EU, FEDER and COMPETE via the Fundação para a Ciência e Tecnologia (FCT) project CERN FP 83524/2008.

Using COMSOL Multiphysics to Describe Solid/Liquid Flows

M. G. Rasteiro*[1], F. A. P. Garcia[1], P.M. Faia[2], R. Silva[1]

[1]CIEPQPF, Department of Chemical Engineering, University of Coimbra, Coimbra, Portugal
[2]Department of Electric and Computers Engineering, University of Coimbra, Coimbra, Portugal
*Presenting and corresponding author: mgr@eq.uc.pt

Abstract: The work which is presented in this manuscript details numerical studies using the Mixture Model present in COMSOL Multiphysics® to simulate the behavior of concentrated solid-liquid suspensions conveyed in pipelines. This model was employed for neutrally buoyant and heavy particles, with varying sizes and particle concentrations. In order to be able to describe adequately these flows several modifications had to be introduced in the Mixture Model. With these modifications good agreement with experimental data was obtained. These modifications depend on the type of particles being conveyed, buoyant particles or heavy particles and, in general, on the flow regime. The Mixture Model, with some modifications to take into account the flow regime, has showed to provide good approximations to the experimental results for different flow velocities and particle concentrations when applied to the description of the flow of solid/liquid suspensions in pipes. Further studies are being conducted for the flow description of oil/water emulsions.

Keywords: Mixture Model, solid-liquid pipe flow, concentrated suspensions.

1. Summary of results for neutrally buoyant particles and heavy particles

A great number of industrial applications heavily depend on the conveying of particles in pipelines. Amongst the ever increasing number of fields where particle conveying is of great importance we can include the production of chemicals, energy, pharmaceuticals or foodstuffs, papermaking, composites and also the transportation of minerals and wastes. The hydraulic conveying of solid-liquid concentrated suspensions is such an example, where particles with different sizes and in diverse concentrations at different flow velocities exhibit complex flow regimens. The ability to correctly predict their behavior is fundamental for the adequate design of pumping equipment and flow systems and to optimize energy consumption.

The team of CIEPQPF working in this field has been dealing with both the flow of concentrated fiber suspensions and of concentrated suspensions of spherical particles.

The work which is presented in this extended abstract details numerical studies using the Mixture Model [1,2,3,4], present in COMSOL Multiphysics®, to simulate the behavior of concentrated solid-liquid suspensions conveyed in pipelines. This model was employed to neutrally buoyant [5] and

heavy particles [6] data from the literature with varying sizes and particle concentrations. Good agreement with experimental data was obtained for the buoyant particles and high concentrations of particles, using the built-in Mixture Model, which employs a Standard / High Reynolds k-ε Turbulence closure [7,8], as can be seen in the pressure drop and vertical solid distribution profiles in Figures 1 and 2.

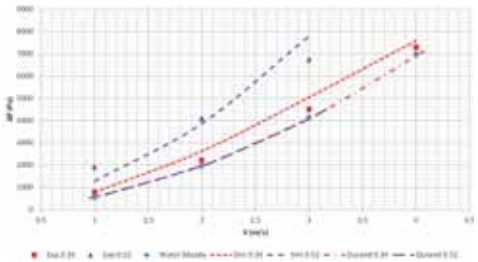

Figure 1 *Numerical and experimental pressure drops for the neutrally buoyant particles.*

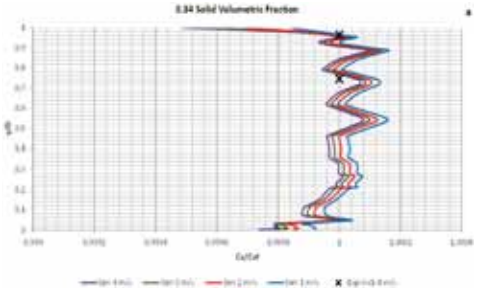

Figure 2 *Numerical and experimental vertical particle distribution profiles for the neutrally buoyant particles.*

The experimental data for the neutrally buoyant particles is well described using numerical studies with the Mixture Model, as seen in Figure 1. Also present in both Figures 1 and 2 are the results obtained with Durand's correlation for these flows.

For the heavy particles, with low particle concentrations, this Mixture Model provided results also with little deviations from experimental data. However, for higher particle concentrations of heavy particles considerable deviations occurred between the experimental and simulated data using the Mixture Model with a Standard / High Reynolds k-ε Turbulence closure. To circumvent the deviations with the previous model a Low Reynolds k-ε Turbulence closure [9,10,11] was incorporated in the Mixture Model, having in mind that the Wall Function in the previous model is an empirical correlation which was developed for single-phase or low concentration particle flow, and is probably inadequate for highly concentrated flows. The Low Reynolds k-ε Turbulence closure has the advantage of solving the equations up to the wall, and thus providing a more accurate representation of the flow characteristics in the vicinity of the wall. With this approach a good agreement was achieved for higher flow velocities and higher concentrations.

In Figure 3, for the experimental data of the heavy particles, turbulence damping for the higher flow velocity is observed. This is a very important phenomenon that the Mixture Model, incorporating a Low Reynolds turbulent closure, was able to represent quite well. Durand's correlation provides reasonable results for the less concentrated flows but fails for the more concentrated ones.

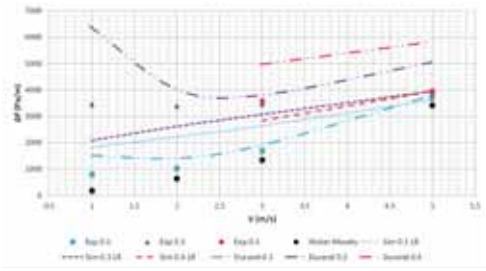

Figure 3 *Numerical and experimental pressure drops for the heavy particles.*

In Figure 4, the vertical particle distribution profiles for the highest volumetric concentration (40% (v/v)) are presented.

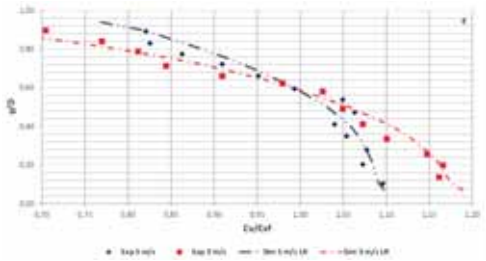

Figure 4 *Numerical and experimental concentration profiles for the heavy particles.*

For both velocities of 3 and 5 m/s the numerical profiles with the Mixture Model and Low Reynolds turbulence closure match quite well the experimental data, further validating the choice of the turbulence closure modification. Figure 5 presents the corresponding velocity profiles obtained for the pipe cross section.

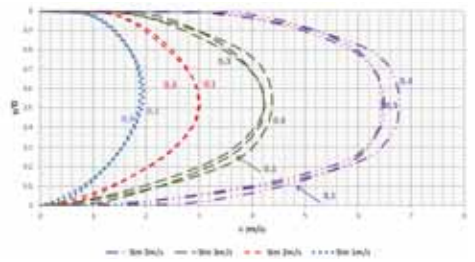

Figure 5 *Numerical velocity profiles using the Low Reynolds closure for the heavy particles.*

In Figure 6 we can as well see the corresponding 3D profiles produced by the COMSOL Multiphysics for this situation.

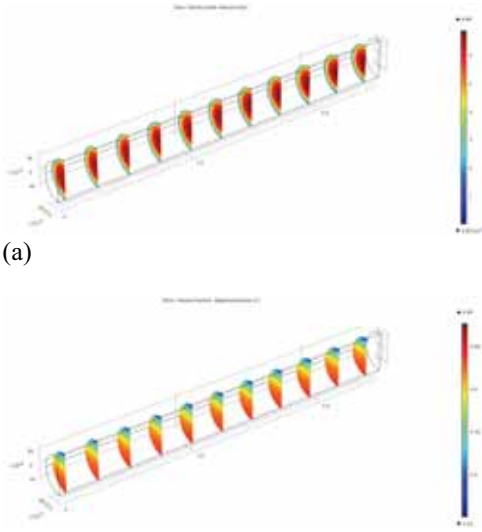

(a)

(b)

Figure 6 *Numerical 3D velocity profiles (a) and concentration profiles (b) using the Low Reynolds closure for the heavy particles.*

As expected, a slight asymmetry is noticed in the velocity profiles and a higher concentration of the particles in the bottom of the pipe can be observed.

Summing up, the Mixture Model, with some modifications to take into account the flow regime, has showed to provide good approximations to the experimental results for different flow velocities and particle concentrations, when applied to the description of the flow of solid/liquid suspensions in pipes.

2. Conclusions

The Mixture Model in COMSOL Multiphysics® presents itself as an accurate model for the study of solid-liquid flows. For neutrally buoyant particles it matches quite well the experimental data. For heavy particles, particularly for highly concentrated flows, a Low Reynolds turbulence closure is preferred.

Future work will be directed to the description of the flow of oil/water emulsions in pipes using, also, COMSOL Multiphysics®.

References

1. COMSOL CFD Module User's Guide, V.4.3.
2. M. Manninen, V. Taivassalo, On the mixture model for multiphase flow, VTT Publications, 288, ESPOO 1996.
3. Pang, M.J. and Jin Jia Wei, 2011.Analysis of drag and lift coefficient expressions of bubbly flow system for low to medium Reynolds number, Nuclear Engineering and Design, Vol. **241**, 6:2204-2213.
4. Visuri, O., G. A. Wierink, V. Alopaeus, 2012. Investigation of drag models in CFD modeling and comparison to experiments of liquid–solid fluidized systems, International Journal of Mineral Processing, **104-105**:58-70.
5. Shook, C. A. Experiments with Concentrated Slurries of Particles with Densities near that of the Carrier Fluid, Can. J. Chem. Eng., 1985, 63, 861.
6. Lahiri, S.L.; Ghanta, K.C. Slurry Flow Modelling by CFD, Chem. Ind. Chem. Eng. Q., 2010, 16, 295.
7. Ekambara K.; Joshi, J.B. Axial mixing in pipe flows: turbulent and transistion regions, Chem. Eng. Sci., 2003, **58**, 2715.
8. Selma, B.; Bannari, R; Proulx, P. A full integration of a dispersion and interface closures in the standard k-ε model of turbulence, Chem. Eng. Sci., 2010, **65**, 5417.
9. Costa, J.J.; Oliveira, L.A.; Blay, D. Test of several versions for the k-ε type turbulence modeling of internal mixed convection flows, Int. J. Heat Mass Transfer, 1999, 42, 4391.
10. Lai, J.C.S.; Yang, C. Y. Numerical simulation of turbulence suppression: Comparisons of the performance of four k-ε turbulence models, Int. J. Heat Fluid Flow, 1997, 18, 575.
11. Bardow, A.; Bischof, C.H.; Bücker, H.M.; Dietze, G.; Kneer, R.; Leefken, A.; Marquardt, W.; Renz, U.; Slusanschi, E. Sensitivity-based analysis of the k–ε model for the turbulent flow between two plates, Chem. Eng. Sci., 2008, 63, 4763.

3. Acknowledgements

This work has been financially supported by the project PTDC/EQU-EQU/66670/2006 from the Fundação para a Ciência e Tecnologia, as well as the individual PhD scholarship SFRH/BD/79247/2011 and Strategic

Research Center Project Pest-C/EQB/UI0102/2013. We acknowledge as well the invitation of the organizers of the 1st Iberian COMSOL Multiphysics Conference to be part of it.

CFD Modeling for Hydrogen Energy Technologies

E. Amores Vera[1,*]

[1] Research Department, Centro Nacional del Hidrógeno.
*Corresponding author: ernesto.amores@cnh2.es - Prol. Fernando El Santo s/n, 13500 Puertollano (C.Real)

Abstract: Hydrogen (H_2) is an ideal energy storage system for the future. In a first step, it can be produced from Renewable Energy (RE) surplus and later it can be used to produce electricity using a fuel cell. However, transition to a RE-H_2 system requires a large R&D effort to improve technologies for production, storage and use of H_2. In this sense, the development of models using CFD simulation software is key to achieving the "hydrogen economy". For example the study of an alkaline electrolysis cell powered by a PV-module or the optimization of H_2/H_2O separator are strategic models to predict and improve the behavior of these technologies.

Keywords: CFD, Hydrogen, Renewable Energy, Energy Storage System.

1. Hydrogen from Renewable Energies

The current fossil fuel-based energy system is not sustainable due to:

- Rapidly growing energy demand in the near future due to population growth.
- Negative environmental impact of fossil fuel combustion.
- Excessive economic dependence on oil producing countries.
- Exhaustion of natural resources.

For the previous reasons, a new energy model is needed. This new energy model could be based on renewable energies, such as PV solar or wind power.

However, renewable energies have a common disadvantage: the generated electricity is not continuous, because they depend on weather conditions. A PV module does not produce electricity if there is not enough solar irradiance; an wind turbine does not produce electricity if there is not enough wind.

Therefore energy storage systems are needed to store energy during periods of high production, with the aim of using this energy in periods without renewable resources.

Among the different energy storage systems available, hydrogen and fuel cells are presented as an "ideal store". A wind or photovoltaic solar system supplies power to a load (for example, a building), but when a electricity production surplus exists, it can be used to generate hydrogen in an electrolyzer. In periods without renewable resource, the stored hydrogen can be used to supply the building, through its transformation into electricity by means of a fuel cell. Figure 1 shows an operation scheme

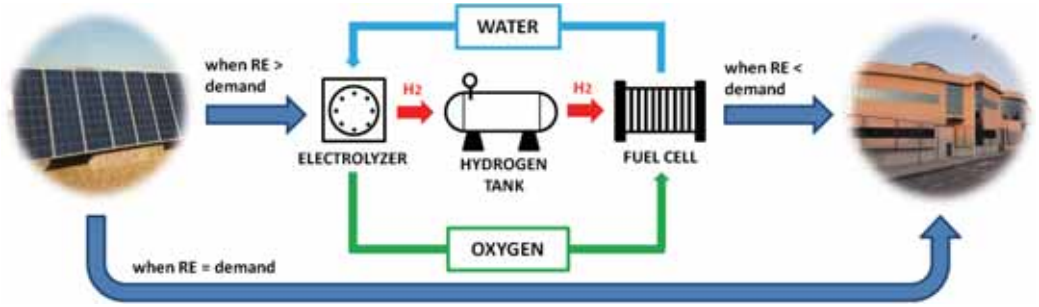

Figure 1 *Operation scheme in which hydrogen and PV solar energy are combined in a "renewable hydrogen-cycle".*

where renewable energies and hydrogen are combined.

The experience gained from over a decade of sustained research, development and demonstration projects corroborates that hydrogen and fuel cell technologies have strong potential to play a significant role in the new energy system that must be defined in the coming years. This energy system should provide adequate and prompt responses to the threats posed by the climate change and energy security issues [1].

Centro Nacional del Hidrógeno (CNH2) works in this direction actively, in order to achieve a sustainable future energy [2].

2. Modeling for Renewable Hydrogen Technologies

H_2 appears as an energy carrier due to the need to have an energy storage system. However, H_2 technologies require significant R&D effort that will achieve more efficient, competitive and less costly processes to introduce the so-called "hydrogen economy". Some of the areas which have to be developed are:

- Improvement in the design of fuel cells and electrolyzers.
- Optimization of fuel cells and electrolyzers for operation with renewable energy.
- Design of auxiliary equipment, such as H_2/H_2O separators.
- Hydrogen hazards and risk analysis.

To achieve these objectives, the modeling using CFD can be a useful tool for the analysis and design of important devices included on H_2 energy technologies. The models require advanced simulation software and high-speed computers to perform the calculations required to simulate the interaction of liquids and gases with surfaces defined by boundary conditions.

Simulations should include all the phenomenology involved but with the necessary simplifications and approximations to reduce computational cost of each model. Figure 2 shows a scheme with the main effects involved in the modeling of electrolyzers, fuel cells and other auxiliary equipment [3]:

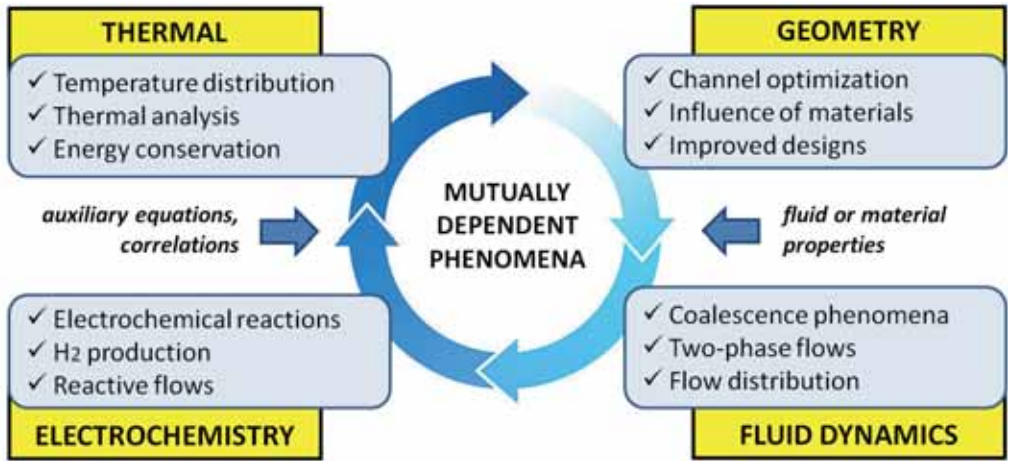

Figure 2 *Mutually dependent phenomena involved in the modeling of energy hydrogen technologies (fuel cells, electrolyzers, separators and risk analysis).*

- Electrochemical effects: They are modeled mainly by equations for electrochemical kinetics, current conservation and species conservation. These equations allow evaluating reactive flows, overpotentials or cell voltage (polarization curve).
- Fluid dynamics effects: They are modelled mainly by mass and momentum balances, with auxiliary equations for turbulent and multiphase flow. The study of multiphase flows is especially important in modelling of hydrogen technologies, since it is common to have mixtures of gas/water in electrolyzers, separators & fuel cells.
- Thermal effects: They are modelled mainly by energy balances.

These effects are strongly interrelated and in turn with the geometry. A variation, for example, in the morphology of an electrolysis cell, involves a new distribution of the flow within it, which can disrupt the removal of the generated gas. As a consequence the voltage necessary for the chemical reaction of the water electrolysis changes, which involves a new heat distribution within the cell.

3. Simulation Activities in CNH2

Related to hydrogen technologies, different CFD simulations activities are performed in *Centro Nacional del Hidrógeno*. The most important simulation activities are described in the following subsections.

3.1 Electrolyzers

Electrolysis is a highly developed technology in the industry and the main way to obtain sustainable hydrogen. Alkaline and proton exchange membrane (PEM) technologies are commercially available, although only alkaline

electrolyzers are industrially well established. On the other hand solid oxide electrolysis cells (SOEC) still need development mainly as regards long-term durability.

Nowadays, commercial electrolyzers are designed for a constant power supply. However, renewable energies are non-dispatchable because of their strong dependence on weather conditions. The fluctuations in power supply to an electrolyzer could cause problems such as generation of explosive mixtures, corrosion of materials, lower efficiency, pressure drops, changes of temperature, etc. The design of electrolyzers powered by renewable energy is a critical issue to avoid these problems.

For these reasons, the CFD simulation is an important design tool to optimize their combination with renewable energies and to evaluate phenomena as [4]:

- Polarization curve.
- Potential and current distribution between electrodes.
- Analysis of coalescence phenomena.
- Flow distribution inside electrolysis cell.
- Gas generation profile and void fraction (occupied space by bubbles) in cathodic and anodic compartments.

There are several published works on the modeling of alkaline electrolyzers. Morel et al. [5] published a model to evaluate the average temperature of an electrolyzer as a function of the electrical current in order to maintain the temperature constant in the cell despite the increased current. Agranat et al. [6] published a CFD model of gas-liquid flow and heat transfer in a high pressure water electrolysis system, which calculated the 3D distributions of pressure, gas and liquid velocities and gas and liquid volume fractions. Jupudi et al. [7] modeled bubble flow and current density distribution in an alkaline electrolysis cell. Hawkes et al. [8] developed an electrochemical CFD model to investigate the high-temperature steam electrolysis in SOEC stacks. Grondin et al. [9] proposed a multiphysics model to predict the SOEC behavior, based on similar charge, mass, and heat transport phenomena as for SOFC using COMSOL® Multiphysics v3.4. Nie and Chen [10] developed a numerical modeling of two-phase flow in the flow field plate of a PEM electrolysis cell.

In Figure 3 [4] a typical polarization curve of an alkaline electrolysis cell obtained with COMSOL® in CNH2 is shown. Oxygen and hydrogen overpotentials are the main source of reaction resistances, and at high current densities, it is very significant the effect of Ohmic losses.

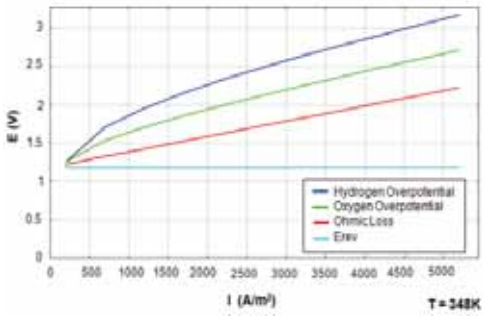

Figure 3 *Polarization curve, including over-potentials and ohmic losses contributions [4].*

3.2 Fuel Cells

Fuel cells constitute the most important and promising energetic application of hydrogen. The proton exchange membrane fuel cell (PEMFC) and the solid oxide fuel cell (SOFC) are well-known technologies to generate electricity. CFD modeling and simulation of PEMFCs and SOFCs are being carried out in order to better understand the fundamental processes taking place and optimize fuel cell designs [1]:

- Polarization curve and electrochemical behavior.
- Study of transport of active species through the porous electrolyte and gaseous diffusion layers (GDL).
- Thermal distribution to avoid hot spots in the membrane.
- Suitable design of flow field to optimize flow distribution, pressure drop and velocity profile.
- Thermal and water management.

The complexity of some of the phenomena involved requires that some simplifications have to be made [1], especially in some of the polarization losses, gas transport through porous media or diffusion of chemical species.

There are many examples in the literature of fuel cell simulations with different configurations and geometries. Ferng and Su [11] investigated the effects of different flow channel designs on the performance of PEMFCs through 3D CFD simulations. Dawes et al. [12] developed a PEM fuel cell CFD model to investigate the effects of water flooding on cell performance parameters. Kvesić et al. [13] presented a CFD model of a five cell short stack, which allows the simulation of an entire PEMFC stack with reasonable computational power and time. Qu et al. [14] predicted the temperature distribution within an anode-supported planar SOFC with corrugated bipolar plates. Peksen [15] performed a 3D thermo-mechanical analysis of a 36-layer planar SOFC stack.

3.3 Gas/Liquid Separators

During electrolysis, H_2 and O_2 are generated and they leave the stack to reach the hydrogen and oxygen separators, respectively. In this kind of device, phases can be separated because the gravity force acts differently on them. In a typical operation, the two-phase flow enters in the separator by the half-height inlet. Gas leaves the separator through the upper outlet and the liquid return to the electrolyzer through the bottom outlet.

However, some technical aspects may produce an non effective gas/liquid separation. In this context, a suitable analysis of separator devices using CFD simulation tools could be a solution to avoid some of these problems [16]:

- Design of gas traps or deflectors inside the separators.
- Study of fluid dynamics gas/liquid mixture and turbulence phenomena.
- Suitable design of gas/liquid separator to avoid that the gas returns to the main circuit (especially in forced convection to avoid explosive mixtures).
- Heat exchange.

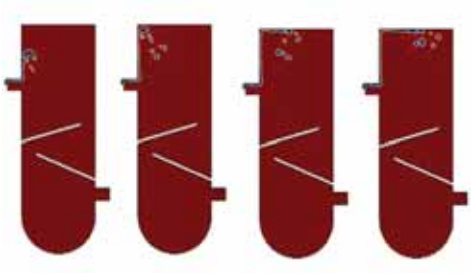

Figure 4 *Separator in which is appreciated as the gas bubbles rise to the liquid/gas interface.*

In Figure 4 the results obtained in CNH2 with COMSOL® are shown, in which is appreciated as the gas bubbles rise to the liquid/gas interface on the inside of a separator. Figure 5 [16] shows the evolution of gas distribution and speed profiles obtained by "turbulent bubbly flow" module.

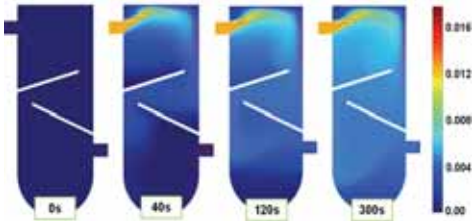

Figure 5 *Gas fraction (surface) and velocity profiles (arrows) obtained by turbulent bubbly flow [16].*

3.4 Hydrogen Leaks and Safety

Hydrogen safety is a very active field of research and international collaboration because it is widely recognized that safety is key issue for the development and commercialization of hydrogen technologies. The main risk related to hydrogen systems is the uncontrolled burning or explosion of an accidental leakage. Due to its low density, gaseous hydrogen will rise and accumulate near the ceiling of an enclosed area during the transitory period as a result of a leak. Afterward, hydrogen, as any other gas, will tend to homogenize its concentration within the enclosure through molecular diffusion [1]. In this context, CFD is a powerful tool for analyzing hydrogen safety scenarios that can help to design the forced ventilation systems and define the number and location of the H_2 sensors [17].

An interesting work on the capabilities of simulation was performed within the activity InsHyde, internal project of the HySafe network of excellence, in the framework of evaluating the capability of various CFD tools and modelling approaches in predicting the short and long term mixing and distribution of hydrogen releases in confined spaces [18].

4. Case Study: modeling Water Alkaline Electrolysis Cell

This section shows the main results obtained in the model presented at the COMSOL Conference 2011 titled "Study of an Alkaline Electrolyzer Powered by Renewable Energy" [4], about the model developed in COMSOL® Multiphysics of an alkaline water electrolysis cell powered by a PV-module.

4.1 Description of the Problem

As indicated in subsection 3.1, commercial alkaline electrolyzers are designed for a constant power supply. However, renewable energies are very fluctuating because of their strong dependence on weather conditions. These fluctuations in power supply to

the electrolyzer can cause problems such as generation of explosive mixtures, corrosion of materials, lower efficiency, pressure drops, changes of temperature, etc.

The design of alkaline electrolyzers powered by renewable energy is a critical issue to avoid these problems. So it is needed to develop a CFD model of the behavior of an electrolysis cell for hydrogen production through PV solar energy.

4.2 Geometry

Taking as reference a modified commercial electrolysis cell, the geometry of the model was built following fluid dynamic requirements. In this way, simplifications were made in order to reduce the model complexity (Figure 6).

4.3 Problem Formulation

Depending of the studied phenomena, the model can be divided into:

- Hydrogen generation by renewable energies, with *Electric Currents* and *Two phase-flow bubbly flow* modules.
- Motion of bubbles next to electrode surface with *Two phase-flow phase field* module of COMSOL®.

A more detailed description of the mathematical formulation used is shown in [4].

4.4 Results and Discussion

The model shows the behavior of an alkaline electrolysis cell powered by a PV-module at different times in a sunny day. Maximum value of solar radiation occurs at 14:00.

Next to the electrode surface, the volume fraction reaches the highest value, and decreases towards the membrane, according with dynamic evolution of gas profiles on cathode, when the cell is powered with PV module profile (Figure 8). In Figure 7, higher values of current in the PV profile correspond with higher applied potential on the cell. Current draws a particular distribution in the cell, being more intense in electrodes extremes.

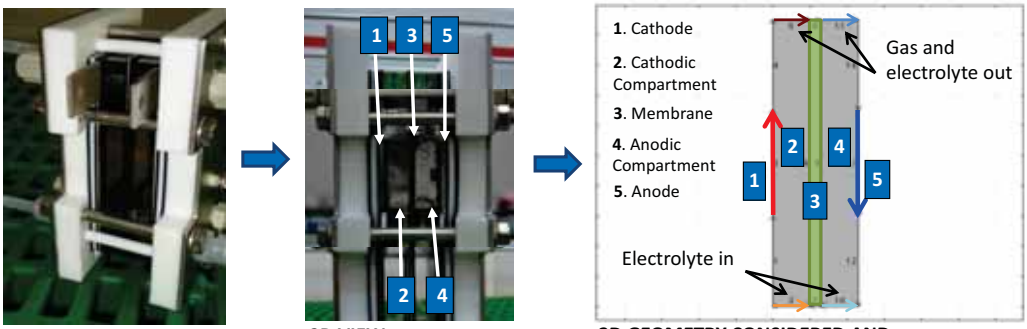

Figure 6 *2D geometry of a modified commercial alkaline electrolysis cell implemented on COMSOL Multiphysics®.*

Finally, Figure 3 shows the polarization curve obtained with the model.

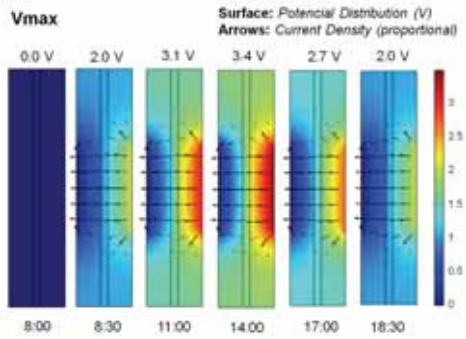

Figure 7 *Potential distribution of electrolysis cell when it is powered by a PV-module [4].*

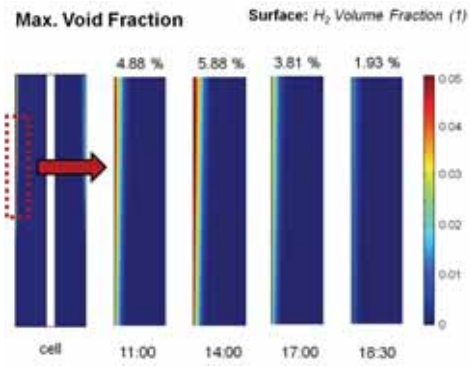

Figure 8 *Hydrogen volume fraction evolution for electrolysis cell during a day operation [4].*

Figure 9 shows a model of coalescence between two bubbles of hydrogen using COMSOL®. During electrolysis of water, the bubbles rise by buoyancy and join in the upper regions of the cell. The study of coalescence lets us know how the gas is accumulated in the output channels of the electrolysis cell.

5. Centro Nacional del Hidrógeno (CNH2)

The *Centro Nacional del Hidrógeno* (CNH2) is a Scientific Research and Technology Development facility (ICTS in its Spanish acronym). CNH2 was created as a public consortium between *Ministerio de Economía y Competitividad* (Spain) and *Junta de Comunidades de Castilla-La Mancha*. They held each one the 50% of the consortium. The Consortium was made up for the facility design, construction, equipping and operation and aims to manage and promote scientific cooperation, technical, economic and administrative between the institutions that comprise it. The Consortium was established on 2007 and the facilities are located in Puertollano (Ciudad Real).

The objectives of the CNH2 are to direct the national strategy in hydrogen technologies, carry out technological development and innovation and promote projects that will serve to demonstrate the efficiency and reliability of these technologies and incorporating them into the national and international energy system, which in turn serves to stimulate the industrial and energy sectors.

CNH2 has focused its activities on producing, storing, purifying and distributing hydrogen generated fundamentally from renewable sources, working with high, medium and low-temperature fuel cell technologies, integrating systems and demonstrating these systems at pilot scale at its facilities [2].

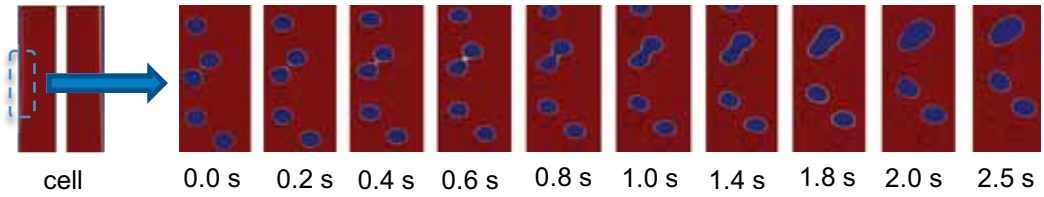

Figure 9 *Detail of coalescence phenomena between hydrogen bubbles [4].*

6. Conclusions

The transition to "hydrogen economy" requires a large R&D effort to improve technologies for production, storage and use of hydrogen. In this sense, the development of models using simulation CFD software is necessary for the analysis, design and optimization of different hydrogen energy technologies.

Centro Nacional del Hidrógeno works actively in this direction by developing models of electrolyzers, fuel cells and auxiliary equipment. CFD also is a powerful tool for analyzing hydrogen safety scenarios.

7. References

1. Gandía LM, Arzamendi G, Diéguez PM. Author, *Renewable Hydrogen Technologies: production, purification, storage, applications and safety*. Elsevier B.V. (2013)

2. Website *Centro Nacional del Hidrógeno*: www.cnh2.es [accesed 15.05.2014]

3. *COMSOL Multiphysics 3.5 - Chemical Engineering Module: Model Library*. COMSOL Inc. (2008)

4. Amores E, Rodríguez J, Merino C, García P. Study of an alkaline electrolyzer powered by renewable energy. *COMSOL Conference 2011*, Stuttgart (Germany)

5. Morel B, Namy P, Belhomme C, Crassous I. Convective movements in an electrolyzer. *COMSOL Conference 2007*, Grenoble (France)

6. Agranat V, Zhubrin S, Maria A, Hinatsu J, Stemp M, Kawaji M. CFD modeling of gas-liquid flow and heat transfer in a high pressure water electrolysis system. *European Fluids Engin. Summer Meeting 2006*, Miami (USA)

7. Jupudi RS, Hongmei Z, Zappi G, Bourgeois R. Modeling bubble flow and current density distribution in an alkaline electrolysis cell. *J of Computational Multiphase Flows*, **1**, 341 (2009)

8. Hawkes G, O'Brien J, Stoots C, Hawkes B. 3D CFD model of a multi-cell high-temperature electrolysis stack. *Int J Hydrogen Energy*, **34**, 4189 (2009)

9. Grondin D, Deseure J, Brisse A, Zahid M, Ozil P. Simulation of a high temperature electrolyzer. *J Appl Electrochem*, **40**, 933 (2010)

10. Nie J, Chen Y. Numerical modeling of three-dimensional two-phase gas–liquid flow in the flow field plate of a PEM electrolysis cell. *Int J Hydrogen Energy*, **35**, 3183 (2010)

11. Ferng YM, Su A. A 3D fuel-cell CFD model used to investigate the effects of different flow channel designs on PEMFC performance. *Int J Hydrogen Energy*, **32**, 4466 (2007)

12. Dawes JE, Hanspai NS, Family OA, Turan A. 3D CFD modelling of PEM fuel cells: An investigation into the effects of water flooding. *Chemical Engineering Science*, **64**, 2781 (2009)
13. Kvesić M, Reimer U, Froning D, Lüke L, Lehnert W, Stolten D. 3D modeling of a 200 cm^2 HT-PEFC short stack. *Int J Hydrogen Energy*, **37**, 2430 (2012)
14. Qu Z, Aravind PV, Boksteen SZ, Dekker NJJ, Janssen AHH, Woudstra N, Verkooijen AHM. Three-dimensional computational fluid dynamics modeling of anode-supported planar SOFC. *Int J Hydrogen Energy*, **36**, 10209 (2011)
15. Peksen M. A coupled 3D thermofluid-thermomechanical analysis of a planar type production scale SOFC stack. *Int J Hydrogen Energy*, **36**, 11914 (2011)
16. Amores E, Rodríguez J. Comparison between turbulent and laminar bubbly-flow for modeling H_2/H_2O separation. *COMSOL Conference 2012*, Milan (Italy)
17. Legg SW, Benavides-Serrano AJ, Siirola JD, Watson JP, Davis SG, Bratteteig A, Laird CD. A stochastic programming approach for gas detector placement using CFD-based dispersion simulations. *Comput Chem Eng*, **47**, 194 (2012)
18. Venetsanos AG, Papanikolaou E, Delichatsios M, Garcia J, Hansen OR, Heitsch M, Huser A, Jahn W, Jordan T, Lacome J-M, Ledin HS, Makarov D, Middha P, Studer E, Tchouvelev AV, Teodorczyk A, Verbecke F, Van der Voort MM. An inter-comparison exercise on the capabilities of CFD models to predict the short and long term distribution and mixing of hydrogen in a garage. *Int J Hydrogen Energy*, **34**, 5912 (2009)

Hydro-Mechanical-Chemical Coupled Modelling of Copper Heap Leaching with iCP

O. Silva[*1], A. Nardi[1], G. Román-Ross[1], J. Molinero[1] and P. Quesada[2]

[1]Amphos 21 Consulting S.L. Spain, [2]Amphos 21 Consulting S:A.C. Peru
*Corresponding author: Passeig de Garcia i Faria 49-51, 1-1, 08019 Barcelona,
orlando.silva@amphos21.com

Abstract: Heap leach pads constitute a common practice in the mining industry. In their design and management it is not common to take into account criteria based on coupled hydro-mechanical-chemical (HMC) processes, and these are of paramount importance for two reasons: (i) they could play an important role on the physical stability of the pad and; (ii) they are keys for the metallurgical efficiency, especially in the mid-long term. Here we present a simulation of a synthetic copper heap leach pad case to demonstrate the relevance of the HMC coupling, as well as the capabilities of the used numerical tool.

Keywords: Heap leaching, hydro-mechanical-chemical coupling.

1. Introduction

Heap leach pads constitute a common practice in the mining industry. In their design and management it is not common to take into account criteria based on coupled hydro-mechanical-chemical processes, and these are of paramount importance for two main reasons: (i) they could play an important role on the physical stability of the pad and; (ii) they are keys for the metallurgical efficiency, especially in the mid-long term. As an example of the relevance of such a complex coupled phenomena, it could be mentioned that geotechnical stability of the heap is related to the distribution of liquid pressures which, at the same time, is related to the permeability through the Darcy's law. In its turn, permeability will be affected by porosity changes, which depends on the consolidation state and the dissolution/precipitation of minerals. Hydrometallurgical performance of the heap ore is strongly linked with the abovementioned coupled processes.

Usual approaches for heap leaching models solve the different phenomena in an uncoupled or just partially coupled way due to their resolution complexity. Some of the existing approaches were formulated to solve hydrodynamics and solute transport (Decker and Tyler, 1999), and soil mechanics and hydrodynamics (Pacheco *et al.*, 2011). In the last decade some efforts for incorporating the chemistry in Hydro-Mechanical (HM) problems have been done (Liu and Brady, 2004; Mata *et al.*, 2005; Mohajeri *et al*., 2011), but most of them only considered simple geochemical models over synthetic cases. Also some attempts to solve the Thermal - Hydro - Mechanical - Chemical (THMC) equations in the context of the design of radioactive waste facilities have been

reported (Guimarães *et al*., 2002). There is a clearly demand of numerical simulators that can help in the design, planning and predicting of leaching operations at industrial scale (Cross *et al.*, 2006; Bennett *et al.*, 2012; McBride *et al.*, 2012a; McBride *et al.*, 2013). Recently, McBride *et al.* (2012b) developed a mathematical model based on CFD technology that consider operational aspects of a leaching process such as actively 3D leached and unleached heap areas. Nevertheless, the flow through the heap is modeled in 1D, which can lead to substantial errors in the prediction of metal recovery as the lateral flow is disregarded. In addition, mechanical phenomena were not considered.

Improving the design of heap leach pads requires performing an integrated analysis of the HMC phenomena. The key aspects of the construction and operation such as mechanical stability and mineral recovery efficiency cannot be estimated accurately without taking into account multiple coupling of a complex chemistry, the soil mechanics and the hydrodynamics. To our knowledge, there is no numerical simulation of a coupled HMC model that accounts for the kinetics of several mineral species and the evolution of a muti-lift heap. In this paper, we present a model that considers all the above mentioned coupled phenomena and a numerical tool for the simulation of copper heap leaching.

2. Methodology

In this work we provide a simulation of a synthetic copper heap leach pad case to demonstrate the relevance of the HMC coupling, as well as the capabilities of the used numerical tool. The methodology followed in this study consists of: (i) development of a numerical tool for the simulation of HMC problems; (ii) application of the numerical tool for simulating copper heap leaching; (iii) demonstration of the potential of the tool for the design, planning and prediction of industrial heap leaching operations.

2.1 Hydro – mechanical - chemical model

In this section we describe the governing equations assumed in the modeling of the heap leaching process. First, the mass balance equation of liquid under isothermal conditions is expressed as follow

$$\rho_l\left(C_m + S_l S\right)\partial_t p_l = \rho_l \nabla\cdot\mathbf{q}_l + \rho_l \partial_t \varepsilon_{vol} + f_{ext}^{w} \quad (1)$$

where ρ_l is the liquid density, S_l is the liquid saturation, C_m is the specific moisture capacity, p_l is the liquid pressure, S is the storage term, $\mathbf{q}_l$ is the liquid flow velocity, ε_{vol} is the volumetric deformation and f_{ext}^{w} is an external source term. The liquid flow velocity equation is given by the Darcy's law (Bear, 1988)

$$\mathbf{q}_l = -\frac{\mathbf{k}k_r}{\mu}\left(\nabla p_l - \rho_l \mathbf{g}\right) \quad (2)$$

where $\mathbf{k}$ is the intrinsic permeability tensor, k_r is the relative permeability, μ is the dynamic viscosity of the liquid and $\mathbf{g}$ is the gravity tensor. The van Genuchten's retention function (van Genuchten, 1980) was considered to account for the relationship between liquid saturation and pressure. Also, the relative permeability was calculated

according to the model of van Genuchten (1980).

On the other hand, we used the so called non-conservative formulation for reactive transport of a chemical species (Bea *et al.*, 2009),

$$\omega\partial_t \mathbf{c} = L_t(\mathbf{c}_a) + f_{ext}^w \mathbf{c}_a^* \rho_l + \omega \mathbf{r}_{eq} + \omega \mathbf{r}_{kin} \quad (3)$$

where $\omega = \phi S_l \rho_l$, $\mathbf{c}$ is the concentration vector of species, $\mathbf{c}_a$ is the concentration vector of aqueous species, $\mathbf{c}_a^*$ is the vector of external concentrations of species, ϕ is porosity, $\mathbf{r}_{eq}$ and $\mathbf{r}_{kin}$ are the vectors of equilibrium and kinetics reactions, respectively. In (3) we have introduced the linear operator accounting for advection, dispersion, diffusion and non-chemical sink-source terms, $L_t(\cdot) = -\rho_l \mathbf{q}_l \cdot \nabla(\cdot) + \nabla(\rho_l \mathbf{D} \cdot \nabla(\cdot)) - f_{ext}^w(\cdot)$, where $\mathbf{D}$ is the tensor of dispersion and diffusion coefficients. The equation (3) consists of a system of N_s equations, where N_s is the number of chemical species. However, it can be reduced to a system of size N_c, the number of chemical components, by eliminating the equilibrium reactions. Chemical components are defined as linear combination of species whose mass is not affected by equilibrium reactions (Steefel and MacQuarrie, 1996; Saaltink *et al.*, 1998),

$$\omega\partial_t \mathbf{m} = L_t(\mathbf{m}_a) + f_{ext}^w \mathbf{m}_a^* + \omega \mathbf{M}\mathbf{r}_{kin} \quad (4)$$

In (4) $\mathbf{m} = \mathbf{M}\mathbf{c}$ is the vector of components, which can be decomposed in subcomponents containing the chemical species of the component present in the aqueous ($\mathbf{m}_a$), gaseous ($\mathbf{m}_g$), mineral ($\mathbf{m}_m$) and sorbed ($\mathbf{m}_d$) phases; $\mathbf{M}$ is a component matrix, which is defined as a matrix that eliminates the equilibrium reactive term, i.e., $\mathbf{M}\mathbf{r}_{eq} = \mathbf{0}$ (Saaltink *et al.*, 1998); and $\mathbf{m}_a^*$ is the vector of external aqueous component concentration.

Finally, the soil mechanics of a heap leach pad was assumed to be governed by the equilibrium equations (Zienkiewicz and Taylor, 1989)

$$\nabla \cdot \boldsymbol{\sigma} + \left((1-\phi)\rho_s + \phi S_l \rho_l\right)\mathbf{g} = 0 \quad (5)$$

where $\boldsymbol{\sigma}$ is the total stress tensor and ρ_s is the soil density. In a variable saturated porous medium the effective stress, $\boldsymbol{\sigma}'$, controls the mechanical behavior. We adopted a simple approach, in which $\boldsymbol{\sigma}' = (\boldsymbol{\sigma} - p_a \mathbf{I}) + \left((S_l - S_{lr})/(1 - S_{lr})\right)(p_a - p_l)\mathbf{I}$, where p_a is the air pressure and S_{lr} is the residual liquid saturation. The Cam-Clay elasto-plastic constitutive law (Wood, 1990) and plane strain conditions were assumed to close the problem.

The initial suction and composition of the ore material layers are represented by p_l^0 and $\mathbf{m}_a^0$, respectively. Initial mechanical conditions assumed are zero strains and stresses for each layer. No flow conditions are assumed at the boundaries of the bedrock. Also, no flow conditions are imposed at the lateral boundaries of the ore layers and the free surface of those layers beneath the current layer under irrigation. Atmospheric pressure and mass outflow conditions are imposed at the lateral boundaries of the drainage system. An inflow condition (q_{in}) is considered at the surface of every layer to reproduce the irrigation process. Horizontal displacement (u_x) at the lateral

boundaries of the rock foundation is set at zero. Also zero vertical (u_y) and horizontal displacements are considered at the bottom boundary of the bedrock. No mechanical constrains and no loads are considered at the remaining boundaries.

2.2 Implementation in COMSOL - PHREEQC

The governing equations (1-5) have been solved with the numerical interface COMSOL-PHREEQC (iCP) (Nardi *et al.*, 2014). iCP is a Java interface that couples COMSOL Multiphysics and the geochemical simulator PHREEQC (Parkhurst and Appelo, 2013). In brief, the tool is based on implementing an operator splitting technique for solving the hydro-mechanical problem on COMSOL and the chemical system of algebraic and differential equations on PHREEQC. A problem is set in iCP with three input files: (i) a COMSOL file for solving the HM phenomena, (ii) a set of PHREEQC files defining the chemical system and (iii) a XML file for linking COMSOL to PHREEQC, specifying the time discretization and outputs. Also, iCP automatically divides the model domain into subdomains where geochemical reactions are solved in parallel by dividing the computation on multiple threads. The present simulation used a mesh with 14641 elements and time steps of 86400 s. It required 1 GB of storage and 1 day of CPU time on a 3.8 GHz processor with 4 cores and 16 GB RAM. These numbers are in the range of other codes and computational methods that only solve flow and reactive transport (e.g., McBride, *et al.*, 2012a; McBride *et al.*, 2012b).

3. Application case: multi-lift leach pad

The present HMC model was applied to simulate the construction and operation of a synthetic copper heap leach pad consisting of 5 ore layers settled on a terrain with a slight slope (2%). Each layer (stacking levels) is simulated sequentially, mimicking the sequence of construction and operation of a real heap leach pad as schematized in Figure 1. In this sequential simulation approach the results obtained during the calculation of the previous layers ($\boldsymbol{u}_{n-1}$, p_{n-1}, c_{n-1}) are used to define the initial ($\boldsymbol{u}_0$, p_0, c_0) and boundary conditions of the next layer.

The construction of each layer is assumed to be performed during 10 days, followed by an irrigation period of 90 days at a constant irrigation rate of $q_{in} = 7.5\ \mathrm{l\ h^{-1}\ m^{-2}}$ applied on the top surface of each layer. The initial liquid pressure in the ore layer (p_l^0) is considered equal to -30 kPa. The temperature of the system is assumed to be 25 ºC. The rock and ore densities were set at 3000 kg/m^3 and 2600 kg/m^3, respectively. An initial porosity of 30% was assumed both for the liner system and ore bed, while the initial intrinsic permeabilities were set at 5×10^{-10} m^2 and 4×10^{-11} m^2, respectively. The longitudinal dispersivities of the liner system and ore bed were assumed equal to 50 m and 10 m, respectively. The respective transversal dispersivities were set at 10 m and 2 m. These values may be representative of industrial heap leaching, where the total heap height

can be up to 200 m and the area under leach can be in the order of 10^6 m^2 (Schlesinger *et al.*, 2011).

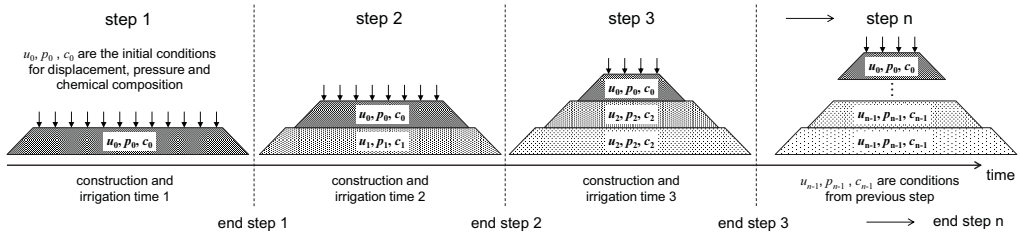

Figure 1 *Sequence of construction of a heap leach pad layer by layer. The layer "n" is represented by "step n". State variables of the problem are displacement (u), liquid pressure (p) and concentration (c).*

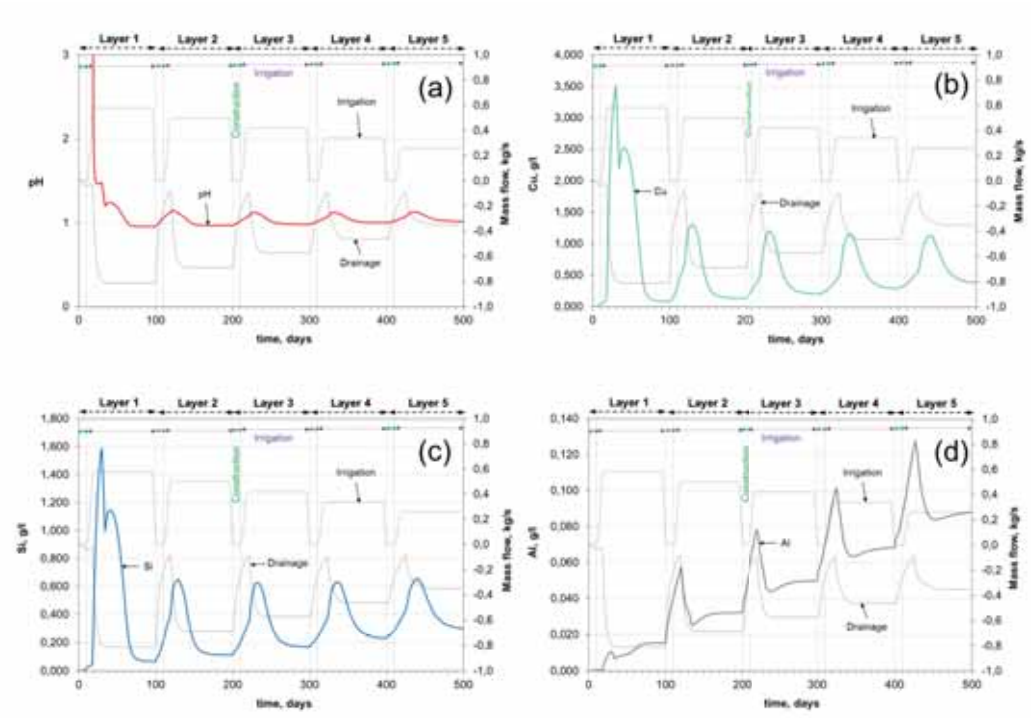

Figure 2 *Evolution of pH (a) and concentrations of Cu (b), Si (c) and Al (d) in the pregnant leach solution. Irrigation and drainage mass flow during each stage are also included.*

Table 1: *Chemical composition of the initial pore water and irrigation solution*

	Initial pore water ($\mathbf{m}_a^0$)	Irrigation solution ($\mathbf{m}_a^*$)
pH	5.95	0.94
Eh, mV	738	1161
Al, mol/l	2.56×10^{-10}	10^{-22}
C, mol/l	3.49×10^{-2}	1.04×10^{-5}
Ca, mol/l	3.49×10^{-2}	2.70×10^{-3}
Cl, mol/l	1.30×10^{-6}	9.63×10^{-2}
K, mol/l	1.89×10^{-2}	6.30×10^{-4}
Fe, mol/l	2.50×10^{-7}	7.50×10^{-6}
Mg, mol/l	3.99×10^{-8}	1.30×10^{-5}
Na, mol/l	10^{-14}	6.10×10^{-4}
S, mol/l	3.79×10^{-2}	4.50×10^{-2}
Si, mol/l	9.25×10^{-17}	3.20×10^{-4}

We assumed that the mineral is composed by Chrysocolla (20% w/w), Chalcopyrite (10% w/w), Pyrite (8% w/w), Albite (30% w/w) and K-Feldspar (32% w/w), and a Cu grade of 0.48%. The chemical evolution of the above minerals is assumed to be governed by kinetics reactions (Dreier, 1999; Kimball *et al.*, 2010; Williamson and Rimstidt, 1994; Chou and Wollast, 1985, Schweda, 1989). Equilibrium precipitation-dissolution reactions of Jarosite-K, Jurbanite, Basaluminite, $Fe(OH)_3(a)$ and Schwertmannite are also taken into account. To simplify the problem, bioleaching of Chalcopyrite was not considered in the model. The chemical compositions of the initial pore water and irrigation solution are shown in Table 1.

4. Results and Discussion

Figure 2 shows the evolution of concentrations of selected dissolved species at the output of the drainage system. The evolution of pH shows the arrival of the acidic solution to the liner system in a time of around 60 days (Figure 2a). Kinetic dissolution of Chrysocolla and Chalcopyrite is triggered by the infiltration of the acidic solution and, as a result, an increase of Cu concentrations is observed in the outlet flow (Figure 2b). The chemical evolution of Si and Al concentrations (Figure 2c and 2d) clearly shows that under this low pH conditions kinetic dissolution of aluminosilicates is also favored. This process is highly dependent on the pH and, over a long period of time, porosity can be significantly modified.

Figure 3 shows the temporal evolution of Chalcopyrite and Chrysocolla concentrations. The concentration of Chalcopyrite practically does not change, while the Chrysocolla is almost completely dissolved at the end of the leaching of each layer. This is due to the combination of three factors: the slow dissolution rate of Chalcopyrite, the fast dissolution rate of Chrysocolla and the initial amounts of both minerals, which are very similar.

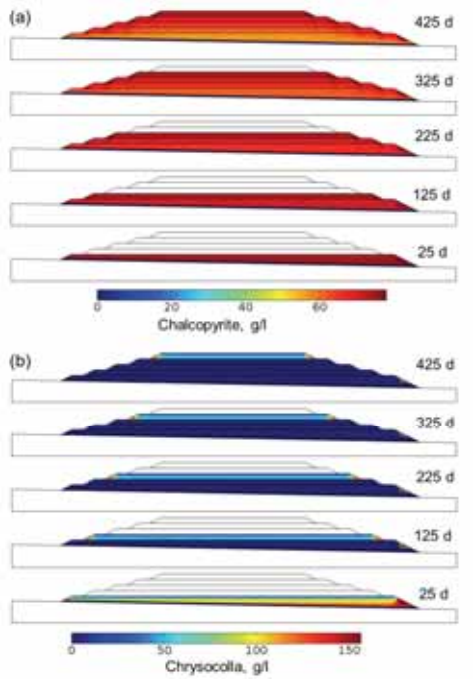

Figure 3 *Evolution of the Chalcopyrite (a) and Chrysocolla (b) concentrations in the leach pad.*

The copper recovery is presented in Figure 4a. Note that the copper recovery associated to the leaching of each layer displays a common pattern that reflects the difference in the leaching rates of Chrysocolla and Chalcopyrite. During the first days of leaching of a new layer, the copper is recovered mainly from Chrysocolla. The fast dissolution rate of Chrysocolla is associated to a higher slope of the recovery curve. Once this has been spent, the copper recovery continues from Chalcopyrite to a lower rate (lower slope of the copper recovery curve). This pattern is more evident during the leaching of the first layer, which provides a copper recovery of about 30%. The copper recovered from the leaching of subsequent layers is about 8%. At the end of the operation (500 days), approximately the 60% of the copper has been recovered. The recovered copper increases due to the leaching of residual mineral from previous layers, depending on the thickness of the loaded layers and the irrigation times.

The competition between Chrysocolla and Chalcopyrite is more evident by looking at the acid sulfuric consumption, which is shown in Figure 4b. During a given irrigation period, the consumed acid increases almost at a constant rate until reaching a plateau coinciding with the construction of a new layer. After 25 days from the start of a new irrigation period, the acid consumption experiments a small decrease, due to the complete dissolution of Chrysocolla. Note that this time coincides with the time at which the copper recovery changes its rate (see Figure 4a). These changes in copper recovery and acid consumption last about 5 days, after which the acid consumption increases again at the initial rate of the current leaching stage. That is, the copper recovery and acid consumption curves directly reflect the different dissolution rates of the mineral species considered in the model, specially the Chrysocolla (fast dissolution rate) and the Chalcopyrite (slow dissolution rate). Also, the plateau of acid consumption is clearly associated to the behavior of the irrigation and drainage flow rates (see Figure 2). In addition, acid consumption during the leaching of a new layer is progressively lower than the acid consumption of previous leaching stages. This is because the mass of mineral of the new layer is lower and

the impact of acid consumption from previous leached layers is minor.

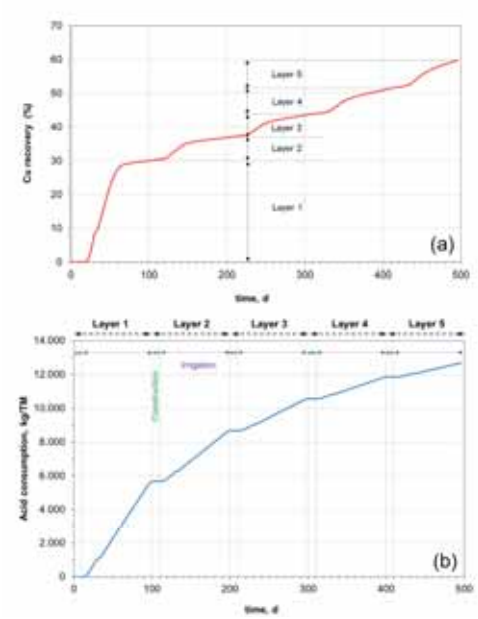

Figure 4 *Predicted copper recovery (a) and acid consumption (b).*

The hydrodynamics behavior of the system is conditioned by the time required for the irrigation solution to saturate the heap as it flows to the drainage system. The evolution of the liquid saturation is shown in Figure 5a. After a short period of time, a quasi-steady state is achieved for every layer. In the present case it takes about 40 days since the layer construction. We have set an observation point to understand the evolution of the liquid pressure (red spot on Figure 5a). As shown in Figure 5b, two stages are found for every leaching step: the construction and the irrigation periods. The effect of construction does not generate pore water pressure (as occurs in undrained conditions) as the ore is mainly unsaturated and the construction has been simulated in a progressive manner. The increase of liquid pressure at the beginning of each leaching step is caused by irrigation. Nevertheless, this increase is progressively lower because the irrigation decreases in the next leaching step. The irrigation time plays an important role in the system behavior. This is due to the influence of irrigation on the liquid pressure and mass of recovered mineral. Some amount of copper remains in the pad close to the slope limits, because irrigation is not very effective on those zones. Ideally, those zones could be exploited as well.

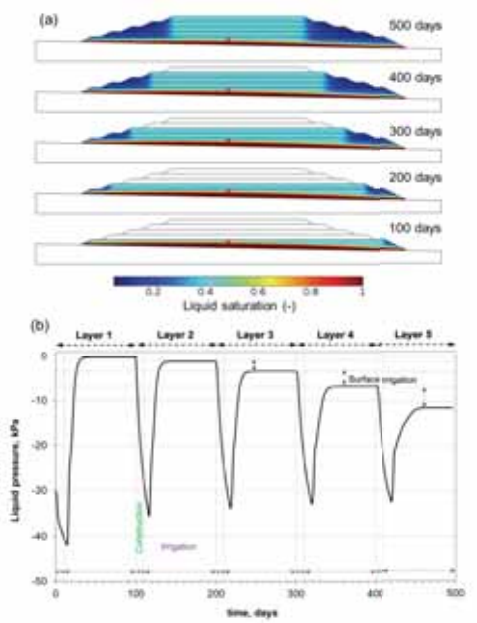

Figure 5 *Evolution of the liquid saturation in the leach pad. The red circle on top (b) denotes the observation point for pressure evolution shown in (b).*

Changes in porosity and permeability due to mineral dissolution/precipitation and irrigation time can affect significantly the hydromechanical behavior of the heap

leach pad. Figure 6a shows the evolution of the global porosity due to the combined hydromechanical and chemical effects. We found that there are zones of the ore where the porosity increases due to the mineral dissolution and other zones where the consolidation of the layers leads to a porosity decrease. The mechanical effects are traduced in an increase in the vertical stress developed mainly on the rock foundation as the layers are progressively loaded. This vertical stress increase also reaches the top of the third layer, where the vertical displacement reaches a maximum.

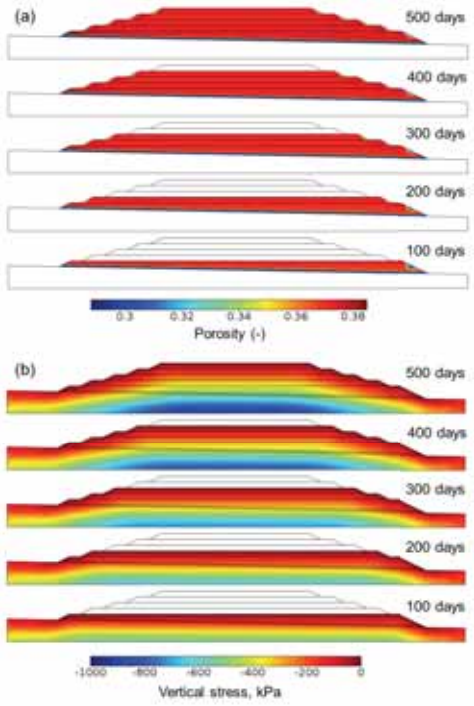

Figure 6 *Evolution of global porosity (a) and vertical stress in the leach pad (b).*

5. Conclusions

We presented iCP, a numerical tool that is able to solve simultaneously unsaturated flow, soil mechanics and reactive transport in porous media. This tool allows integrating in a single framework hydromechanical and geochemical coupled phenomena and the processes involved in the construction and operation of heap leach pads. Geochemical changes affecting porosity and permeability are coupled explicitly in the hydraulic and geomechanical calculations. The model calibration may be conducted in a two-stage optimization process based on (i) experimental data from batch tests and kinetics test columns for reaction rate parameters optimization in PHREEQC and (ii) field scale measurements and operational indicators (e.g., pressures, flow rates, copper recovery, acid consumption) for inverse modeling of hydro-mechanical-solute transport parameters in COMSOL.

The simulation results show that changes in porosity due to mineral dissolution/precipitation and irrigation time affect significantly the hydromechanical behavior of the heap leach pad, and vice versa. For the synthetic case of a multi-lift heap considered in the study, the simulated copper recovery and acid consumption responds directly to the dissolution rates of the copper bearing minerals considered in the model. A strong advantage of the present model is that it can treat multiple chemical species simultaneously, providing solutions that are best for interpreting all the chemical interactions within a leaching system. In addition, the stability of the pad and the ore recovery efficiency can be predicted with more accuracy because the model considers the interaction between variable saturated flow, mechanical

deformation and chemical reactions during the construction and irrigation of the different layers of the heap. Finally, the modeling methodology presented in this work can help to improve the stability of the heap pad and optimize the mineral recovery efficiency.

6. References

1. Bea, S. A., Carrera, J., Ayora, C., Batlle, F. and Saaltink, M. W., CHEPROO: A Fortran 90 object-oriented module to solve chemical processes in Earth Science models, *Computers & Geosciences*, **35(6)**, 1098–1112 (2009)

2. Bear, J., *Dynamics of fluids in porous media*, page numbers. Dover, New York (1988)

3. Bennett, C. R., McBride, D., Cross, M. and Gebhart, J. E., A comprehensive model for copper sulphide heap leaching Part 1 Basic formulation and validation through column test simulation, *Hydrometallurgy*, **127–128**, 150–161 (2012)

4. Chou L. and Wollast, Steady-state kinetics and dissolution mechanisms of albite, *American Journal of Sciences*, **285**, 963-993 (1985)

5. Cross, M., Bennett, C., Croft, T. N., McBride, D. and Gebhart, J. E., Computational modeling of reactive multi-phase flows in porous media: Applications to metals extraction and environmental recovery processes, *Minerals Engineering*, **19**, 1098–1108 (2006)

6. Decker, D. L. and Tyler, S. W., Hydrodynamics and solute transport in heap-leach mining. *Closure, remediation and management of precious metals heap-leach facilities*. Univ. of Nevada, Reno, 1–13 (1999)

7. Dreier, J. E., *The chemistry of copper heap leaching*, http://jedreiergeo.com/copper/article1/Chemistry_of_Copper_Leaching.html (1999)

8. Guimarães, L., Gens, A., and Olivella, S., Modelling the geochemical behaviour of an unsaturated clay subjected to heating and hydration, *Proc. 3rd Int. Conf. on Unsaturated Soils*, 71–76 (2006)

9. Kimball, B. E., Rimstidt, J. D. and Brantley, S. L., Chalcopyrite dissolution rate laws, *Applied Geochemistry*, **27(7)**, 972-983 (2010)

10. Liu, J. and Brady, B. H., Simulations of a coupled hydro-chemo-mechanical system in rocks, *Geotechnical & Geological Engineering*, **22(1)**, 121–133 (2004)

11. Mata, C., Guimarães, L. D. N., Ledesma, A., Gens, A. and Olivella, S., A hydro-geochemical analysis of the saturation process with salt water of a bentonite crushed granite rock mixture in an engineered nuclear barrier, *Engineering Geology*, **81(3)**, 227–245 (2005)

12. McBride, D., Gebhart, J. E. and Cross, M., A comprehensive gold oxide heap leach model: Development and validation, *Hydrometallurgy*, **113–114**, 98–108 (2012a)

13. McBride, D., Cross, M. and Gebhart, J. E., Heap leach modelling employing CFD technology: A 'process' heap model, *Minerals Engineering*, **33**, 72–79 (2012b)

14. McBride, D., Croft, T. N., Cross, M., Bennett, C. and Gebhart, J. E., Optimization of a CFD – Heap leach model and sensitivity analysis of

process operation, *Minerals Engineering*, http://dx.doi.org/10.1016/j.mineng.2013.11.010 (2013)
15. Mohajeri, A., Muhlhaus, H., Gross, L., and Baumgartl, T., Coupled mechanical-hydrological-chemical problems in elasto-plastic saturated soils and soft rocks using *escript*, *Advances in Bifurcation and Degradation in Geomaterial*, Springer Netherlands, 269–275 (2011)
16. Nardi, A., Idiart, A., Trinchero, P., de Vries, L. M. and Molinero, J., Interface Comsol-PHREEQC (iCP), an efficient numerical framework for the solution of coupled multiphysics and geochemistry, *Computers & Geosciences*, doi:10.1016/j.cageo.2014.04.011 (2014)
17. Pacheco, P. G. M., Purizaga, M., Huertas, J., and Romanel, C., Flow analysis and dynamic slope stability in a copper ore heap leach, *Geotechnical Conference*, 7 (2011)
18. Parkhurst, D. L., and Appelo, C. A. J., *Description of input and examples for PHREEQC version 3—A computer program for speciation, batch-reaction, one-dimensional transport, and inverse geochemical calculations*, U.S. Geological Survey Techniques and Methods, book 6, chap. A43, 497 p., available only at http://pubs.usgs.gov/tm/06/a43/ (2013).
19. Saaltink, M. W., Ayora, C., and Carrera, J., A mathematical formulation for reactive transport that eliminates mineral concentrations, *Water Resources Research*, **7(34)**, 1649–1656 (1998)
20. Schweda, P., Kinetics of alkali feldspar dissolution at low temperatures, D. L. Miles, ed., Water-rock interaction 6: Proceedings Sixth International Symposium on Water-Rock Interaction, Edmonton, International Association of Geochemistry and Cosmochemistry and Alberta Research Council, pp. 609–612 (1989)
21. Schlesinger, M. E., King, M. J., Sole, K. C. and Davenport, W. G., *Extractive Metallurgy of Copper*, Elsevier, Fifth Edition (2011)
22. Steefel, C. I. and MacQuarrie, K. T., Approaches to modelling reactive transport in porous media, *Reviews in Mineralogy and geochemistry*, **34(1)**, 85–129 (1996).
23. van Genuchten, M. Th., A closed-form equation for predicting the hydraulic conductivity of unsaturated soils, *Soil Science Society of America Journal*, **44**, 892–898 (1980)
24. Williamson, M. A. and Rimstidt, D., The kinetics of electrochemical rate-determining step of aqueous pyrite oxidation, *Geochimica et Cosmochimica Acta*, **58(24)**, 5443-5454 (1994)
25. Wood, D. M., *Soil behaviour and critical state soil mechanics*, Cambridge University Press, New York (1990)
26. Zienkiewicz, O. C. and Taylor, R. L., *The finite element method*, McGraw Hill, vol. 1 (1989)

7. Acknowledgements

We want to acknowledge the partners of the iMaGe consortium (www.image-modelling.net) for supporting the iCP development.

Mixed Elasticity with Discontinuous Pressure Interpolation

J. J. Anza[1,*]

[1]Department of applied mathematics, University of the Basque Country, Bilbao, Spain
*Alameda de Urkijo s/n, Bilbao 48013, Spain , juanjose.anza@ehu.es

Abstract: In this paper we are interesting in using COMSOL as a platform for new developments. The work presented deals with elasticity in the incompressible limit where standard formulation has to be substituted by the mixed one, and finite element interpolations might be ill conditioned conducting to pathological behavior. This work implements using first the pde interfaces and after the Physics Interface builder (PIB), a mixed formulation with continuous displacements and discontinuous pressure which gives good precision and performance, and allows to work with linear elements, extending COMSOL capabilities that only supports quadratic elements near the incompressible limit.

Keywords: Incompressibility, mixed elasticity, COMSOL pde interfaces, COMSOL interface builder.

1. Introduction

COMSOL offers in the Structural Mechanics toolbox, a mixed formulation that represents the pressure as a dependent variable in addition to the displacement components, when near incompressibility is activated. This formulation is implemented with continuous quadratic interpolation of displacements and continuous linear interpolation of pressure, a good combination to avoid mesh locking and pressure modes (ref.1) but not the only one. The discontinuous interpolation of pressure allows the use of linear displacement elements, and the elimination of pressure at the element level, although this will not be possible with COMSOL architecture.

A 2D prototype is first easily developed with the pde interfaces of basic COMSOL and with this basis two new 3D interfaces are implemented with the help of the Physics Interface builder (PIB), one for linear elastic material and other for nonlinear hyperelastic material.

2. Modeling with the mathematical PDE interfaces

2.1. Linear plane strain elasticity

The displacement field $\{u,v\}$ of a linear plane deformation elasticity problem with zero volume forces can be obtained solving the 2 PDE for the stresses $\boldsymbol{\sigma}$:

$$\nabla\cdot\boldsymbol{\sigma}=0\rightarrow\left\{\begin{array}{l}\dfrac{\partial\sigma_x}{\partial x}+\dfrac{\partial\sigma_{xy}}{\partial y}=0\\[2ex]\dfrac{\partial\sigma_{xy}}{\partial x}+\dfrac{\partial\sigma_y}{\partial y}=0\end{array}\right\}\quad(1)$$

Stresses $\boldsymbol{\sigma}$ are linearly related to strains $\boldsymbol{\varepsilon}$,

$$\left\{\begin{array}{l}\sigma_x=\lambda e+2\mu\varepsilon_x\\\sigma_y=\lambda e+2\mu\varepsilon_y\\\sigma_{xy}=\mu\varepsilon_{xy}\end{array}\right\}\text{ with }\left\{\begin{array}{l}e=\varepsilon_x+\varepsilon_y+\varepsilon_z\\\varepsilon_z=0\\\sigma_z=\dfrac{-\nu}{E}(\sigma_x+\sigma_y)\end{array}\right\}\quad(2)$$

and strains $\boldsymbol{\varepsilon}$ are related with the displacements:

$$\left\{\begin{array}{ll}\varepsilon_x=\dfrac{\partial u}{\partial x}; & \varepsilon_y=\dfrac{\partial v}{\partial y}\\[2ex]\multicolumn{2}{c}{\varepsilon_{xy}=\dfrac{\partial u}{\partial y}+\dfrac{\partial v}{\partial x}}\end{array}\right\}\quad(3)$$

It is well known that the variable e represents de volumetric deformation and is related to the stress pressure σ_m through the bulk modulus κ:

$$\kappa=\frac{3\lambda+2\mu}{3}\;;\;\sigma_m=\frac{\sigma_x+\sigma_y+\sigma_z}{3}=\kappa e\quad(4)$$

$$\text{where}\left\{\begin{array}{l}\text{Lame Coefs:}\left\{\begin{array}{l}\lambda=\dfrac{\nu E}{(1+\nu)(1-2\nu)}\\[2ex]\mu=\dfrac{E}{2(1+\nu)}\end{array}\right.\\[2ex]\text{and}\left\{\begin{array}{l}E=\text{Young modulus}\\\nu=\text{Poisson modulus}\end{array}\right.\end{array}\right.\quad(5)$$

We can solve this 2D problem by means of the mathematical interface: "General form PDE" (pdeg), but defining two dependent variables $\{u,v\}$, instead of the usual one u. Than the conservative flux Γ has two components for each dependent variable: $\{\Gamma_{11},\Gamma_{12}\}$ and $\{\Gamma_{21},\Gamma_{12}\}$, and when COMSOL solves the 2 PDE defined by the general form:

$$\nabla\cdot\Gamma=0\rightarrow\left\{\begin{array}{l}\dfrac{\partial\Gamma_{11}}{\partial x_1}+\dfrac{\partial\Gamma_{12}}{\partial x_2}=0\\[2ex]\dfrac{\partial\Gamma_{21}}{\partial x_1}+\dfrac{\partial\Gamma_{22}}{\partial x_2}=0\end{array}\right\}$$

we are solving (1), (2) and (3) if:

* Define in the settings of "General form PDE":

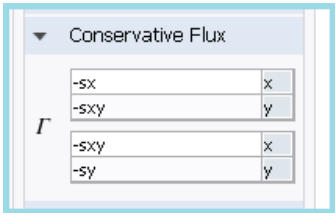

* Define the parameters:

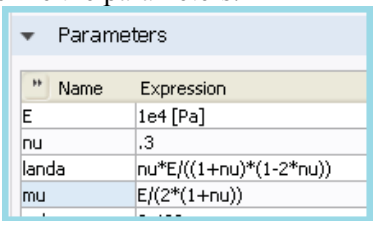

And define the new variables

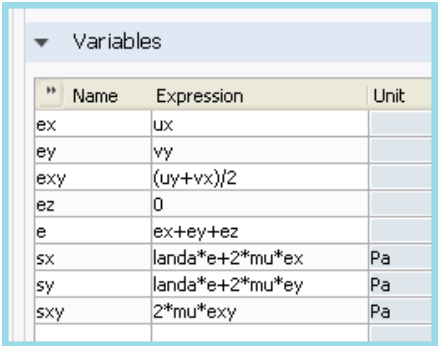

Now we have all the COMSOL power to define and mesh any 2D geometry, choose any shape function for the FEM approximation, apply boundary conditions, choose any solver and represent results.

For example, for the cantilever beam (ref 1) of rectangular cross section (base b=1, height $2c$=4) and length L=16 units, with transversal load P=27 at the free end, we show the

deformation (E=1e4) and the longitudinal stress (sx) for a mesh with 16x4 square elements. Only the upper half of the beam has been modeled, being the bottom line antisymmetric. All deformations are shown with an amplification factor of 5.

Figure 1 corresponds to Poisson modulus 0.3, and linear interpolation of displacements (d1). Maximum longitudinal stress sx (152) and transversal tip displacement (v) (0.64) adjust well to strength of materials formulas (162, 0.66) shown below table 1.

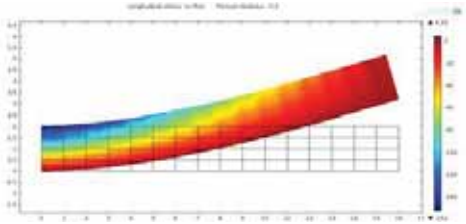

Figure 1 *sx stress for v*=0.3*, linear interpolation of displacements. (pdeg, d1)*

We can not use the value $\mu = 0.5$ because coefficient blows up (5), but we can approximate a nearly incompressible material with $\mu = 0.499$ and observe the mesh locking phenomena with useless stress values and shorter tip displacement (0.2), than expected (0.555).

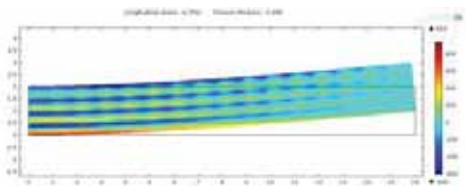

Figure 2 *sx stress for v=0.499, linear interpolation of displacements. (pdeg, d1)*

Nevertheless, it is immediate to check that locking disappears in this problem with quadratic shape functions (d2).

It is also easy to check that all previous results can be repeated with the regular solid mechanics interface of COMSOL (see table 1), but now you can activate "near incompressibility" to avoid mesh locking. Anyway, "near incompressibility" is formulated in COMSOL with quadratic shape functions for displacements and continuous linear for pressure (d2_p1c), but regular quadratic displacements perform well in this problem giving similar results with "near incompressibility" activated or not.

2.2. Linear mixed elasticity

Near incompressibility formulation is based on the mixed version of elasticity where a new independent variable p is added and two constitutive equations are considered, instead of the one in (2)

$$\left\{\begin{matrix}\sigma_x = -p + 2\mu\varepsilon_x \\ \sigma_y = -p + 2\mu\varepsilon_y \\ \sigma_{xy} = \mu\varepsilon_{xy}\end{matrix}\right\} \text{ and } \{-p = \lambda e\} \qquad (6)$$

Now you have 3 unknowns $\{u,v,p\}$ but one more condition $\{-p = \lambda e\}$ which transforms to the incompressibility condition

$$e = \varepsilon_x + \varepsilon_y + \varepsilon_z = \nabla \cdot \mathbf{u} = 0\,;$$

when $\nu = 0.5$. This way the mixed formulation is also valid in the incompressible limit.

COMSOL approximates the displacements:

$$u(\mathbf{x}) \approx \sum_j u_j N_j(\mathbf{x})\ ;\ v(\mathbf{x}) \approx \sum_j v_j N_j(\mathbf{x}) \qquad (7)$$

with finite element basis functions $N_j(\mathbf{x})$ and to find the coefficients $\{u_j,v_j\}$ uses the weak form of (1) or principle of virtual work

$$\int_\Omega \boldsymbol{\sigma}:\delta\boldsymbol{\varepsilon}\,d\Omega = \int_\Omega \mathbf{f}\cdot\delta\mathbf{u}\,d\Omega + \int_\Gamma \mathbf{t}\cdot\delta\mathbf{u}\,d\Gamma \qquad (8)$$

where the test functions (virtual displacements $\delta\mathbf{u}$) are constructed from (7). As a consequence, basis functions $N_j(\mathbf{x})$ appear one time differentiated in $\boldsymbol{\sigma}$ and $\delta\boldsymbol{\varepsilon}$, and its gradient has to be at least piecewise continuous in order to assure the existence of the integral in the first member of (8).

In the same way, the approximation of the dependent variable p is based on a second set $\tilde{N}_j(\mathbf{x})$ of basis functions:

$$p(\mathbf{x}) = \sum_j p_j \tilde{N}_j(\mathbf{x})$$

and the constraint (6) is set in integral form:

$$\int_\Omega (e + p/\lambda)\delta p\,d\Omega = 0 \qquad (9)$$

but now the functions $\tilde{N}_j(\mathbf{x})$ do not appear differentiated under the integral symbol, and can be element piecewise discontinuous if desired.

The new variable p and the condition (9) can be considered in COMSOL with the addition of a "weak form pde" defining the name "p" of the new variable, and the integrand of (9) in the settings of the interface

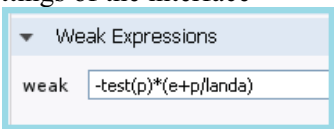

This simple way you have the mixed formulation of elasticity on, and you can choose any shape functions continuous for displacements and continuous or discontinuous for $p(\mathbf{x})$ among the Lagrange shape functions offered by COMSOL.

To avoid mesh locking near the incompressible limit ($\nu = 0.5$), linear continuous displacement interpolation with constant discontinuous $p(\mathbf{x})$ interpolation (d1_p0d), is a good choice (refs 1,3,4), as can be seen in figure 3.

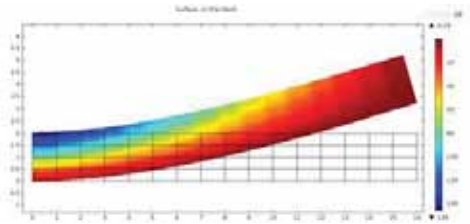

Figure 3 *sx stress for ν = 0.499, linear displacements and constant disc. pressure. (pdeg, d1_p0d)*

Numerical results for last, previous and other cases are reported in Table 1 of the appendix.

3. Interface implementation

"COMSOL Physics Interface Builder (PIB)" allows to implement this specific development as a new physics interface that we will call "mxe" and will appear in the wizard together with other standard COMSOL physic interfaces. This way we will have the new formulation at hand for any geometry and interpolation, where the definition of new variables and the use of the mathematical PDE interfaces is automatic.

COMSOL PIB uses a high level language that allows to define scalars vectors and matrixes functionality of the interface. For this reason we have been able to implement directly the general 3D case, as is shown in figure 4.

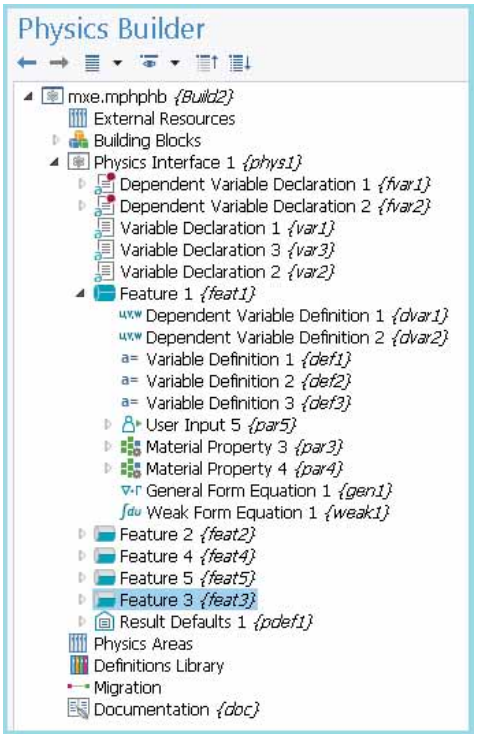

Figure 4 *Physics interface builder tree for 3D mixed elasticity (mxe).*

- Dependent variable declaration 1: declares the displacement **u** as a vector (3x1).
- Dependent variable declaration 2: declares *p* as a scalar quantity.
- Variable declaration 1: declares strain tensor *e* as a matrix (3x3).
- Variable declaration 2: declares stress tensor *s* as a matrix (3x3).
- Variable declaration 3: declares volumetric deformation *J* (previously *e*) as a scalar.

Feature 1 defines the contents of the variables and the PDE to solve. Features 2, 4 and 5 implement inputs for Dirichlet boundary conditions and feature 3 input for Neumann BC.

In feature 1:

- Dependent variable definition 1: defines continuous Lagrange shape functions for the interpolation of displacements (the degree is chosen by the user in runtime).
- Dependent variable definition 2: defines discontinuous Lagrange shape function for the interpolation of variable *p* (the degree is chosen by the user in runtime).
- Variable definition 1:
  e = 0.5*(gradient(u) + transpose(gradient(u)))
- Variable definition 2:
  s = –p*I+2*mu*e
- Variable definition 3:
  J = mxe.exx + mxe.eyy + mxe.ezz
- Material properties 3 and 4 define inputs for Lamé constants λ and μ.
- General form equation 1: defines $\Gamma = -s$
- Weak form equation 1: defines the integrand (J + p/landa)*test(p)

This new interface "mxe" was designed and tested as a prototype for minimum functionality, under COMSOL 4.2a, and has been imported to COMSOL 4.4, but does not benefit from the significant improvements of PIB 4.4 versus PIB 4.2a.

Once the interface is finished, you first save the file mxe.mphphb, and second, you have to include this file, under "development files", in the Physics Builder Manager window, whenever you want to use the interface. Alternatively, you can convert the file in a mxe.jar file which has to be included in the "plugins" directory of the COMSOL installation.

4. Modeling and implementation of the non linear case with large displacements and deformations.

Next step has been to improve the development to the non linear case of large displacements and deformations for "near incompressibility" with a neohookean material, using Green and second Piola as strain and stress tensors respectively (see refs 3 and 4).

4.1 Formulation

Given a trial for the displacement {u,v,w} and pressure p, compute the:

-Deformation gradient: $\mathbf{F}=\mathbf{I}+\nabla\mathbf{u}$

-Rigth Cauchy Green tensor: $\mathbf{C}=\mathbf{F}^T\mathbf{F}$

-Green deformation tensor: $\mathbf{E}=0.5\cdot(\mathbf{C}-\mathbf{I})$

-Volumetric deformation: $J=\frac{\Delta v}{v}=\sqrt{\det(\mathbf{C})}$

$-\mathbf{C}$ first invariant: $I_1=C_{xx}+C_{yy}+C_{zz}$

$-\bar{\mathbf{C}}$ first invariant: $\bar{I}_1=J^{-2/3}I_1$

-Neohookean isocoric energy density:

$$\bar{W}_s=0.5\mu(\bar{I}_1-3)$$

-Volumetric energy density: $W_v=0.5\kappa(J^2-1)$

-Pressure from displacement field: $pp=-\frac{\partial W_v}{\partial J}$

-Isocoric Piola II stress tensor: $\bar{\mathbf{S}}=2\frac{\partial\bar{W}_s}{\partial\mathbf{C}}$

-Piola II stress tensor: $\mathbf{S}=-pJ\mathbf{C}^{-1}+\bar{\mathbf{S}}$

-Internal Forces: $\mathbf{F}^{int}=\int_\Omega\mathbf{S}:\delta\mathbf{E}\,d\Omega$

-Constraint $(\mathrm{p}\rightarrow\mathrm{pp})$: $\int_\Omega(p-pp)\delta p\,d\Omega=0$

Finally, compute the residual:

$$\mathbf{R}(\mathbf{u})=\mathbf{F}^{int}(\mathbf{u})-\mathbf{F}^{ext},$$

add the constraint, and solve the nonlinear problem $\mathbf{R(u)}=0$ plus the constraint.

4.2 Interface implementation

The new interface is called "mxh" and its structure is very similar to the previous one in section 3. The following variables are declared: displacement **u** (3x1), scalar pressure p, F(3x3), eG (3x3), scalars: *J*, I1, Ib1, scalar energies *Wb*s and *W*v, scalar stress pressure pp, stress tensors (3x3) Sb and S, and scalar kapa. Then feature 1 defines the contents of the variables:

* input I,
* F = I + gradient(u), input C,
* eG = 0.5*(C−I)
* J=sqrt(C.1.1*C.2.2*C.3.3+2*C.1.2*C.1.3* C.2.3-C.1.1*C.2.3^2-C.2.2*C.1.3^2- C.3.3*C.1.2^2)
* I1 = C.1.1 + C.2.2 + C.3.3
* Ib1 = (J^(−2/3))*I1
* Wbs = 0.5*mu*(Ib1−3)
* Wv = 0.5*kapa*(J−1)^2
* pp = −d(Wv,J)
* Sb = 2*d(Wbs,C)
* S = −p*J*inverse(C) + Sb
* kapa = landa + (2/3)*mu

Input I, input C define the contents of tensor unity and tensor **C**, because it has not been possible to define directly nor **I**, nor **C** = transpose(F)*F.

For **C**, we will write on position (1,1): "Fxx^2+Fyx^2+Fzx^2", and so on.

Feature 1 also defines the two weak forms with the two integrands, to compute the internal forces and the contribution of the constraint to the system of equations:

- WF1 → S:test(eG)
- WF2 → (p−pp)*test(p)

Features 2, 3 ,4 and 5 implement the boundary conditions as before. This

way the new "mxh interface" will give the information COMSOL needs to compute the part of the residuals depending on the two unknown fields: displacement and pressure. COMSOL then proceeds with the trial and error Newton algorithm to obtain the solution if the non linear problem. All the solving machinery: Newton Raphson with damping (line search) and load stepping, is now available.

4.3 Results

We presents the results obtained with a torus subjected to compression (ref 2) as shown in figure 5. For modeling simplicity, the load is distributed as a constant vertical stress of value 1.5 over the outer half of the torus surface. Figure 5 also shows the discretization of one eighth of the torus, valid due to the symmetry of the problem.

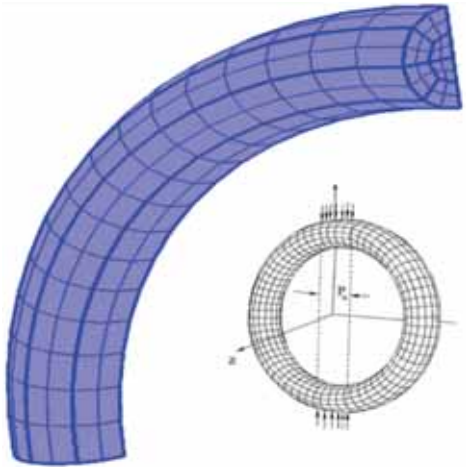

Figure 5 *Vertically compressed torus and discretization of one eighth of the torus respectively.*

Inner and outer radius of the torus are 8 and 10 respectively. Young and Poisson modulus are 1000 and 0.4999. All the results are presented with an amplification factor of 1.

Figure 6 shows Von Misses stress and deformation for the standard hyperelastic formulation obtained with the "solid mechanics interface" with linear interpolation of displacements.

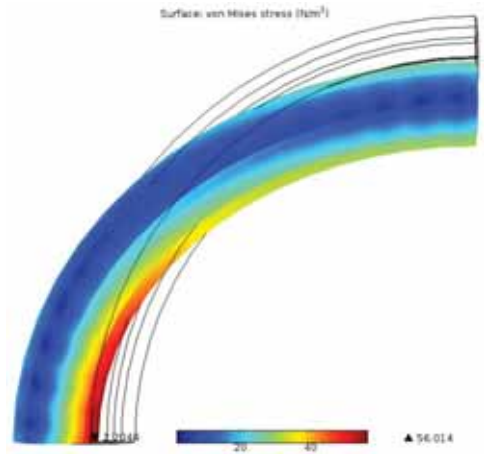

Figure 6 *Von Misses stress, hiper. linear displacements. (solid, d1)*

The expected mesh locking associated to this formulation is confirmed when the torus deforms much more in figure 7, that corresponds to the "near incompressibility" case of the "solid mechanics interface" with quadratic displacement and continuous linear pressure interpolation.

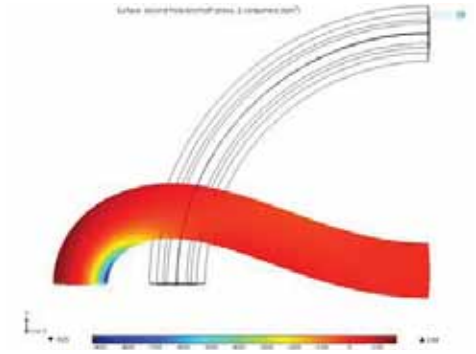

Figure 7 *PiolaII z stress, hiper. quadratic displacements and cont. linear pressure. (solid, d2_p1c)*

Solving with the new "mxe" interface shows improper deformation in figure 8, typical of a linear deformation formulation applied to a non linear large deformation problem.

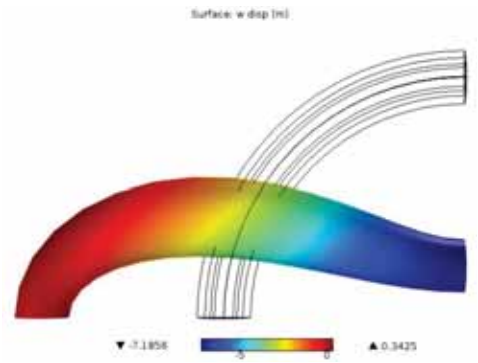

Figure 8 *Vertical elastic displacement, linear displacements and disc. constant pressure. (mxe, d1_p0d)*

Finally, figure 9 shows the deformation obtained with the new "Hyperelastic Mixed Model (mxh)" interface, with linear displacement and discontinuous constant pressure interpolation. This deformation is very similar to the one obtained in the case of figure 7, as well as the PiolaII stress, but now the computations are faster and the memory required much less.

Nevertheless, to obtain similar precision the number of elements has to be doubled and then the performance is similar.

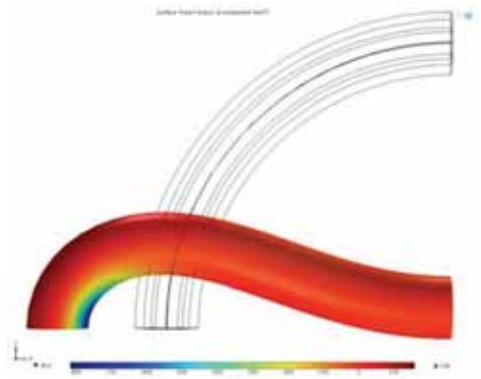

Figure 9 *PiolaII z stress, hiper. linear displacements and disc. constant pressure. (mxh, d1_p0d*)*

Numerical results for last, previous and other cases are reported in Table 2 of the appendix.

5. Conclusions

PDE interfaces are a powerful way to program and solve specific formulations not included in COMSOL basic software. Then, new developments can be implemented with the PIB in new physics interfaces that can be added to the standard ones, and general tools for meshing, solving and multiphysics interaction remain available. A prototype for mixed elasticity allowing discontinuous Lagrange interpolation of pressure, shows the process, and can be useful for teaching purposes and in incompressible elasticity applications where linear interpolation of displacements are required or convenient.

Extensions like considering stresses and deformations decoupled in volumetric and deviatoric parts, or the three field formulation considering also the volumetric deformation as

dependent variable, seem straightforward.

6. References

1. T. J. Hugues, "The Finite Element Method. (Linear Static and Dynamic Analysis)", *Prentice Hall*, 1987.
2. K. S. Chavan, B. P. Lamichhane, B. I. Wohlmuth, "Locking-free finite element methods for linear and non linear elasticity in 2D and 3D"Non linear continuum mechanics for finite element analysis", *Computer Methods in Applied Mechanics and Engineering,* **Volume** 196 issue 41-44 p. 4075-4086, 2007.
3. J. Bonet, R. D. Wood, "Non linear continuum mechanics for finite element analysis", *Cambridge University Press*, 1997.
4. G. Holzapfel, "Non linear solid mechanics", *John Wiley and Sons*, 2001.

7. Acknowledgements

This work and the participation in the conference has been possible with the support of the Applied Mathematics Department of the University of Basque Country.

8. Appendix

Numerical results are presented in two tables, as ratios of the obtained values to the exact.

Table 1: Plane strain cantilever beam ν=0,4999 except when indicated

Case	Stress ratio : σ_r	Displacement. ratio: v_r
pdeg, d1, ν=0.3	0.9383	0.96965
pdeg , d1		0.35715
pdeg, d1_p0d, ν=0.3	0.9012	0.97866
pdeg, d1_p0d	0.8951	0.98918
pdeg , d1_p1c		0.07768
pdeg , d2	1	0.99999
pdeg, d2_p1d	1	0.99998
solid, d1		0.35715
solid, d2_p1c	1	0.99999

Exact formulas for the cantilever beam, considering shear deformation, are shown below:

$$I=\frac{2bc^3}{3}\ ;\ \tilde{E}=\frac{E}{(1-\nu^2)}\ ;\ \tilde{\nu}=\frac{\nu}{(1-\nu)}$$

$$\tilde{v}_{\max}=\frac{PL^3}{3\tilde{E}I}\ ;\ \left(\tilde{v}_{\max}\right)_s=\tilde{v}_{\max}\left(1+(4+5\tilde{\nu})\frac{c^2}{2L^2}\right)$$

$$\left(\tilde{\sigma}_z\right)_{\max}=\frac{PLc}{2I}\ ;\ \sigma_r=\frac{\left(\sigma_z\right)_{\max}}{\left(\tilde{\sigma}_z\right)_{\max}}\ ;\ v_r=\frac{v_{\max}}{\left(\tilde{v}_{\max}\right)_s}$$

Table 2: 3D compressed torus

Case	Stress ratio : σ_r	Displacement. ratio: v_r
Solid, d1		0.1287
Solid, d2	Does not	converge
Solid, d2_p1c	1.0244	0.9998
Solid, d2_p1c*	1.0000	1.0000
mxe, d1_p0d		0.8481
mxh, d1_p0d	0.7763	0.9269
mxh, d1_p0d*	0.9003	0.9808
mxh, d2_p1d	1.0078	0.9997
mxh, d2_p1d*	1.0011	1.0000

* star means double number of elements
Solid, d2_p1c* is considered the exact solution.
PiolaII "z" component is the reference stress.

$$\sigma_r=\frac{\left(S_z\right)_{\max}}{\left(\tilde{S}_z\right)_{\max}}\ ;\ v_r=\frac{w_{\max}}{\tilde{w}_{\max}}$$

Generalized Plane Strain Problem: Application to Heterostructure Nanowires

H. T. Mengistu[1*] and A. Garcia-Cristóbal[1]

[1] Institute of Material Science, University of Valencia, P.O.Box 22085, E-46071, Valencia, Spain
*Heruy.Mengistu@uv.es

Abstract: In this work we first present a general theoretical framework for the two-dimensional (2D) modeling of the elastic deformation of translationally invariant three-dimensional (3D) systems. This approach is called here the Generalized Plane Strain (GPS) problem. Then, a computational methodology is developed and implemented on the COMSOL Multiphysics software platform, that allows to solve efficiently a wide class of problems. Finally, we apply the procedure to the calculation of the strain fields in lattice - mismatched heterostructure (core-shell) nanowires.

Keywords: Structural Mechanics, Finite Element Method, Generalized Plane Strain, Nanowires.

1. Introduction

Numerical simulations of discretized three-dimensional (3D) elastic problems are in general expensive in terms of memory requirements and computing time. Therefore, the disposal of two-dimensional (2D) approaches to problems originally posed in a 3D geometry is always desirable, since they reduce significantly the computing resources needed. One standard approach accomplishing this goal is the Plane Strain (PS) approximation, in which the antiplane displacement $\boldsymbol{u_3}$ is forced to vanish [1]. However, there are many problems where the elastic medium develops out-of-plane axial ($\boldsymbol{\varepsilon_{33}}$) and shear ($\boldsymbol{\varepsilon_{13}}$ and $\boldsymbol{\varepsilon_{23}}$) strain components that cannot be captured by the above hypothesis.

In Sec. 2 we report on a more general 2D approach, based on the idea that for (indefinite) systems with geometry, material properties and loads independent of the coordinate $\boldsymbol{x_3}(\equiv \boldsymbol{z})$, the strain depends only on the in-plane coordinates, $\boldsymbol{\varepsilon_{ij}}(\boldsymbol{x_1}, \boldsymbol{x_2})$. Under this sole hypothesis, the original 3D problem can be reformulated into a 2D mathematical framework called here the Generalized Plane Strain (GPS) problem [2]. The GPS problem is expected to be a good approximation for finite but long 3D systems, where the state of deformation is mostly uniform along the $\boldsymbol{x_3}$ axis (except near the end surfaces).

In order to perform numerical calculations based on the GPS approach, an attractive option is to use the finite element method, as implemented, for instance, in the COMSOL Multiphysics software platform. In Sec. 3 we give details of how to arrange the GPS problem in a way that can be easily implemented within the COMSOL software.

Finally, the above procedure is illustrated in Sec. 4 by calculating the

strain fields in a free-standing lattice-mismatched core-shell nanowire.

2. The Generalized Plane Strain Problem

We first recall the general formulation of a linear elasticity 3D problem in a domain *D*. Cartesian index notation ($\boldsymbol{i,j,k,l = 1,2,3}$ and $\boldsymbol{\alpha,\beta = 1,2}$) and Einstein summation convention for repeated indices are used throughout the paper.

The kinematic relations connecting the displacement $\boldsymbol{u_i}$ with the strain tensor $\boldsymbol{\varepsilon_{ij}}$ are:

$$\boldsymbol{\varepsilon_{ij}} = \frac{1}{2}\left(\frac{\partial u_i}{\partial x_j} + \frac{\partial u_j}{\partial x_i}\right) \quad (1)$$

The equilibrium equations are given by:

$$\frac{\partial \sigma_{ij}}{\partial x_j} = -f_i \quad (2)$$

where σ_{ij} is the stress tensor, which is related to the strain through the constitutive relation:

$$\sigma_{ij} = C_{ijkl}\varepsilon_{kl} \quad (3)$$

or, schematically,

$$\sigma = C : \varepsilon$$

where C_{ijkl} are the elastic constants. f_i is the force per unit voume acting on the elastic body.

It can be shown that the particular problem of an heterogeneous lattice-mismatched body containing regions with different elastic constants $[C_{ijkl}(\boldsymbol{r})]$ and lattice parameters $[a_k(\boldsymbol{r})]$ can be mapped to a standard elastic problem by the introduction of an equivalent body force:

$$f_i^{(0)} = \frac{\partial}{\partial x_j}\left[\, C_{ijkl}(\boldsymbol{r})\varepsilon_{kl}^{(0)}(\boldsymbol{r})\right]$$

$$\varepsilon_{kl}^{(0)}(\boldsymbol{r}) = \frac{a_k^{(\mathrm{ref})} - a_k(\boldsymbol{r})}{a_k(\boldsymbol{r})}\,\delta_{kl}$$

where $a_k^{(\mathrm{ref})}$ are the parameters of a convenient reference lattice. In this case, the total deformation with respect to the local lattice is given by $\varepsilon_{kl}^{(T)}(\boldsymbol{r}) = \varepsilon_{kl}^{(0)}(\boldsymbol{r}) + \varepsilon_{kl}(\boldsymbol{r})$.

The equations (1), (2) and (3), supplemented with appropriate boundary conditions constitute the complete mathematical definition of a linear elasticity 3D problem.

Direct simulations of 3D problems require large computing resources. However, if certain additional conditions are required, the above framework can be cast into a mathematically 2D problem. Those conditions are as follows: Let us assume that we have a system, indefinite along one longitudinal direction (taken to be the $x_3 \equiv z$ axis), whose transverse geometrical description (i.e., cross-section), material properties, loads, and eventual boundary or interface conditions are independent of the x_3 coordinate. For such a system all the cross sections along the longitudinal axis can be considered to be at identical conditions and, therefore, one can make the ansatz [2]:

$$\varepsilon_{ij} = \varepsilon_{ij}(x_1, x_2) \quad (4)$$

By using Eq. (4) together with Eq. (1) the displacement field is shown to have the following structure [2]:

$$\begin{aligned} u_1 &= U_1(x_1,x_2) - \frac{A}{2}{x_3}^2 + \Theta\, x_2 x_3 \\ u_2 &= U_2(x_1,x_2) - \frac{B}{2}{x_3}^2 - \Theta\, x_1 x_3 \\ u_3 &= U_3(x_1,x_2) + (Ax_1 + Bx_2 + C)x_3 \end{aligned} \quad (5)$$

The corresponding strain can then be written as:

$$\varepsilon_{ij} = \varepsilon_{ij}^{(U)} + \varepsilon_{ij}^{(ABC\Theta)} \quad (6)$$

$$\varepsilon_{ij}^{(U)} \leftrightarrow \begin{pmatrix} \frac{\partial U_1}{\partial x_1} & \frac{1}{2}\left(\frac{\partial U_1}{\partial x_2}+\frac{\partial U_{j2}}{\partial x_1}\right) & \frac{1}{2}\frac{\partial U_3}{\partial x_1} \\ sym. & \frac{\partial U_2}{\partial x_2} & \frac{1}{2}\frac{\partial U_3}{\partial x_2} \\ sym. & sym. & 0 \end{pmatrix}$$

$$\varepsilon_{ij}^{(ABC\Theta)} \leftrightarrow \begin{pmatrix} 0 & 0 & \frac{1}{2}\Theta\, x_2 \\ sym. & 0 & -\frac{1}{2}\Theta\, x_1 \\ sym. & sym. & Ax_1 + Bx_2 + C \end{pmatrix}$$

and the equilibrium equation (2) becomes:

$$\frac{\partial}{\partial x_\alpha}\left[C_{i\alpha kl}\varepsilon_{kl}^{(U)}\right] + \frac{\partial}{\partial x_\alpha}\left[C_{i\alpha kl}\varepsilon_{kl}^{(ABC\Theta)}\right] = -f_i \quad (7)$$

Here, U_i is the mathematically 2D (i.e., dependent only on (x_1, x_2)) displacement, C is the axial strain, A and B are bending strains, and Θ characterizes the torsion of the system.

The above equations must be supplemented with conditions on the boundary limiting the cross section of the body, and boundary conditions at the far end surfaces $S_\pm$ (at $x_3 \to \pm\infty$). These latter conditions are usually required not pointwise but in an integrated sense, e.g, by specifying the average force and torque:

$$\boldsymbol{F} = \int_{S_+} \boldsymbol{t}\, dS \quad \text{and} \quad \boldsymbol{M} = \int_{S_+} \boldsymbol{r}\times\boldsymbol{t}\, dS \quad (8)$$

where $t_i = \sigma_{i3}$ are the components of the traction vector field at S_+.

The set of equations (4)-(7), together with boundary conditions (8), define a mathematical 2D problem, where we have to find displacement $U_i(x_1, x_2)$ and constants (A, B, C, Θ). This problem is here called the Generalized Plane Strain (GPS) problem. We note that the GPS approach is able to accommodate any cross section geometry and elastic symmetry, and a wide range of compatible boundary conditions, corresponding to different kinds of externally applied stresses (such as hydrostatic pressure, bending moments...). The GPS problem refers of course to an idealized situation, but it is supposed to be a good approximation for a 3D finite but long system fulfilling the translational invariance conditions mentioned above. The quality of this approximation is illustrated by the numerical simulations in Sec. 4.

3. COMSOL Multiphysics implementation

In order to perform numerical calculations based on the GPS approach, an attractive option is to use the finite element method as implemented in the Structural Mechanics module of the COMSOL Multiphysics software platform [3]. In this module the elastic equilibrium condition is implemented via the virtual work principle, leading to a weak formulation of Eq. (2), which can be written schematically as [4]:

$$\mathbf{0} = \int_{\boldsymbol{D}} \boldsymbol{u_{test}} \cdot (\boldsymbol{\nabla}.\boldsymbol{\sigma} + \boldsymbol{f}) \quad (9)$$

where $\boldsymbol{u_{test}}$ are the test functions for the displacement field.

The Structural Mechanics module allows to use the standard Plane Strain approximation within the Plane Strain application mode [4]. However, neither the antiplane displacement variable $\boldsymbol{U_3}$ nor the strain $\boldsymbol{\varepsilon_{ij}^{(ABC\Theta)}}$ are available or easily implementable in the Plane Strain application mode, so it is not useful to make computations of the GPS problem.

We have instead implemented the GPS problem within the Structural Mechanics module of COMSOL by means of the following procedure. First, we note that, by using Eq. (6), the weak condition (9) becomes:

$$\int_D \left(-\boldsymbol{C}:\boldsymbol{\varepsilon}^{(U)}\cdot\boldsymbol{\varepsilon}_{test}^{(U)}+\boldsymbol{f}\cdot\boldsymbol{U}_{test}\right)+\boldsymbol{surf.term}+$$
$$+\int_D \left(-\boldsymbol{C}:\boldsymbol{\varepsilon}^{(ABC\Theta)}\cdot\boldsymbol{\varepsilon}_{test}^{(U)}-\boldsymbol{\sigma}\cdot\boldsymbol{\varepsilon}_{test}^{(ABC\Theta)}\right)=\mathbf{0} \quad (10)$$

The terms in the first line of Eq. (10) correspond to the "partial" elastic problem associated to displacement $\boldsymbol{U_i}(\boldsymbol{x_1},\boldsymbol{x_2})$. This problem can be solved by using the 3D application mode on a finite length slice of the original infinitely extended system. The cross section is conveniently meshed. In order to force the dependence on $(\boldsymbol{x_1},\boldsymbol{x_2})$ we use the following trick: We mesh the length of the slice with only one quadrilateral element (what simply doubles the total number of elements used to mesh the cross section) and require periodic boundary conditions to connect the top and bottom surfaces of the slice. This trick effectively imposes that the numerical solution, that is to be interpreted as $\boldsymbol{U_i}$, does not depend on $\boldsymbol{x_3}$.

However, it still remains to incorporate the contribution of $\boldsymbol{\varepsilon}^{(\boldsymbol{ABC}\Theta)}$ to the weak condition (10). This is implemented as follows: Since $(\boldsymbol{A},\boldsymbol{B},\boldsymbol{C},\Theta)$ can be considered as degrees of freedom that are constant throughout the modeled cross section, it is convenient to include them in the COMSOL program as extra unknown global variables [5]. Then, the contributions containing those variables in the second line of Eq. (10) are added as weak terms to the 3D problem related to $\boldsymbol{U_i}$ by means of the "Weak Contribution" feature of COMSOL [5].

The boundary conditions (8) can eventually be implemented by making use of the "Weak Constraint" feature of COMSOL [5].

The solution of the 3D application mode modified as explained above gives the desired results for $\boldsymbol{U_i}(\boldsymbol{x_1},\boldsymbol{x_2})$ and constants $(\boldsymbol{A},\boldsymbol{B},\boldsymbol{C},\Theta)$.

4. Numerical Results

In order to illustrate the GPS problem and its implementation in COMSOL we have performed numerical calculations of the strain distribution in an infinite hexagonal core-shell nanowire. The core is made of Ge and the shell is made of Si. Both materials exhibit cubic elastic symmetry. The longitudinal axis coincides with the [111] crystallographic direction. In Fig. 1(a) we display the cross section mesh used for the GPS problem. The X- and Y-axes are taken along $[\bar{1}10]$ and $[11\bar{2}]$ crystallographic directions, respectively. We assume that the nanowire is free from external tractions and body forces, so that the strain is solely induced by the internal lattice-mismatch body force $f_i^{(0)}$. Material parameters can be found in Table I. In this case, the GPS solution presents axial strain $C=-0.0079$, and no bending $(A,B=0)$ nor torsion $(\Theta=0)$, though there is a nonnegligible warping of the cross section $(U_3\neq 0\rightarrow \varepsilon_{13},\varepsilon_{23}\neq 0)$. In order to test the quality of our GPS approach we have also performed standard 3D calculations for a finite but long nanowire. The longitudinal mesh employed is displayed in Fig. 1 (b).

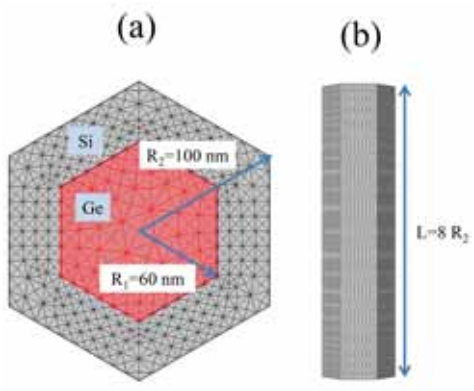

Figure 1 *Geometry of the core-shell nanowire investigated with details about the meshes employed.*

	Si	Ge
Lattice parameter		
a_0 (Å)	5.430	5.652
Elastic constants		
C_{11}(GPa)	162.0	128.5
C_{12}(GPa)	62.8	45.7
C_{44}(GPa)	77.2	66.8

Table 1: *Parameters used in the numerical calculations.*

In Fig. 2 we present the comparison of X-axis linescans of the strain (cylindrical) components (ε_{rr}, $\varepsilon_{\phi\phi}$, ε_{zz}, ε_{rz}, $\varepsilon_{\phi z}$ and $\varepsilon_{r\phi}$) corresponding to the GPS problem and to the central cross section of the finite 3D problem. We see that the agreement between the strain profiles of both approaches is excellent virtually indistinguishable in the figure thus showing the reliability of the GPS approach to simulate the central region of large aspect-ratio elastic problems.

Figures 3 and 4 show details of the total strain ($\varepsilon^{(T)} = \varepsilon^{(0)} + \varepsilon$) distribution throughout the nanowire cross section, as obtained within the GPS approach. We show only the radial, $\varepsilon_{rr}^{(T)}(x_1, x_2)$, and angular, $\varepsilon_{\phi\phi}^{(T)}(x_1, x_2)$, components. The Ge core is essentially compressed (negative strain) as a result of the smaller lattice constant of the shell material (Si). On the other hand, the angular (radial) strain in the shell is tensile (compressive) near the interface with the core, but tends to relax towards zero when going to the nanowire surface.

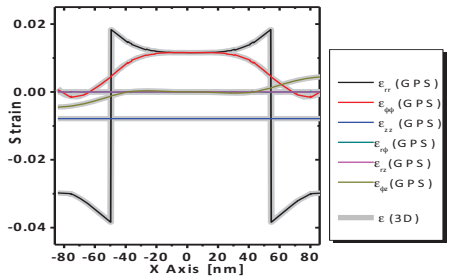

Figure 2 *Comparison of the strain components obtained from the GPS approach and the direct 3D calculations.*

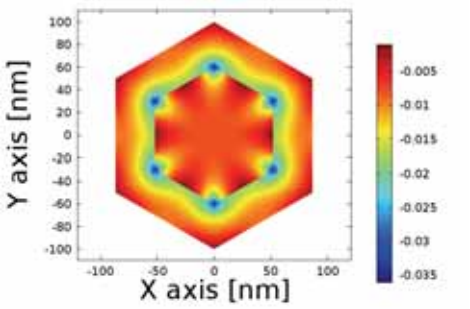

Figure 3 *Total strain* $\varepsilon_{rr}^{(T)}(x_1, x_2)$.

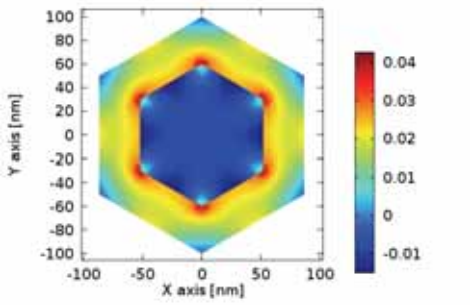

Figure 4 *Total strain* $\varepsilon_{\phi\phi}^{(T)}(x_1, x_2)$.

5. Conclusions

In this paper we have presented a theoretical framework called Generalized Plane Strain problem (GPS) and implemented a computational methodology within the COMSOL Multiphysics software platform that allows efficient and inexpensive numerical calculations of the strain distribution in a wide class of translationally invariant systems. We have performed model simulations in a core-shell nanowire that show an excellent agreement when compared with direct 3D calculations for a long nanowire. This agreement shows the reliability of the GPS approach to obtain efficiently accurate strain distributions for wire-like systems.

6. References

1. M. H. Saad, *Elasticity: Theory, Applications, and Numerics* (Elsevier Academic Press, Amsterdam, 2005).

2. S. G Lekhnitskii, *Theory of elasticity of an anisotropic elastic body* (San Francisco: Holden-Day, San Francisco, 1963).

3. http://www.comsol.com/comsol-multiphysics. In this work we have employed COMSOL Multiphysics version 4.2a.

4. See the *Structural Mechanics Module User's Guide* for more details.

5. See the *COMSOL Multiphysics User's Guide* for more details.

7. Acknowledgement

This work has been financially supported by the European Union through the Grant Agreement No.265073-NANOWIRING of the Seventh Framework Program, and by the Ministry of Finances and Competitiveness (MINECO) of Spain through Grants CSD2010-00044 of the Programme ''Consolider Ingenio 2010'' and MAT2012-33483.

NO_x Remediation in Monolith Channel with NH_3-SCR

U. De La Torre[1*], F. Dhainaut[2], B. Pereda-Ayo[1] and J.R. González-Velasco[1*]

[1]Chemical Engineering Department, Faculty of Science and Technology, University of the Basque Country, UPV/EHU, Leioa, 48940, Spain
[2]UCCS, Université Lille 1, Villeneuve d'Ascq, France.
*Presenter: unai.delatorre@ehu.es; Corresponding author: juanra.gonzalezvelasco@ehu.es

Abstract: In this work kinetic modelling was used for modelling NH_3 selective catalytic reduction (SCR) of NO_x over a Cu-ZSM-5 catalyst. First, in order to determine the number of active sites in the catalyst, NH_3 adsorption-desorption experiments were performed and compared with experimental data. Then, an SCR kinetic model with six elementary reactions has been created. In our model, a 3D single channel is the NO_x reduction environment. In order to compare channel geometries, in addition to typical square channels, cylindrical shapes where also simulated. The removal of NO_x with different NO/NO_2 ratios in the feed has been simulated with parameters determined by fitting experimental data at 200 ºC and the conversion of NO_x is predicted fairly well. The main objective of this study is to create a model which fits our available experimental data as well as verify if the use of 2D axisymmetric space dimension in COMSOL is a valid geometry in order to decrease computational time or, on the contrary, high differences in the catalytic behavior advice to rule out this type of geometry.

Keywords: NH_3-SCR catalyst, monolith, channel, NO_x elimination.

1. Introduction

Diesel engines have the highest thermal efficiency, and consequently release less CO_2 into the atmosphere as main gas contributing to global warming. The engine operates in excess of oxygen, with an air-to-fuel ratio higher than stoichiometric, making the conventional three-way catalyst (TWC) ineffective under such net oxidizing environment [1]. Among different alternatives, engine manufacturers and catalyst suppliers are considering the use of SCR with NH_3 as reductant for NO_x removal in end-of-pipe technologies. Additionally, the automobile application requires the use of structured catalysts (Figure 1) in order to limit the pressure drop under real operation. Thus, the walls of a cordierite monolith (2 cm in length and diameter, 175 channels) were washcoated with a layer of previously exchanged Cu-zeolite catalyst where NH_3-SCR reaction occurs.

2. Use of COMSOL Multiphysics

The modelling was performed with COMSOL Multiphysics version 4.4 and the reaction engineering module. This program takes diffusion and convection into account along with kinetics of chemical reactions. The

behavior of a single channel was simulated for three different application models. First, NH_3 adsorption-desorption experiments were fitted in order to determine the amount of adsorption sites, which is a critical value when performing the NH_3-SCR model. Then, SCR model consisting of six reactions was computed in square geometry channel varying the NO/NO_2 feeding ratio in order to find out sensitivity of the model to changes in the feed composition and verify agreement with results in literature. Finally, the same model was used in a cylindrical channel to compare the SCR reaction behavior with different geometries. Table 1 shows the general parameters for the model

Parameter	Value
Catalyst Mass (mg)	6.0
ρ (kg·m^{-3})	0.85
μ (Pa·s)	3.605×10^{-5}
v_0 (m^3·s^{-1})	2.76×10^{-7}

Table 1 *General parameters.*

Diffusivity coefficients where calculated according to Wilke-Lee formulas and are shown in Table 2.

Species	Value (m^2·s^{-1})	Species	Value (m^2·s^{-1})
NO	6.86×10^{-5}	N_2	6.48×10^{-5}
O_2	7.74×10^{-5}	H_2O	7.83×10^{-5}
NH_3	7.06×10^{-5}	N_2O	4.88×10^{-5}
NO_2	5.02×10^{-5}		

Table 2 *Diffusivity of gases at 473 K.*

2.1 Reactions and kinetics

In our model, we consider that NH_3 has to be adsorbed at the surface of the catalyst before reacting with NO in the gas phase. This step can be written as

$$NH_3 + * \rightleftarrows NH_3^* \quad (1)$$

Reaction (1) has also been used to determine the amount of adsorption sites available in our experimental results.

A second step was considered for the oxidation of ammonia, in which chemisorbed ammonia reacts with O_2 to produce N_2 and H_2O:

$$2NH_3^* + \tfrac{1}{2}O_2 \rightarrow N_2 + 3H_2O + 2* \quad (2)$$

On the other hand, the standard SCR reaction occurs between adsorbed NH_3 species and NO and O_2 reacting from the gas phase:

$$4NH_3^* + 4NO + O_2 \rightarrow 4N_2 + 6H_2O + 4* \quad (3)$$

In addition, three more side-reactions can occur simultaneously: fast SCR, slow SCR and N_2O formation

$$2NH_3^* + NO + NO_2 \rightarrow 2N_2 + 3H_2O + 2* \quad (4)$$

$$4NH_3^* + 3NO_2 \rightarrow 3.5N_2 + 6H_2O + 4* \quad (5)$$

$$2NH_3^* + 2NO_2 \rightarrow N_2 + N_2O + 3H_2O + 2* \quad (6)$$

NO oxidation was not considered as our catalyst oxidizes NO only at temperature above 350 ºC. The rate equations for reactions (1)-(6) over Cu-ZSM-5 were borrowed from literature [2]:

$$r_1 = k_{1,f} C_{NH_3} \theta_S - k_{1,b} \theta_{NH_3} \quad (7)$$

$$r_2 = k_2 C_O \theta_{NH_3} \quad (8)$$

$$r_3 = k_3 C_{NO} \theta_{NH_3} \quad (9)$$

$$r_4 = k_4 C_{NO} C_{NO_2} \theta_{NH_3} \quad (10)$$

$$r_5 = k_5 C_{NO} \theta_{NH_3} \quad (11)$$

$$r_6 = k_6 C_{NO} \theta_{NH_3} \quad (12)$$

The units for the rate constants were given in mol·(mol sites)$^{-1}$·s^{-1}. The rate constants with temperature were assumed to follow the Arrhenius expression:

$$k_i = A_i \exp\left(-\frac{E_i}{RT}\right) \quad (13)$$

Frequency factors and activation energies for equation (13) were assumed as in ref. [2], with values shown in table 3.

Frequency Factors	Values	Activation Energy ($kJ \cdot mol^{-1}$)	Values
A_1	0.93	E_1	0
A_{-1}	1.0×10^{-11}	E_{-1}	181.5
A_2	1.2×10^{-11}	E_2	162.4
A_3	2.3×10^{-8}	E_3	84.9
A_4	1.9×10^{-12}	E_4	85.1
A_5	1.1×10^{-7}	E_5	72.3
A_6	3.6×10^{-4}	E_6	43.3

Table 3 *Frequency factors and activation energies for reactions (1)-(6).*

It is worth to note that units of frequency factor should be in agreement with dimension homogeneity of equations (7)-(12), needing to be adapted for COMSOL simulation program.

2.2 Model Geometry

The monolithic reactor consists of a ceramic material with parallel square channels with cross sectional dimensions of about 1×1 mm (Fig. 1). The walls of the channels are coated with a porous Cu-ZSM-5 catalyst, which is later defined as "washcoat". The model represented a single channel and it is thus assumed that all other channels in the monolith operated under identical conditions. The model channel edge was 1 mm, the channel length was 2 cm and, considering the small washcoat width (8 μm, estimated from SEM images of the catalyst), it was assumed that reactions occurred in the walls of the cordierite monolith. In contrast, in the case of the cylindrical channel, a 1 mm diameter channel was drawn.

2.3 Governing equations initial and boundary conditions

The governing equations for the Laminar Flow are listed below:

$$\rho(\mathbf{u}\cdot\nabla)\mathbf{u} = \nabla\cdot\left[-p\mathbf{I}+\mu\left(\nabla\mathbf{u}+(\nabla\mathbf{u})^T\right)-\frac{2}{3}\mu(\nabla\cdot\mathbf{u})\mathbf{I}\right]+\mathbf{F} \quad (14)$$

$$\nabla\cdot(\rho\mathbf{u}) = 0 \quad (15)$$

For the momentum balance a laminar inflow was used, defining a flow rate and also no slip and 0 Pa outlet pressure boundary conditions were used at the monolith surface.

On the other hand, the governing equations for the Transport of Diluted Species are the following:

$$\frac{\delta c_i}{\delta t}+\nabla\cdot(-D_i\nabla c_i)+\mathbf{u}\cdot\nabla c_i = R_i \quad (16)$$

$$\mathbf{N}_i = -D_i\nabla c_i+\mathbf{u}c_i \quad (17)$$

The velocity field has been linked with the Laminar Flow. The concentration initial values for all the species were set as 0 $mol\cdot m^{-3}$ and convective flow was defined at the outflow. Transport of Diluted Species was linked with Surface Reaction by a Flux defined in the walls of the channel according to the following equation:

$$-\mathbf{n}\cdot\mathbf{N}_i = \mathbf{N}_{0,i} \quad (18)$$

Finally, the governing equations for the Surface Reaction are written as follows

$$\frac{\delta c_{S,i}}{\delta t}+\nabla_t\cdot(-D_i\nabla_t c_{S,i}) = R_{S,i} \quad (19)$$

$$\mathbf{N}_{S,i} = --D_i\nabla_t c_{S,i} \quad (20)$$

$$\theta_i = \frac{c_{S,i}\sigma_i}{\Gamma_s} \quad (21)$$

$$\frac{\delta c_{S,i}}{\delta t} = R_{b,i} \quad (22)$$

Initially, the number of free sites has been defined as θ_s=1 and the boundary condition that no flux at the edges of the channel was applied for all the species.

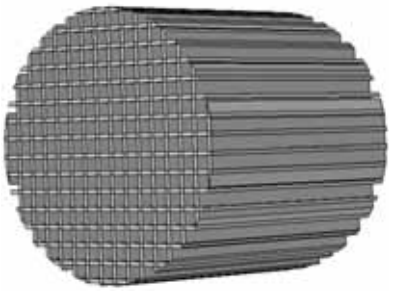

Figure 1 *Cordierite monolith (2 cm in length and diameter).*

2.4 Simulated Conditions

2.4.1 NH_3-TPD.

NH_3-TPD experiments were performed in an Autochem II set-up located in the TQSA group laboratories. There is a difference between the experimental NH_3 concentration (50,000 ppm in Ar, total flow $2.16 \cdot 10^{-6}$ $m^3 \cdot s^{-1}$) and the modeled one in COMSOL, where the inlet composition for the channel was 5000 ppm NH_3, as the latter let us observe more accurately the catalyst saturation curve. The adsorption-desorption simulations were carried out at 373 K in order to compare with available data. For this section, a simplified 2D model with axial symmetry has been used, thus saving big amount of memory and computational time compared with using 3D models.

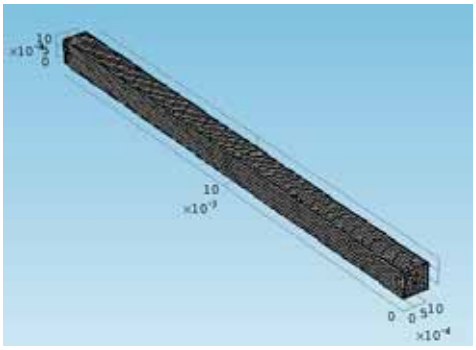

Figure 2 *Mesh used consisting of a total of 38,000 elements.*

2.4.2 SCR experiments.

For the SCR simulations, the inlet composition was 750 ppm NO, 750 ppm NH_3, 6% O_2, in Ar as balance. NO/NO_2 ratios used in the modeling where 1:0 (only NO in the feed), 1:1 (equimolecular feeding) and 0:1 (only NO_2 in the feed). The flow rate and temperature of the gas are 2.76×10^{-7} m^3 s^{-1} and 473 K, respectively. At these conditions the space velocity resulted in 90,000 h^{-1} and the average residence time 0.05 s. In this case, a 3D model has been used, and the simulations were computed with both square and cylindrical channel geometries.

2.5 Model Simulation

When simulating the program, first only the Laminar Flow module was used. Then, Transport of Diluted Species and Surface Reactions modules have been incorporated, as the velocity field has been linked previously. The resulting model had 31,325 degrees for the stationary solver and a virtual

memory of 1.75 GB was used. On the other hand, the time dependent solver had about 57,000 degrees of freedom and 20,510 internal DOFs, which required 1.92 GB virtual memory. In order to achieve convergence it was necessary to simulate the Time Dependent solver with an unscaled method for the absolute tolerance and the steps taken by the solver where considered strict.

2.6 Mesh

The mesh used in the SCR simulations is shown in Figure 2. The mesh is fine enough in the gas channel and the wall. A thinner mesh in the washcoat should give a more precise profile inside the catalyst layer, but at the cost of spending unavailable memory.

3. Results

3.1 NH_3 adsorption-desorption

The amount of NH_3 adsorption sites is a critical factor in NH_3-SCR modelling. For this purpose, the amount of adsorbed NH_3 in a real catalyst bed has been calculated from TPD experiments (Figure 3), which resulted in 5.742×10^{-4} mol NH_3. It can be observed an initial uptake of ammonia during the first 700 seconds. After this time, NH_3 concentration increases gradually while the catalyst is being completely saturated.

In the channel geometry, an ammonia slip is occurring and the COMSOL calculation has been considering that reaction only occurs on the walls of the monolith. Consequently, to determine the concentration of adsorption sites, the amount of adsorbed NH_3 calculated must be equal to the experimental one.

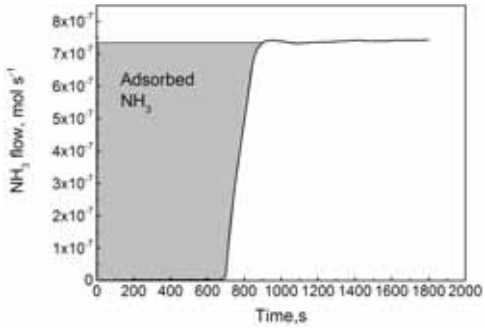

Figure 3 *NH_3-TPD experiment for NH_3 adsorption-desorption with powder form catalysts.*

The ending solver time must be higher compared to the powder form TPD example, because the percentage of ammonia interacting with the catalyst is much lower.

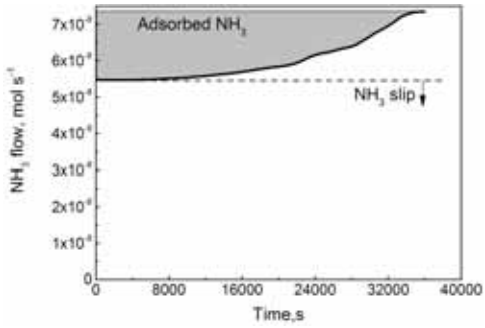

Figure 4 *NH_3 adsorption evolution for a square channel, calculated with COMSOL.*

Figure 4 shows the calculated NH_3 adsorption-desorption flow. In this case, during the first 6000 seconds, ammonia at the outlet is due to the NH_3 slip and afterwards the concentration starts increasing until the steady-state is reached.

Finally, from this model a number of sites of 8.5×10^{-2} (mol·sites)·$g_{zeolite}^{-1}$ has been calculated .

3.2 SCR reaction modelling

Figure 5 and 6 show the typical concentration and velocity profiles of a single monolith channel when NO_x, NH_3 and O_2 are fed in the catalyst, while Figure 7 shows the NO concentration at the outlet of the catalyst.

As it is shown in Figure 5, the velocity at the walls of the channel is negligible, while the highest value is located at the center of the channel.

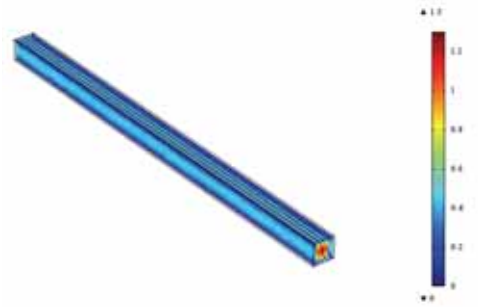

Figure 5 *Velocity profile along the channel.*

As it is shown in Figure 5, the velocity at the walls of the channel is negligible, while the highest value is located at the center of the channel.

As the mixture of NH_3, NO and O_2 in Ar flows down the channel, the ammonia adsorbs on the surface allowing reaction of NO and NO_2 with adsorbed ammonia to form the products. Thus, as it can be observed in Figure 6, the NO concentration decreases along the channel with a total conversion close to that of the walls of cordierite.

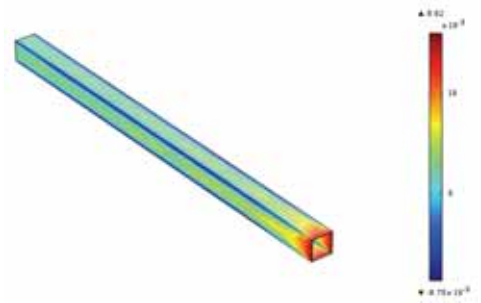

Figure 6 *NO concentration profile along the channel after 2000 seconds for NO/NO_2 1:0 feeding ratio.*

However, with these kinetic values, there is a concentration profile for NO with maximum values in the center of the channel, as shown in Figure 7.

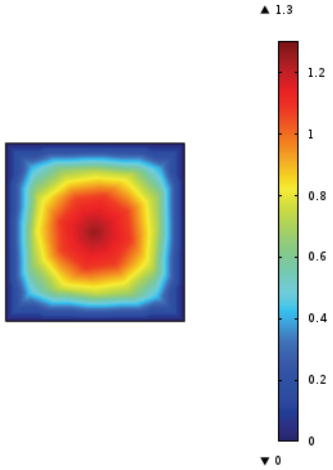

Figure 7 *NO concentration profile at the exit of the channel after 2000 seconds for NO/NO_2 1:0 feeding ratio.*

Figure 8 shows the outlet NO_x concentration evolution during first 2000 seconds as a function of the NO/NO_2 feed ratio. The obtained values are in good agreement with the experimental data obtained at 200 ºC (about 40 % of NO_x converted when only NO was fed [3]).

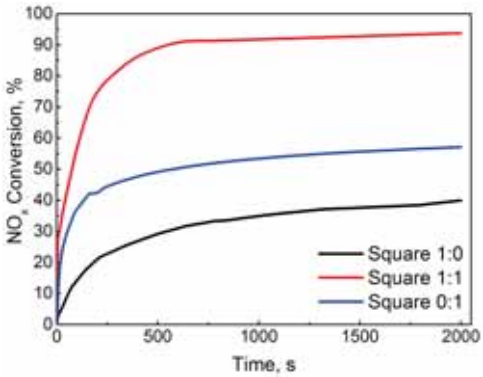

Figure 8 *NO concentration vs. time for different NO/NO$_2$ ratio feedings.*

Nevertheless, this model needs to be improved, e.g. some computational data should be obtained at different temperatures in order to validate the model.

Among the different feeding compositions, equimolecular NO/NO$_2$ mixture is the optimal for maximizing NO$_x$ conversion, in line with the stoichiometry of the fast SCR reaction (4). This result agrees with previous work [4, 5], where it was reported that higher NO$_x$ conversions are achieved in the 150-350 ºC temperature region. Nevertheless, the influence of temperature is out of the scope of this paper and will be studied in future works.

3.3. Influence of the geometry

In Figure 9, the NO concentration profile in a cylindrical channel can be observed at steady-state for the 1:1 NO/NO$_2$ ratio. In line with square form channels, the NO concentration decreases along the channel and the conversion is total close to the surface of the cordierite channel. Also, the concentration at the center of the channel is maximum, due to the limitation of the radial diffusion processes in the channel.

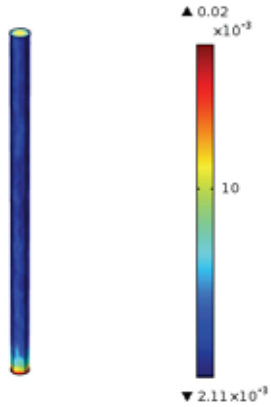

Figure 9 *NO concentration profile along the cylindrical channel geometry after 2000 seconds.*

On the other hand, comparison made between both geometries allowed us to affirm that the use of a square channels improved NO$_x$ conversion compared to cylindrical geometry. In Figure 10 both geometries are compared, plotting first 2000 seconds NO$_x$ conversion for different NO/NO$_2$ ratios.

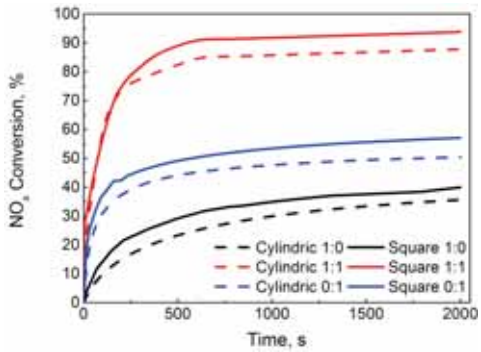

Figure 10 *NO concentration vs. time for different NO/NO$_2$ ratio and different channel geometries.*

The main reason for a lower NO_x conversion in rounded shape channels is in the difference in the volume-to-surface ratio of this type of channels. This result confirms that when 2D axisymmetric approximation is used in order to save some computational time, a loss of activity exists due to lower catalytic surface. Therefore, some calculations should be done with identical surface square/cylindrical channels in order to compare catalytic activity of both geometries.

4. Conclusions

In this work a kinetic model was used for simulating NH_3 selective catalytic reduction (SCR) of NO_x over a Cu-ZSM-5 catalyst. The results obtained for NH_3 adsorption-desorption model allowed us to determine the number of adsorption sites in our catalyst, which was 8.5×10^{-2} mol-sites$\cdot g_{zeolite}^{-1}$. On the other hand, the SCR model based on six elementary reactions reproduced NO_x elimination in our catalyst at 200 ºC fairly well, although other temperatures should be modelled as well. Also, the behavior of the catalyst in NO_x remediation has been well reproduced when different NO/NO_2 ratios were used, in line with the literature results. Finally, it can be affirmed that a loss of activity exists in cylindrical geometry catalyst's NO_x elimination due the lower surface of this type of channel, assuring that, with 2D axisymmetric model approximation, a non-real catalytic behavior is obtained, although some computational time has been saved. It can be finally concluded that a kinetic model which fits available data has been performed with COMSOL Multiphysics.

5. References

1. J.R. González-Velasco, M.A. Gutiérrez-Ortiz, J.L. Marc, M.P. González-Marcos, G. Blanchard, Selectivity of high surface area $Ce_{0.68}Zr_{0.32}O_2$ for the new generation of TWC under environments with different redox character, *Appl. Catal. B: Environmental*, **33**, 333–314 (2001).
2. Olsson L., Sjövall H., Blint R.J., A kinetic model for ammonia selective catalytic reduction over Cu-ZSM-5, *Appl. Catal B: Environ*, **81**, 203-217 (2008).
3. B. Pereda-Ayo, U. De La Torre, M. Romero-Sáez, A. Aranzabal, J.A. González-Marcos, J.R. González-Velasco, Influence of the washcoat characteristics on NH_3-SCR behavior of Cu-zeolite monoliths, *Catal. Today*, **216**, 82-89 (2013).
4. C. Ciardelli, I. Nova, E. Tronconi, D. Chatterjee, B. Bandl-Konrad, M. Weibel, B. Krutzsch, Reactivity of NO/NO_2–NH_3 SCR system for diesel exhaust aftertreatment: Identification of the reaction network as a function of temperature and NO_2 feed content, *Appl. Catal B: Environ*, **70**, 80-90 (2007).
5. M. Colombo, I. Nova, E. Tronconi, Detailed kinetic modeling of the NH_3–NO/NO_2 SCR reactions over a commercial Cu-zeolite catalyst for Diesel exhausts after treatment, *Catal Today*, **197**, 243-255 (2012).

6. Acknowledgements

The authors wish to thank to the Spanish MICINN (CTQ2012-32899)

and the Basque Government (GIC IT657-13) for their financial support. One of the authors (UDLT) also acknowledges Basque Government for the research grant (BFI-2010-330) and the COMSOL Support team for the advices provided.

7. Nomenclature

Symbol		Units
θ_{NH3}	Ammonia surface coverage	-
θ_S	Available sites fraction	-
C_i	Concentration of *i*	$mol \cdot m^{-3}$
$C_{s,i}$	Concentration of surface species *i*	$mol \cdot m^{-2}$
ρ	Density of flux at 200 ºC	$kg \cdot m^{-3}$
Γ	Density of sites	$mol \cdot m^{-2}$
D_i	Diffusitity of *i* at 200ºC	$m^2 \cdot s^{-1}$
v_0	Inlet velocity	$m^3 \cdot s^{-1}$
k_i	Rate constants *i*	Depending on the reaction
r_i	Surface rate of reaction *i*	$mol \cdot mol\text{-}sites^{-1} \cdot s^{-1}$
T	Temperature	K
μ	Viscosity of flux at 200 ºC	Pa·s

Committees

Scientific committee

Anders Ekerot. COMSOL AB, Sweden.

M.Sc. in engineering physics, specialized in scientific computing. Anders has been with COMSOL since 1999, starting out at the development department. He currently works with global technical support and product development at the Swedish office.

José Manuel González Vida. University of Málaga.

Manager of the HySEA super-computation platform, at the Numerical Methods Laboratory at UMA. He is principal investigator in an international project with the NOAA Centre for Tsunami Research (U.S.A.), in which they apply numerical methods for tsunami simulations produced by submarine landslides.

Jesús Lucio García. University of Valladolid.

He is Physicist and PhD at University of Valladolid. He specialised in Electronics and has worked since then on many simulations, most of them with finite element software COMSOL Multiphysics (solar refrigeration by methanol adsorption on active charcoal, transitory study of a turbine, house heating and cooling by Trombe wall, aluminium melting by laser, and others). Main methods which he has worked with have been time series, neural networks and finite elements. Prof.Lucio has published several papers on international rated journals. He teaches Physics at University of Burgos since 1993.

Emilio Ruiz Reina. University of Málaga.

His research is mainly focused in the electrokinetics and rheology of concentrated nanoparticle suspensions and he successfully uses different numerical analysis methods. The collaboration with research groups and engineering companies in the field of finite element method simulations is among his regular activities, as well as teaching in specialized courses about COMSOL Multiphysics.

Jorge Carbonell. Polytechnic University of Valencia.

He is Telecommunications Engineer and PhD in Electronics (1998, European Label) by the University of Lille (France). He worked in the Institutd'Electronique et de Microélectronique du Nord (IEMN), University of Lille, where his researchdealt with the electromagnetic analysis of active and passive devices for space applications, including photonic crystals in particular. Among 1999 and 2003, he joined successively Siemens, Retevisión Móvil and Telefónica Móviles, where he worked on second and third generation telephonic networks, mainly in radic-communications engineering. Since 2004, he got a full position in the Polytechnic University of Valencia, where his teaching and research activity have been focused mainly in microwave engineering, periodic structure analysis and metamaterials.

Organizing committee

Emilio Ruiz Reina
Departamento de Física Aplicada II, Universidad de Málaga.
[+34] 95 195 22 91
eruizr@uma.es

Juan Antonio Rubio
Addlink Software Cientifico, S.L.
[+34] 93 415 49 04
jrubio@addlink.es